Control of Spacecraft for Rendezvous Maneuver in an Elliptical Orbit

by

Piotr Felisiak, **M.Sc.**

A dissertation submitted to the
Faculty of Mechanical and Power Engineering
in partial fulfillment of the requirements for the degree of

Doctor of Philosophy in Mechanical Engineering and Machine Building

Department of Cryogenic, Aviation and Process Engineering
Wrocław University of Technology
Wrocław, Poland
June, 2015

Abstract

Rendezvous maneuver is one of a key elements of space flight technology. Orbital rendezvous maneuver denotes the technology that two satellites attain the same position and velocity, both vectors relative to the Earth, at the same time. The present development directions of automatic control methods for rendezvous maneuver problem are focused on autonomy of spacecraft performing maneuver, assurance of safety during the maneuver and enabling of impromptu maneuvers execution.

So far, the major vast of rendezvous maneuvers was performed in circular orbits of the target satellite. Future missions will require an execution of maneuvers completed with concatenation of satellites in an elliptical orbit. This motivates a development of suitable models of relative motion dynamics as well as automatic control methods for such case.

The conducted investigation concerns a problem of spacecraft control for rendezvous maneuver with assumption that the target satellite is moving in a Keplerian elliptical orbit. A method based on model predictive control, also referred as control with receding horizon, has been proposed in order to find a quasi-optimal maneuver trajectory. The relative motion is represented by a controlled variables vector, namely vector of relative position and velocity in Cartesian reference frame. One of the basic assumptions during control algorithm design has been an extension of initial conditions set, for which exists a possibility of control objective accomplishment.

Mathematical model of relative motion dynamics plays a key role in the control algorithm. The vast majority of control methods developed so far utilizes linearized models of relative motion, such as Hill-Clohessy-Wiltshire equations for the case of circular orbit of the target satellite, or Tschauner-Hempel equations for the elliptical case. The accuracy of that class of models degrades quickly together with increasing of the separation between spacecraft and target satellite, what restricts the set of initial conditions for which the maneuver can be successfully accomplished.

Described peculiarity of linearized models was one of the reasons for which the

proposed control method utilizes full, nonlinear and time-variant model of relative motion. It was applied as an internal model for the predictive controller, enabling process output prediction and state estimation. The model directly considers the dependency of the process dynamics on propellant mass expelled by spacecraft thrusters.

Another assumption for the controller design was an ability of utilization of quadratic programming procedure for solving of the optimal control problem. This assumption was motivated by peculiarities of nonlinear optimization procedures, which do not guarantee predictable time required for finding of solution, or the result found by them is only a local solution. Reduction of the optimization procedure to a quadratic optimization problem was obtained using a method proposed by author, involving the generation of local linear models distributed within prediction horizon. The proposed algorithm considers variance of the model parameters within a prediction horizon, what enables for more accurate prediction of the process output. Consideration of system dynamics variance was implemented owing to mechanism of prediction of model parameters, which are dependent on time and trajectories of state and control. The dependency of model parameters on control trajectory enforced application of heuristic method for preliminary estimation of future control trajectory. This allowed for avoidance of direct consideration of model parameters dependency on control trajectory in optimization procedure, what would lead to a nonlinear optimization problem.

Conducted numerical experiments denote that the proposed predictive control algorithm enables for satisfying of requirements for rendezvous maneuver in an elliptical orbit. The proposed output prediction system with consideration of model parameters variance over prediction horizon allowed for improvement of control process quality. Significant improvement was achieved in terms of the set of feasible initial conditions. The algorithm proposed by author enables for maneuver control with initial separation between satellites more than 36 000 km, what far exceeds the range of reliable operation of the present algorithms for orbital relative motion control.

The main problems belonging to the original author's contribution include: an output prediction method with consideration of model parameters variance over prediction horizon, a method for estimation of future model parameters, formulation of predictive control algorithm utilizing the mentioned methods and simulations of the control loop involving the proposed algorithm.

Streszczenie

Technologia manewrów spotkania jest jedną z kluczowych w technice kosmicznej. Orbitalny manewr spotkania polega na obraniu przez statek kosmiczny oraz obiekt docelowy (np. stację kosmiczną) takich samych wektorów prędkości i położenia względem Ziemi, obu w tym samym momencie. Obecne kierunki rozwoju technologii automatycznego sterowania dla problemu manewru spotkania skupione są na zwiększeniu autonomii statków wykonujących manewr, zapewnieniu bezpieczeństwa podczas manewru jak również umożliwieniu wykonywania przez statek manewrów improwizowanych.

Zdecydowana większość manewrów spotkania została do tej pory wykonana na kołowej orbicie obiektu docelowego. Przyszłe misje będą wymagać wykonania manewrów zakończonych połączeniem statków na orbicie eliptycznej. Z tego względu celowym jest stworzenie dla takiego wariantu odpowiednich modeli dynamiki ruchu względnego oraz metod sterowania automatycznego.

Podjęte badania dotyczą zagadnienia sterowania statkiem kosmicznym w celu wykonania manewru spotkania, przy założeniu, że satelita docelowy przemieszcza się po keplerowskiej orbicie eliptycznej. W celu znalezienia quasi-optymalnej trajektorii manewru zaproponowano metodę opartą o sterowanie predykcyjne, zwane również sterowaniem z przesuwnym horyzontem predykcji. Sterowaniu podlega ruch względny, czyli względne położenie oraz prędkość wyrażone w kartezjańskim układzie współrzędnych. Jednym z założeń podjętych na etapie projektowania algorytmu sterowania było rozszerzenie przestrzeni warunków początkowych, dla których możliwe jest osiągnięcie celu sterowania.

W algorytmie sterowania kluczową rolę odgrywa model matematyczny dynamiki ruchu względnego. Większość metod sterowania opracowanych do tej pory wykorzystuje zlinearyzowane modele ruchu względnego, takie jak równania Hill'a-Clohessy-Wiltshire'a dla przypadku kołowej orbity obiektu docelowego czy też równania Tschaunera-Hempla dla przypadku eliptycznego. Dokładność tego typu modeli jest

szybko tracona wraz ze zwiększaniem początkowej separacji pomiędzy statkiem a obiektem docelowym, co zawęża zbiór warunków początkowych, dla których manewr jest wykonalny.

Opisana właściwość modeli zlinearyzowanych była jednym z powodów, dla których w opracowanej metodzie sterowania zdecydowano się na wykorzystanie pełnego, nieliniowego oraz niestacjonarnego (nieautonomicznego) modelu ruchu względnego. Posłużył on jako model wewnętrzny dla regulatora predykcyjnego, pozwalając na predykcję wyjścia oraz estymację stanu procesu. Model w bezpośredni sposób uwzględnia zależność dynamiki procesu od masy gazu pędnego wyrzuconego przez silniki statku.

Kolejnym z założeń dotyczących projektu regulatora była możliwość wykorzystania programowania kwadratowego do rozwiązywania zagadnienia sterowania optymalnego. Założenie to podyktowane jest właściwościami procedur optymalizacji nieliniowej, które nie pozwalają przewidzieć czasu potrzebnego na znalezienie dokładnego rozwiązania, bądź też znajdują jedynie rozwiązanie lokalne. Sprowadzenie procedury optymalizacji do programowania kwadratowego rozwiązano za pomocą metody zaproponowanej przez autora, polegającej na generacji lokalnych modeli liniowych wzdłuż horyzontu predykcji. Metoda uwzględnia zmienność parametrów modelu wzdłuż horyzontu predykcji, co pozwala na dokładniejszą prognozę wyjścia procesu. Uwzględnienie zmienności dynamiki systemu jest zrealizowane dzięki mechanizmowi predykcji parametrów modelu, zależnych od czasu, trajektorii stanu oraz trajektorii sterowania. Zależność parametrów modelu od trajektorii sterowania wymusiła zastosowanie heurystycznej metody do wstępnej estymacji przyszłej trajektorii sterowania. Uniknięto w ten sposób bezpośredniego uwzględnienia zależności parametrów modelu od trajektorii sterowania w procedurze optymalizacji, co prowadziłoby do zagadnienia optymalizacji nieliniowej.

Przeprowadzone eksperymenty numeryczne wskazują, że zaproponowany algorytm regulacji predykcyjnej pozwala na spełnienie warunków stawianych manewrowi spotkania na orbicie eliptycznej. Mechanizm predykcji wyjścia uwzględniający zmienność parametrów modelu wzdłuż horyzontu predykcji pozwolił na poprawę jakości sterowania. W zdecydowany sposób uzyskano poprawę w zakresie dopuszczalnego zbioru warunków początkowych. Przedstawiony przez autora algorytm pozwala na sterowanie dla manewru z początkową separacją pomiędzy statkami ponad 36 000 km, co znacznie przekracza zakres poprawnego działania większości obecnych algorytmów

sterowania orbitalnym ruchem względnym.

Główne zagadnienia należące do oryginalnego dorobku autora stanowią: metoda predykcji wyjścia uwzględniająca zmienność parametrów modelu wewnątrz horyzontu predykcji, metoda estymacji przyszłych parametrów modelu, sformułowanie algorytmu sterowania predykcyjnego korzystającego z wymienionych metod oraz symulacje zachowania pętli sterowania wykorzystującej zaproponowany algorytm.

Moim Rodzicom

Acknowledgments

First, I would like to thank the main supervisor of the dissertation, Prof. Krzysztof Sibilski. His wisdom, enthusiasm and patience were necessary for the completion of this investigation. I am grateful for the support of the assistant supervisor, Dr. Wiesław Wróblewski.

Inspirational discussions with Dr. Krzysztof Tomczuk and Dr. Piotr Bania have their reflection in many concepts considered during this research.

Finally, I would like to thank everyone who has assisted me in my academic career.

Piotr Andrzej Felisiak

Table of Contents

List of Tables

List of Figures

Nomenclature

$\Delta\mathbf{u}$ - control vector increment
μ - standard gravitational parameter
ρ - relative position vector
$\mathbf{\Theta}$ - vector of control increment weights
Ω - longitude of the ascending node
ω - angular velocity vector or argument of periapsis
$\mathbf{\Xi}$ - output set-point vector
$\mathbf{A}$ - state matrix
a - semi-major axis of an orbit
$\mathbf{a}_u$ - acceleration produced by satellite thrusters
$\mathbf{B}$ - input matrix
b - semi-minor axis of an orbit
$\mathbf{C}$ - output matrix
$\mathbf{D}$ - feedthrough matrix
E - eccentric anomaly
e - orbit eccentricity
f - true anomaly
G - universal gravity constant
g - gravity of the Earth
$\mathbf{H}$ - Hessian matrix or angular momentum
$\mathbf{h}$ - massless angular momentum
$\mathbf{I}$ - identity matrix
I_{sp} - specific impulse
k - current sampling instant
M - mean anomaly
m - general mass
m_d - mass of the deputy satellite

m_{dry} - mass of the deputy satellite without propellant

m_{p0} - initial amount of propellant

N_c - control horizon

N_p - prediction horizon

n - mean angular motion

$\hat{\mathbf{o}}_r$, $\hat{\mathbf{o}}_\theta$, $\hat{\mathbf{o}}_h$ - LVLH frame orientation vectors

p - *semilatus rectum* (parameter of an orbit)

$\mathbf{r}$ - general position vector

$\mathbf{r}_c$ - position vector of the chief satellite

r_c - current radius of the chief satellite orbit

$\mathbf{r}_d$ - position vector of the deputy satellite

r_d - current radius of the deputy satellite orbit

$\mathbf{u}$ - control vector

$\mathbf{x}$ - state vector

$\mathbf{y}$ - vector of output variables

Chapter 1

Introduction

The orbital maneuvers involving two satellites and completed with concatenation of them into a complex structure are commonly referred to as rendezvous operations. Expressed formally, orbital rendezvous maneuver denotes the technology that two satellites attain the same position and velocity, both vectors in an inertial frame at the same time.

Orbital rendezvous is a key operational technology, required for missions such as assembly in orbit of larger units, re-supply of orbital platforms and stations, repair of spacecraft in orbit or capture and return of spacecraft to ground. Historically, the first rendezvous and docking between two spacecraft took place on 16 March 1966, when Neil Armstrong and Dave Scott manually performed the maneuver in a Gemini vehicle and then docked with an unmanned Agena target spacecraft. The first automatic rendezvous maneuver took place on 30 October 1967, when the Soviet spacecraft Cosmos 186 and 188 docked. In the past half-century, hundreds of orbital rendezvous missions were performed. The spacecraft engaged in these missions can be divided into more than ten series, including Gemini, Apollo, space shuttle, Experimental Satellite System-11 (XSS-11), Demonstration of Autonomous Rendezvous Technology (DART), Autonomous Space Transport Robotic Operations (ASTRO) from USA, the Soyuz and Progress spacecraft from Russia or the former Soviet Union, the automated transfer vehicle (ATV) from the European Space Agency (ESA), the Engineering Test Satellite VII (ETS-VII), H-II Transfer Vehicle (HTV) from Japan and the Shenzhou spaceship from China.

Relative orbital dynamics and control, inherently connected with the problem of spacecraft orbital rendezvous are an active research field for more than 50 years. An automatic and autonomous control methods are currently the main development

directions in orbital rendezvous technology. The missions planned in the future may be much more focused on satellite autonomy and include an impromptu maneuvers.

Typically, satellite rendezvous maneuvers are described assuming motion of a "deputy" satellite, often called chaser spacecraft, relative to a "chief" satellite, frequently referred as target satellite. Figure 1.1 presents typical phases of the rendezvous process. They include phasing, close-range rendezvous, final approaching and docking. Usually, the close-range rendezvous phase is divided into the homing and closing phases.

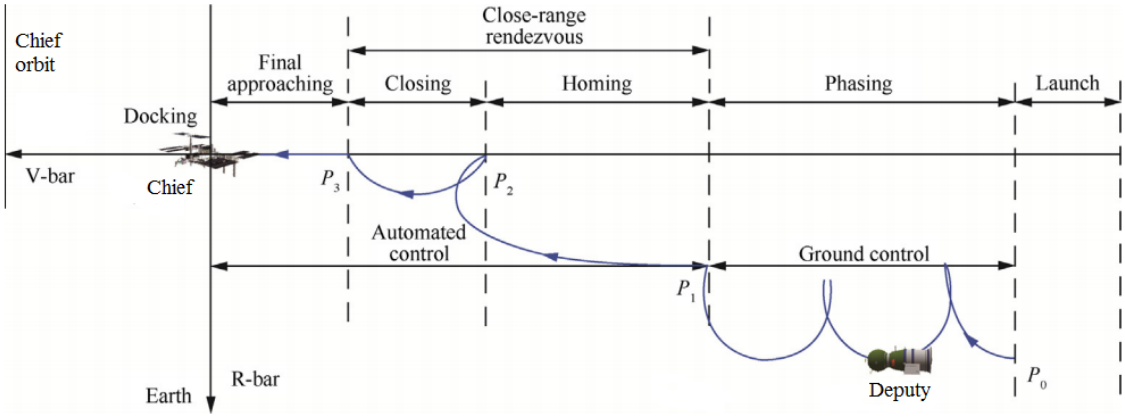

Figure 1.1: Typical spacecraft rendezvous and docking process (reproduced from Reference [1]).

In the phasing stage, the deputy spacecraft perform several maneuvers under the guidance of the ground command station. The basic aims of the phasing stage are adjusting of the phase angle between the two satellites, increasing the orbital height, reducing the orbital plane differences and initiating of the relative navigation. During this stage, motion of the satellites is typically described using inertial reference frame.

In the homing phase, the deputy spacecraft is controlled autonomously by its on-board control system. This eliminates the problem of delays present in the case where the maneuvers are controlled based on telemetry by the ground command center. The result of this phase is reduction of the relative velocity and occupation of the chief satellite orbit by the deputy. The final position of the deputy vehicle in the homing phase is a station-keeping point located a couple kilometers away from the chief satellite. In the closing phase, the deputy reduces the relative distance further, and its position is transferred to a station-keeping point located hundreds of meters

away from the chief satellite. During close-range rendezvous, relative navigation and control are mainly used.

The final approaching phase is completed when the deputy touches the chief satellite. In this phase, the deputy approaches the chief along a straight line, in order to satisfy strict requirements of docking for the relative position, velocity and attitude. During final approaching, orbit and attitude combined six-degree of freedom control is used.

1.1 Problem Background

The problems investigated in this dissertation belong to two fields of knowledge: the space flight mechanics and the control theory. The former is represented by derivation and description of mathematical model of orbital relative dynamics, whilst the latter provides tools for finding a solution for the orbital rendezvous problem.

This investigation attempts to find a control strategy for the rendezvous problem, where the chief satellite is moving in a highly elliptical orbit. In essence, this dissertation treats control of the rendezvous maneuver as a control of relative motion between the deputy and chief satellites, namely control of relative position and velocity in Cartesian coordinate frame.

The relative motion between two satellites is described by several mathematical models. The classical description is provided by the Hill-Clohessy-Wiltshire model, represented by a set of linearized time-invariant ordinary differential equations. However, this model assumes a circular chief orbit and it is valid only for small initial separations between the satellites.

Assumption of elliptical shape of the chief satellite orbit results in time-varying differential equations. In this work, such model is represented by the Tschauner–Hempel equations. However, since the applicability of this model is also limited to small initial separations between the satellites, this investigation deploys it only for comparative purposes.

The principal control method proposed in this investigation is based on full nonlinear time-variant model of relative motion. The utilization of such model is motivated by desire of closed-loop behavior enhancement and liberation from the restriction on initial separation between the satellites.

Historically, the control of relative motion have been solved using a variety of approaches, such as: PID control, linear-quadratic regulator, linear-quadratic-Gaussian controller, Lyapunov theory, rapidly exploring random tree or model predictive control. This dissertation assumes utilization of the model predictive control where the nonlinear model plays an essential role. However, presented algorithm differs from conventional solutions through consideration of model parameters variability. Nevertheless, a strong emphasis was placed on its relative simplicity and achievable application of quadratic optimization procedure, providing reliable operation of the controller.

Classically, in case of single-spacecraft mission, the term *control* refers to maintaining and altering of the spacecraft attitude. The manipulation of trajectory on the scale of an orbit is termed as *guidance*, usually performed as activity supervised from the ground. In the orbital rendezvous literature, the notion of *control* also refers to maintenance of a close proximity between two spacecraft which represents high level of autonomy.

The autonomous control strategy presented in this dissertation concerns the separation between satellites ranging from hundreds of meters, typical for closing phase, up to distances commonly reserved for phasing stage, for example tens of thousands kilometers. For this reason, in this investigation the term *control* frequently refers to classical meaning of guidance.

1.2 Scope of Dissertation

The proposed control method is based on mathematical model of the relative orbital dynamics, hence the derivation of the model is presented in detail, starting with the basic laws of orbital mechanics. The relative motion model is derived considering the two-body problem, therefore an orbital perturbations are treated as stochastic disturbances. The chief satellite orbit is assumed to have Keplerian shape.

Solution for the rendezvous control problem is obtained using proposed formulation of nonlinear model predictive control algorithm. This dissertation is focused on predictive controller design and presents a detailed description of the controller structure. However, this investigation assumes only a simple state observer, without consideration of stochastic disturbances. Such approach can be justified by the principle of separation of estimation and control, which states that under some assumptions

the problem of designing an optimal feedback controller for a stochastic system can be solved by designing an optimal observer for the state of the system, which feeds into an optimal deterministic controller. Thus the problem can be broken into two separate parts. More on the separation principle can be found in Ref. [3].

1.3 Motivation

The vast majority of the orbital rendezvous maneuvers were performed in circular orbits. Till now, the circular chief orbit case has been quite thoroughly investigated. Linearized models and control methods for the elliptical chief orbit case are less addressed in the literature. Upcoming challenges facing space technology necessitate a more detailed examination of relative dynamics for elliptical case and application of its models.

Literature studies conducted by the author denote that the vast majority of model predictive control applications for an orbital rendezvous problem exploit linear models of spacecraft relative motion. Accuracy of linearized models degrades quickly with increasing of the initial separation between satellites. Such approach enables for relative motion control only in a close proximity of the chief satellite. Moreover, imperfections of dynamics modeling leads to more inefficacious control loop behavior, such as protracted control process or needless expenditure of a propellant. Application of the full nonlinear model lets hope for an improvement of initial conditions range and control loop behavior.

An another motivation for the presented research was the design of relative simple model predictive controller able to cope with a strongly nonlinear process, described by time-variant model.

1.4 Theses of Dissertation

Following theses are formulated:

1. Algorithm proposed by author provides quasi-optimal solution for problem of spacecraft rendezvous control in a highly elliptical orbit, ensuring accomplishment of the control objective.

2. Consideration of model parameters variance within prediction horizon enables improvement of model predictive control performance.

3. Application of exact nonlinear time-variant model of relative motion for prediction and state estimation in predictive control algorithm significantly extends a set of initial conditions for which the accomplishment of the rendezvous maneuver objective is possible.

4. The method of model parameters prediction proposed by author enables reduction of the optimization problem present in predictive control algorithm to a quadratic programming problem.

1.5 Objectives of Investigation

Since the mathematical modeling of orbital relative motion represents underlying issue for further investigation, one of main objectives is derivation of suitable mathematical model and systemization of the knowledge on orbital motion. One of required attributes of the model is a direct consideration of spacecraft mass, which is variable due to expulsion of a propellant.

The principal step is a design and implementation of model predictive controller which attempts to prove the theses of this dissertation. The primary requirements for the controller are:

1. ability to guide the state of orbital relative motion described by presented nonlinear time-variant model to the control objective,

2. possible utilization of a standard quadratic programming procedure, providing predictable and reliable behavior of the control algorithm,

3. implementation of the output prediction system with consideration of model parameters variability over prediction horizon,

4. relative simplicity.

The next step is realization of a simulation environment and conducting of series of numerical experiments for confirmation of the dissertation theses.

Side objectives contain design and implementation of alternative controllers for comparative purposes.

1.6 Literature Review

Section 1.6.1 provides an overview on the relative orbital dynamics, in majority represented by linearized models as the most common description of the spacecraft relative motion. The vast majority of these approaches are valid for relatively small separations only.

Section 1.6.2 describes modern approaches to automated control for spacecraft rendezvous. Majority of these approaches consider close-range operations.

1.6.1 Mathematical Models of Relative Motion

In the case where chief satellite is moving in a circular orbit, the orbital relative motion can be described using Hill-Clohessy-Wiltshire (HCW) equations described in Ref. [4], [5]. Principal assumption for application of HCW equations is distance of separation between chief and deputy satellites less than 1 km.

As one of the first, Lawden found a closed-form solution for linearized relative motion in the case of elliptic reference orbits [6]. The next milestone for the elliptic orbit case was obtained by Tschauner & Hempel, through a reduction of the relative motion problem to a system of linear differential equations described in Ref. [7]. Melton derived in Ref. [8] the state transition matrix (STM) of the Tschauner–Hempel equations for orbits with small eccentricity, based on the solution of the HCW equation and using a perturbation theory. Carter found a singularity in Lawden's solution and then provided a state-transition matrix that depends explicitly on the true and the eccentric anomaly, overcoming the singularity [9]. Yamanaka and Ankersen proposed in Ref. [10] an analytical solution to the Tschauner-Hempel equations given in the form of a time-explicit state-transition matrix, simpler than Carter's. Minimum-time orbital rendezvous between neighboring elliptic orbits has been studied by Alfriend and Kashiwagi in Ref. [11].

In order to improve the precision of relative dynamics equations, the second-order terms of relative positions and velocities should be taken into account. Such approach was presented by London in Ref. [12]. He derived system of equations with quadratic terms, and obtained its approximate solution based on the solution of the HCW equations. Karlgaard and Lutze presented in Ref. [13] an approximate solution of the second-order relative motion equation set in spherical coordinates. Kechichian described in Ref. [14] an application of the second-order equations set to a rendezvous

trajectory with an initial relative distance of 2000 km. Extension of the second-order equations set in order to include constant thrusts was performed in Ref. [15] by Zhu and Li with consideration of a small eccentricity.

A several modifications of the relative dynamics have been developed to include relative effects of perturbations, for example consideration of inhomogeneous gravitational field caused by Earth's oblateness, based on an assumption that gravitational field is a sum of spherical harmonics, where the J_2-term plays the dominating role. In Ref. [16] Ross derived a set of relative dynamics time-variant equations considering the J_2 perturbations. Gim and Alfriend derived in Ref. [17] a complicated state transition matrix for elliptic orbits under perturbations. More computationally efficient set of equations with constant coefficients based on the HCW equations was provided by Schweighart and Sedwick in Ref. [18] by adding the long-term effect of the J_2 perturbations. Pollock et al. presented in Ref. [19] an analytical solution for relative dynamics subject to Lorentz-force perturbations. State transition matrices for the elliptical case are presented in Ref. [20] and [21].

An alternative to description using Cartesian frames is an utilization of orbital elements. The accuracy of models based on orbital elements seems to not degrade as rapidly with the separation distance as in the case of models employing Cartesian coordinates, as shown in Ref. [22]. Assuming the orbital elements as a state vector, the relative dynamics can be propagated using Gauss' Variation Equations (GVEs). A state transition matrix capable of propagating spacecraft with large separations in elliptical orbits and incorporate the effects of J_2 is presented in Ref. [23]. Labourdette and Baranov derived in Ref. [24] a relative dynamics equations set based on orbital elements differences with the J_2 perturbation, and used it to calculate maneuvers of a long-time rendezvous mission on a Mars orbit. In Ref. [25], Zhang et al. corrected and extended this equations set and applied it to a long-time multi-spacecraft rendezvous mission in a low Earth orbit. A discrete input effect matrix that incorporates the effects of J_2 perturbations and use a combined linear time-varying orbital dynamics is presented in Ref. [26]. The dynamics of the relative motion problem in a perturbed orbital environment is exploited based on Gauss' variational equations by Okasha and Newman in Ref. [27].

An another approach, utilizing difference in argument of latitude, the difference in orbital radii, and their first-order derivatives to describe relative trajectories is presented by Baranov in Ref. [28]. This equations set was used in the phasing stage

of Russian and the former Soviet Union rendezvous missions.

A wide overview on the relative motion models is presented in Ref. [1] and [29].

1.6.2 Control of Relative Motion

A very wide range of modern control techniques has been developed to solve orbital rendezvous problem. One of these approaches, represented by multi-input multi-output design for arbitrary non-cooperating chief vehicles and an assumption of relative motion with 6 degrees of freedom is developed in [30]. Karr and Freeman in Ref. [31] and Chen and Xu in Ref. [32] proposed different rendezvous fuzzy control methods. Youmans and Lutze proposed in Ref. [33] a rendezvous control method based on artificial neural network. An Extended Kalman Filter (EKF) for position estimation and fly around as well as general control design is performed in Ref. [34]. Shibata and Ichikawa proposed in Ref. [35] a feedback controller for circular and elliptic rendezvous by using the property of null controllability with vanishing energy for the Hill-Clohessy-Wiltshire and Tschauner–Hempel equations. Leader-following approach to satellite formation keeping in Earth orbit is described in [36]. Sharma et al. presented in Ref. [37] a near-optimal feedback control methodology for minimum-fuel rendezvous near an elliptic orbits accounting for nonlinear differential gravity. An excellent survey on spacecraft formation guidance and control can be found in Ref. [38]. Cairano et al. proposed in Ref. [39] a model predictive control approach for spacecraft rendezvous and proximity maneuvering which could effectively handle the constraints on thrust magnitude, line-of-sight, and approach velocity. A two Kalman filter design with relative and inertial data fusion is developed in Ref. [40]. An impulsive feedback control approach is performed in Ref. [41]. Yang et al. considered in Ref. [42] the impulse controlled rendezvous process as a switching system and proposed a novel feedback control approach based on linear matrix inequality and genetic algorithm. Non Gaussian navigation in elliptic orbits is proposed in [43] using a maximum likelihood optimization in Kalman and Huber filters. Gao et al. designed in Ref. [44] an H_∞ state-feedback controller for spacecraft rendezvous systems subject to parameter uncertainties, external perturbation, control input constraints, and poles constraint via a Lyapunov approach, which could guarantee the closed-loop systems to meet the multi-objective design requirements. Ref. [45] presents control of distributed spacecraft systems using convex fuel/time-optimal optimization. Zhou et

al. proposed in [46] a controller based on Lyapunov differential equations for an elliptical rendezvous problem by considering both magnitude and energy constraints. A classical feedback design in polar coordinates to boundary conditions along a docking axis is performed in [47]. A direct method for rapid generation of combined time-propellant near-optimal trajectories of proximity maneuvers based on the synthesis of the optimal control via the Pontryagin maximum principle is presented in Ref. [48]. An analysis on the impact of sensing noise upon the performance of model predictive control of formation flying spacecraft is performed by Breger et al. in Ref. [49]. Robust model predictive control for spacecraft rendezvous using the HCW model is proposed in Ref. [50]. Model predictive control system design and implementation for spacecraft rendezvous in an elliptical orbit can be found in Ref. [51]. Kalman filter to determine relative attitude, position, and gyro biases is developed in Ref. [52]. Model predictive control and extended command governor for improving robustness of relative motion guidance and control is proposed in Ref. [53]. Model predictive control for spacecraft rendezvous in Mars Sample Return scenario is presented in Ref. [54]. Ref. [55] develops an approach for spacecraft relative motion control based on the application of linear quadratic model predictive control with dynamically reconfigurable constraints.

An excellent handbook which approximates digital control techniques and specific application for formation flying, deployment, station keeping, and reconfiguration is represented by Ref. [56]. Another recommendable handbook is given in Ref. [57].

1.7 Main Contributions

The main objectives and contributions of this dissertation are in the field of model predictive control. Nevertheless, a detailed derivation of the orbital relative dynamics will be derived by author. A description of the main contributions is listed below:

1. A detailed, partly redefined derivation of the fundamental laws of the two-body problem will be performed.

2. A complete, peculiar derivation of the nonlinear model of relative motion will be elaborated.

3. A novel model of the deputy spacecraft mass will be derived, and used to form an augmented model of relative motion, enabling consideration of the variable

spacecraft mass in the overall process dynamics.

4. A distinctive output prediction system for the model predictive control algorithm will be derived, enabling more accurate prediction of the process described by time-variant model.

5. The guidance/control algorithm will be designed. The formulated relative motion model will serve as a basis for a novel formulation of model predictive control algorithm. The main distinguishing features of the control algorithm will be utilization of nonlinear time-variant model and consideration of model parameters variance within prediction horizon.

1.8 Dissertation Outline

The dissertation is organized as follows:

- **Chapter** 2 presents formulation of the relative motion model which will serve to formulate an internal model of predictive controller. The model is derived in details, starting from the basic laws of orbital mechanics. The chapter includes relative orbital dynamics as well as a formulation of mass model for the deputy spacecraft.

- **Chapter** 3 describes principles and theoretical aspects of model predictive control, serving as an introduction to the control algorithm description.

- **Chapter** 4 defines the control strategy proposed as a solution for the problem formulated in this dissertation. A detailed description of the control algorithm is presented, as well as an alternative version is proposed for comparative purposes.

- **Chapter** 5 presents chosen aspects of the software implementation used for research and simulations.

- **Chapter** 6 depicts the results of the rendezvous process simulations, considering various controller configurations and initial conditions sets.

- **Chapter** 7 deliberates on the obtained results. A comparison of the control quality between the chosen controllers is performed and general evaluation of the proposed solution is performed.

- **Chapter** 8 summarizes the most significant conclusions obtained during investigation as well as indicates a directions of further improvements and development of the proposed solution.

Chapter 2

Mathematical Models

This chapter contains definitions of mathematical models which forms basis for further investigation. Models described here are used by predictive controller as well as they are used for simulation of the control object.

Section 2.1 describes basic laws of orbital motion relative to the Earth. These laws are used to formulate model of relative motion between orbiting bodies described in Section 2.2. Finally, Section 2.3 formulates assumed model of spacecraft mass.

2.1 Orbital Motion Relative to the Earth

In 1543 the Polish astronomer Mikołaj Kopernik (Latin: *Nicolaus Copernicus*) published the groundbreaking work *De revolutionibus orbium coelestium*. His work, which postulated Heliocentrism, was the first one which changed perception of the center of the known Universe. Due to quality of observation methodology in his time, Kopernik assumed circular model of celestial body orbit.

The first great Kopernik's successor was Danish astronomer Tycho Brahe. He proved to be meticulous in the collection and recording of accurate data on positions of the planets. In 1601 Brahe gave Johannes Kepler his scrupulous observations of planetary motion. Brahe's work, especially observations of the Mars orbit, indicated relevant deviation from the Kopernik's circular model. That triggered Kepler's curiosity, who managed to explain Brahe's observations using elliptical model. In 1609 Kepler published his first two laws of planetary motion, and third law in 1619. His famous laws are listed below:

1. The orbit of each planet is an ellipse, with the Sun at a focus.

2. The line joining the planet to the Sun sweeps out equal areas in equal times.

3. The square of the period of a planet is proportional to the cube of its mean distance from the Sun.

Still, Kepler's laws were only a description, not an explanation of planetary motion. In years 1665 - 1667, among development of the fundamental concepts of the differential calculus and the famous laws of motion, Newton discovered the law of universal gravitation and the ensuing analytical solution of the two-body problem. However, these breakthrough achievements were published 20 years later, in 1687, as famous *Philosophiae Naturalis Principia Mathematica*.

Interesting facts about historical background of the orbital mechanics development can be found in Ref. [58]. Another recommendable handbook on orbital mechanics is represented by Ref. [59]. Ref. [60] provides an useful theory on chosen aspects of space flight mechanics. A comprehensive handbook is provided by Ref. [61]. A general introduction into the space technology, including orbital dynamics is given in Ref. [62].

An analytic solutions of the two-body problem with variable mass is derived in Ref. [63]. Integrals of motion for the two-body problem with drag are provided by Ref. [64]. A numerical approach to the orbital dynamics analysis is presented in Ref. [65].

Derivation of laws in this section was reproduced, with some modifications, on the basis of Ref. [66] and Ref. [67].

In this dissertation, the orbital motion with respect to the Earth is assumed as Keplerian motion, while the equations of motion are derived using Newton's Law of Universal Gravitation. Theory described in this section is known as the two-body problem. The scope of the problems presented here was limited to only those which are relevant to this dissertation.

2.1.1 Geometry of Keplerian Orbit

Although Newton proved that all of the conic sections could be feasible orbits, here we are interested in closed orbit, modeled by an ellipse. An example of such orbit is presented in Figure 2.1.

The shape of the orbit is determined by semi-major axis a and semi-minor axis b

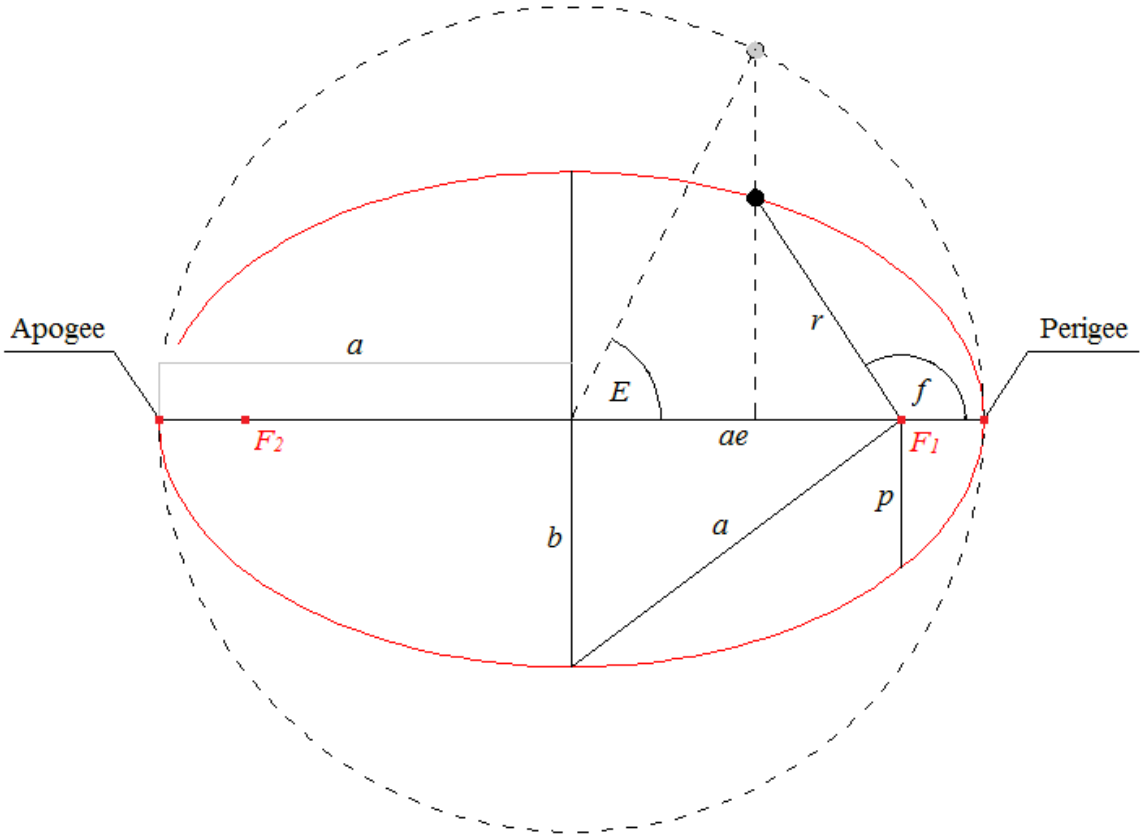

Figure 2.1: Geometry of an elliptic orbit

where $a \geqslant b$. Every orbit has two focal points, in Figure 2.1 denoted by F_1 and F_2. In special case, $a = b$, the ellipse has form of circle and both focal points occupy the same point.

The line segment p called *semilatus rectum* is perpendicular to the major axis and represents the distance between the focal point and the orbit.

The angle f between position vector $\mathbf{r}$ and the semi-major axis a is called the true anomaly. True anomaly is measured from perigee, therefore the closest point on the ellipse to the focus occurs at $f = 0$.

An important parameter that describes the shape of an elliptical orbit is non-dimensional constant e referred as the eccentricity. In case of the ellipse, the value of e is in the range $0 \leqslant e < 1$.

Let us assume that vector $\mathbf{r}$ represents the position of a body in the orbit relative to focal point F_1, whereas magnitude of that vector is denoted by r. By using some geometrical dependencies, we can find the radial distance r as the function of the true

anomaly f:

$$r = \frac{p}{1 + e\cos f} \tag{2.1}$$

Wherein a relationship exists between *semilatus rectum* p and the orbit eccentricity e:

$$p = a\left(1 - e^2\right) \tag{2.2}$$

The semi-minor axis b can be found using semi-major axis a and e:

$$b = a\sqrt{1 - e^2} \tag{2.3}$$

Note that for $e = 0$ the orbit has circular shape and $a = b$.

It is not always mathematically convenient to express the current location in the orbit using the true anomaly f. Therefore, the concept of the eccentric anomaly E was introduced. The angle E is defined in Figure 2.1. The orbiting body is projected onto circular reference orbit (dashed line). The eccentric anomaly E is the angle between the major axis and projected position relative to ellipse center.

Derivation of direct relationship between the eccentric anomaly and the true anomaly f can be found in Ref. [66]. The dependency is presented below:

$$\tan\frac{f}{2} = \sqrt{\frac{1+e}{1-e}}\tan\frac{E}{2} \tag{2.4}$$

2.1.2 Equations of Motion Relative to the Earth

In the following investigation we will consider bodies as particles having a mass m. This line of reasoning is excused by the fact of spherical shape of massive celestial bodies and large relative distances between them.

In order to describe the motion of a satellite with respect to the Earth, let us assume two particles of mass m_1 and m_2. The position of mass m_2 relative to m_1 is expressed by vector $\mathbf{r}$:

$$\mathbf{r} = \mathbf{r}_2 - \mathbf{r}_1 = r\hat{\mathbf{i}}_r \tag{2.5}$$

where vectors $\mathbf{r}_1$ and $\mathbf{r}_2$ represent position relative to inertial frame (fixed with respect to the fixed stars) and $\hat{\mathbf{i}}_r = \frac{\mathbf{r}}{r}$. The problem is illustrated in Figure 2.2. Furthermore, assume that there are two kinds of forces acting on both bodies: mutual gravitational attraction and some disturbance forces $\mathbf{F}_{d1}$ and $\mathbf{F}_{d2}$ as presented in Figure 2.2. The

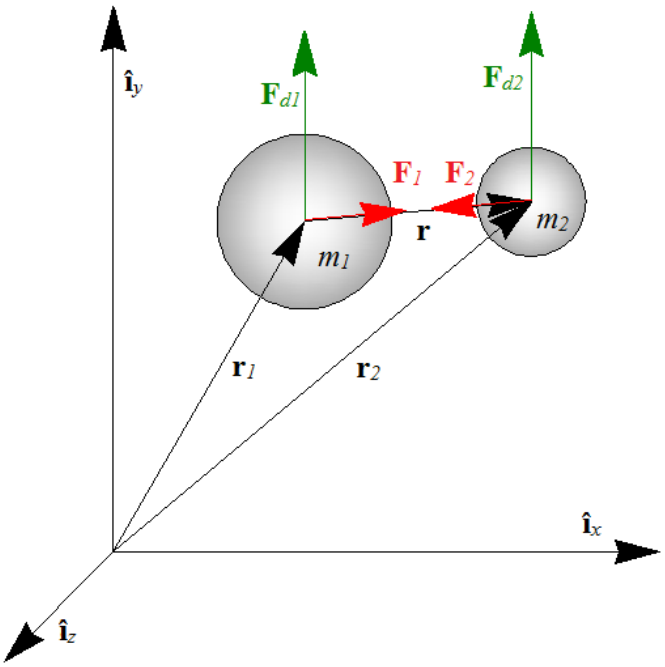

Figure 2.2: Inertial coordinate frame

gravitational attraction forces $\mathbf{F}_1$ and $\mathbf{F}_2$ are given by the Newton's Law of Universal Gravitation:

$$\mathbf{F}_1 = -\mathbf{F}_2 = \frac{Gm_1m_2}{r^2}\frac{\mathbf{r}}{r} \tag{2.6}$$

where $G \approx 6{,}673\,84 \cdot 10^{-11}\ \frac{\mathrm{m}^3}{\mathrm{kg\,s}^2}$ is the universal gravity constant.
The disturbance forces $\mathbf{F}_{d*}$ may be of different nature. They could represent drag of the rarified atmosphere in low Earth orbit, gravitational attraction of another celestial body or, in case of controllable spacecraft, thrust force produced by its thrusters.

Let us consider Newton's Second Law:

$$\mathbf{F} = m\ddot{\mathbf{r}}_n \tag{2.7}$$

where $\mathbf{F}$ is the sum of all forces acting on body having mass m and inertial position vector $\mathbf{r}_n$. Using general Equation 2.7, the inertial equations of motion for both the bodies can be expressed as:

$$m_1\ddot{\mathbf{r}}_1 = \mathbf{F}_1 + \mathbf{F}_{d1} \tag{2.8}$$

$$m_2\ddot{\mathbf{r}}_2 = \mathbf{F}_2 + \mathbf{F}_{d2} \tag{2.9}$$

After substituting of Equation 2.6:

$$m_1\ddot{\mathbf{r}}_1 = \frac{Gm_1m_2}{r^3}\mathbf{r} + \mathbf{F}_{d1} \tag{2.10}$$

$$m_2\ddot{\mathbf{r}}_2 = -\frac{Gm_1m_2}{r^3}\mathbf{r} + \mathbf{F}_{d2} \tag{2.11}$$

By dividing the Equations 2.10 and 2.11 by m_1 and m_2, respectively, we will obtain:

$$\ddot{\mathbf{r}}_1 = \frac{Gm_2}{r^3}\mathbf{r} + \frac{1}{m_1}\mathbf{F}_{d1} \tag{2.12}$$

$$\ddot{\mathbf{r}}_2 = -\frac{Gm_1}{r^3}\mathbf{r} + \frac{1}{m_2}\mathbf{F}_{d2} \tag{2.13}$$

Here, let us define the standard gravitational parameter μ. Its general definition has a form:

$$\mu = G\left(m_1 + m_2\right) \tag{2.14}$$

If we will consider artificial satellite of mass m_2 in the Earth's orbit, and we will assume that m_1 is the mass of the Earth, it turns out that $m_1 \gg m_2$ and gravitational parameter μ can be approximated as:

$$\mu \approx Gm_1 \tag{2.15}$$

Considering Equation 2.15, the value of gravitational parameter for the Earth can be approximated as $\mu_\oplus \approx 398{,}6 \cdot 10^{12}\ \frac{\mathrm{m}^3}{\mathrm{s}^2}$.

Assume the disturbance acceleration vector $\mathbf{a}_d$:

$$\mathbf{a}_d = \frac{1}{m_2}\mathbf{F}_{d2} - \frac{1}{m_1}\mathbf{F}_{d1} \tag{2.16}$$

Then, by taking the difference between Equations 2.13 and 2.12 and using Equation 2.14 we can write:

$$\ddot{\mathbf{r}} = \ddot{\mathbf{r}}_2 - \ddot{\mathbf{r}}_1 = -\frac{\mu}{r^3}\mathbf{r} + \mathbf{a}_d \tag{2.17}$$

In the case of two-body system, disturbed by gravitational force coming from a third body, where the distance between the first two bodies is relatively small in comparison with the distance to the third body, the two components of the disturbance acceleration in Equation 2.16 are near cancellation. For example, such situation has a place

in the system consisting of artificial satellite and the Earth, with the Sun's gravitational attraction as the external disturbance. Referring to this line of reasoning, in this investigation the effect of the third bodies is neglected in mathematical models.

Assuming that both the bodies (e.g. artificial satellite and the Earth) are exclusively under influence of mutual gravitational attraction, Equation 2.17 takes simpler, familiar form:

$$\ddot{\mathbf{r}} = -\frac{\mu}{r^3}\mathbf{r} \tag{2.18}$$

2.1.3 Conservation of Angular Momentum

Let us consider a rotating coordinate frame placed in the center of mass m_1 with the unit orientation vectors represented by the triad $\left\{\hat{\mathbf{i}}_r, \hat{\mathbf{i}}_\theta, \hat{\mathbf{i}}_h\right\}$. The situation is illustrated in Figure 2.3. The angular momentum $\mathbf{H}$ of body m_2 relative to m_1 is the

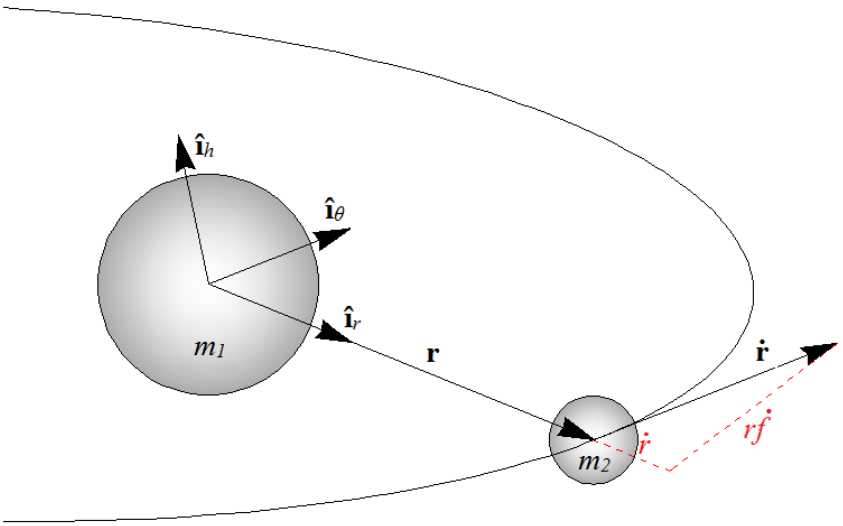

Figure 2.3: Planar orbital motion

cross product of relative position vector $\mathbf{r}$ and linear momentum $m_2\dot{\mathbf{r}}$, where $\dot{\mathbf{r}}$ is the velocity of m_2 relative to m_1:

$$\mathbf{H} = \mathbf{r} \times m_2\dot{\mathbf{r}} \tag{2.19}$$

Let us divide Equation 2.19 by m_2 and assume $\mathbf{h} = \frac{1}{m_2}\mathbf{H}$. Then $\mathbf{h}$ is angular momentum of m_2 per unit mass and takes the form:

$$\mathbf{h} = \mathbf{r} \times \dot{\mathbf{r}} = h\hat{\mathbf{i}}_h \tag{2.20}$$

The vector $\mathbf{h}$ is referred as specific angular momentum or massless angular momentum and is commonly used in orbital mechanics. The units of $\mathbf{h}$ are $\frac{\mathrm{m}^2}{\mathrm{s}}$.

To analyze what type of motion is possible with Equation 2.17, let us take the first time derivative of $\mathbf{h}$:

$$\dot{\mathbf{h}} = \dot{\mathbf{r}} \times \dot{\mathbf{r}} + \mathbf{r} \times \ddot{\mathbf{r}} \tag{2.21}$$

Having regard to the fact that $\dot{\mathbf{r}} \times \dot{\mathbf{r}} = \mathbf{0}$ and substituting Equation 2.17 we obtain:

$$\dot{\mathbf{h}} = \mathbf{r} \times \left(-\frac{\mu}{r^3}\mathbf{r} + \mathbf{a}_d\right) = -\frac{\mu}{r^3}\left(\mathbf{r} \times \mathbf{r}\right) + \mathbf{r} \times \mathbf{a}_d = \mathbf{r} \times \mathbf{a}_d \tag{2.22}$$

Equation 2.22 implies the fact that for the case of external disturbances absence, $\mathbf{a}_d \approx \mathbf{0}$, the angular momentum vector $\mathbf{h}$ remains constant since $\dot{\mathbf{h}} = \mathbf{0}$. This fact states that all possible motions will lie in inertially fixed plane perpendicular to $\hat{\mathbf{i}}_h$. Now, according to the Figure 2.3, let us express the velocity vector $\dot{\mathbf{r}}$ as:

$$\dot{\mathbf{r}} = \dot{r}\hat{\mathbf{i}}_r + r\dot{f}\hat{\mathbf{i}}_\theta \tag{2.23}$$

where $\dot{f}$ is the true anomaly rate. According to Equation 2.20, by making use of Equations 2.5 and 2.23 we can write:

$$\mathbf{h} = \mathbf{r} \times \dot{\mathbf{r}} = r\hat{\mathbf{i}}_r \times \left(\dot{r}\hat{\mathbf{i}}_r + r\dot{f}\hat{\mathbf{i}}_\theta\right) = r^2\dot{f}\hat{\mathbf{i}}_h \tag{2.24}$$

Comparing the right-hand sides of Equations 2.20 and 2.24 gives:

$$h = r^2\dot{f} \tag{2.25}$$

Since h is constant, Equation 2.25 is the proof of Kepler's Second Law of Planetary Motion.

2.1.4 Eccentricity Vector Integral

This section will introduce the concept of the eccentricity and develop relevant dependencies.

Since the angular momentum vector $\mathbf{h}$ is perpendicular to both vectors $\mathbf{r}$ and $\dot{\mathbf{r}}$, the cross product $\dot{\mathbf{r}} \times \mathbf{h}$ lies in the orbit plane. Furthermore, since $\dot{\mathbf{h}} = \mathbf{0}$, the first

derivative of $\dot{\mathbf{r}} \times \mathbf{h}$ has a form:

$$\frac{d}{dt}\left(\dot{\mathbf{r}} \times \mathbf{h}\right) = \ddot{\mathbf{r}} \times \mathbf{h} \tag{2.26}$$

With the assumption of $\mathbf{a}_d = \mathbf{0}$ we can use Equation 2.18 in order to express $\ddot{\mathbf{r}}$. Then, by using Equation 2.20 we can write:

$$\frac{d}{dt}\left(\dot{\mathbf{r}} \times \mathbf{h}\right) = -\frac{\mu}{r^3}\mathbf{r} \times \left(\mathbf{r} \times \dot{\mathbf{r}}\right) \tag{2.27}$$

By use of the trigonometric identity known as the *bac-cab* rule:

$$\mathcal{A} \times (\mathcal{B} \times \mathcal{C}) \equiv \mathcal{B} \cdot (\mathcal{A} \cdot \mathcal{C}) - \mathcal{C} \cdot (\mathcal{A} \cdot \mathcal{B}) \tag{2.28}$$

and Equations 2.5 and 2.23 for substitution, the derivative given by Equation 2.27 can be written as:

$$\frac{d}{dt}\left(\dot{\mathbf{r}} \times \mathbf{h}\right) = \frac{\mu}{r^2}\left(r\dot{\mathbf{r}} - \dot{r}\mathbf{r}\right) \tag{2.29}$$

This allows us to rewrite Equation 2.29 in the form of a exact differential:

$$\frac{d}{dt}\left(\dot{\mathbf{r}} \times \mathbf{h}\right) = \mu\frac{d}{dt}\left(\frac{\mathbf{r}}{r}\right) \tag{2.30}$$

Integration of Equation 2.30 leads to:

$$\dot{\mathbf{r}} \times \mathbf{h} = \mu\left(\frac{\mathbf{r}}{r}\right) + \mathbf{c} \tag{2.31}$$

where $\mathbf{c}$, further called eccentricity vector, is constant.

By making use of identity:

$$\mathcal{A} \cdot (\mathcal{B} \times \mathcal{C}) \equiv \mathcal{C} \cdot (\mathcal{A} \times \mathcal{B}) \tag{2.32}$$

we can find that:

$$\mathbf{r} \cdot \mathbf{c} = \mathbf{r} \cdot \left(\dot{\mathbf{r}} \times \mathbf{h} - \mu\left(\frac{\mathbf{r}}{r}\right)\right) = h^2 - \mu r \tag{2.33}$$

Assume that $c = \|\mathbf{c}\|$ and α is the angle between the vectors $\mathbf{r}$ and $\mathbf{c}$. According to the dot product definition:

$$\mathbf{r} \cdot \mathbf{c} = rc\cos\alpha \tag{2.34}$$

Equating the right-hand sides of Equations 2.33 and 2.34 we obtain:

$$r = \frac{\frac{h^2}{\mu}}{1 + \frac{c}{\mu}\cos\alpha} \tag{2.35}$$

Comparison between Equations 2.35 and 2.1 entails the proof of the Kepler's First Law of Planetary Motion which states that orbit of celestial body is an ellipse. Furthermore, this comparison leads to useful relationship between angular momentum magnitude and the semilatus rectum p:

$$h^2 = \mu p \tag{2.36}$$

Finally, the angle α between the vectors $\mathbf{r}$ and $\mathbf{c}$ has proved to be the true anomaly f.

2.1.5 Conservation of Energy

This section presents investigation of energy conservation principle in case of orbital motion. In Section 2.1.4, by taking the cross product of $\ddot{\mathbf{r}}$ given by Equation 2.18 and specific angular momentum $\mathbf{h}$ we received the Keplerian orbit formula, Equation 2.35. Now we will investigate the dot product of Equation 2.18 and linear momentum per unit mass.

The linear momentum per unit mass is just the velocity:

$$\frac{m_2\dot{\mathbf{r}}}{m_2} = \dot{\mathbf{r}} \tag{2.37}$$

hence the dot product of Equation 2.18 and massless linear momentum:

$$\ddot{\mathbf{r}} \cdot \dot{\mathbf{r}} = -\frac{\mu}{r^3}\mathbf{r}\dot{\mathbf{r}} \tag{2.38}$$

First let us consider the left-hand side of Equation 2.38. Assume the vector $\mathbf{v} = \dot{\mathbf{r}}$ express the velocity of m_2 mass relative to the m_1. Since $\mathbf{v} \cdot \mathbf{v} = v^2$:

$$\ddot{\mathbf{r}} \cdot \dot{\mathbf{r}} = \frac{1}{2}\frac{d}{dt}\left(\dot{\mathbf{r}} \cdot \dot{\mathbf{r}}\right) = \frac{1}{2}\frac{d}{dt}\left(\mathbf{v} \cdot \mathbf{v}\right) = \frac{1}{2}\frac{d}{dt}v^2 = \frac{d}{dt}\left(\frac{v^2}{2}\right) \tag{2.39}$$

Now let us consider the right-hand side of Equation 2.38. Recalling that $\mathbf{r} \cdot \mathbf{r} = r^2$

and $\frac{d}{dt}\frac{1}{r} = -\frac{\dot{r}}{r^2}$:

$$\frac{\mu}{r^3}\mathbf{r}\dot{\mathbf{r}} = \mu\frac{r\dot{r}}{r^3} = \mu\frac{\dot{r}}{r^2} = -\frac{d}{dt}\left(\frac{\mu}{r}\right) \tag{2.40}$$

Substitution of Equations 2.39 and 2.40 into Equation 2.38 gives:

$$\frac{d}{dt}\left(\frac{v^2}{2}\right) = \frac{d}{dt}\left(\frac{\mu}{r}\right) \tag{2.41}$$

Integration of Equation 2.41 yields:

$$\frac{v^2}{2} - \frac{\mu}{r} = \varepsilon \tag{2.42}$$

where ε is a constant. The $\frac{v^2}{2}$ component of Equation 2.42 is the kinetic energy per unit mass, while the $-\frac{\mu}{r}$ component is the potential energy per unit mass of the body m_2 in the gravitational field of m_1. Equation 2.42 is commonly known as the *vis-viva* (living force) equation. It states that the specific mechanical energy is the same at all points of the trajectory. Since the total mechanical energy per unit mass ε is constant, we can find its formula in terms of orbital constants by examination of Equation 2.42 at periapsis.

The periapses radius r_p can be found using Equation 2.1, by substitution of $f = 0$. By making use of Equation 2.2 we can write:

$$r_p = \frac{p}{1+e} = a\left(1-e\right) \tag{2.43}$$

Since at periapsis the radial velocity $\dot{r}_p = 0$, according to Equation 2.23 it turns out that the periapses velocity $v_p = r_p\dot{f}$. For this reason, Equation 2.25 allows us to write:

$$v_p = r_p\dot{f} = \frac{h}{r_p} \tag{2.44}$$

Thus, by using Equations 2.2, 2.36 and 2.43, the periapses velocity v_p can be found by:

$$v_p^2 = \frac{h^2}{r_p^2} = \frac{\mu a\left(1-e^2\right)}{a^2\left(1-e\right)^2} = \frac{\mu\left(1+e\right)}{a\left(1-e\right)} \tag{2.45}$$

The use of Equation 2.43 and substitution of Equation 2.45 into Equation 2.42 enables

us to find the total energy of a body ε:

$$\varepsilon = \frac{1}{2}\frac{\mu\,(1+e)}{a\,(1-e)} - \frac{\mu}{r_p} = \frac{\mu\,(1+e)}{2a\,(1-e)} - \frac{\mu}{a\,(1-e)} = -\frac{\mu}{2a} \tag{2.46}$$

Let us substitute Equation 2.46 into Equation 2.42. The result is an elegant form of *vis-viva* equation in terms of semi-major axis a:

$$v^2 = \mu\left(\frac{2}{r} - \frac{1}{a}\right) \tag{2.47}$$

An useful possibility is to express the velocity vector $\mathbf{v} = \dot{\mathbf{r}}$ in terms of its radial and tangential components $v_r = \dot{r}$ and $v_\theta = r\dot{f}^2$, respectively. By using Equations 2.25 and 2.36 we can write:

$$v_\theta^2 = \frac{\mu p}{r^2} \tag{2.48}$$

Equation 2.47 enables us to find the corresponding radial velocity component:

$$v_r^2 = \dot{r}^2 = v^2 - v_\theta^2 = \mu\left(\frac{2r-p}{r^2} - \frac{1}{a}\right) \tag{2.49}$$

An another useful expression representing the radial velocity $\dot{r}$ is presented below [67]:

$$v_r = \dot{r} = \frac{\mu e}{h}\sin f \tag{2.50}$$

2.1.6 Kepler's Equation

This section describes a way to determine the angular position of the body in orbit at any instance of time t.

Let us consider a reference frame associated with the orbit plane with origin placed in the center of the m_1 mass and unit direction vectors $\left\{\hat{\mathbf{i}}_e, \hat{\mathbf{i}}_p, \hat{\mathbf{i}}_h\right\}$. Assume that the $\hat{\mathbf{i}}_e$ vector points in the direction of periapsis, $\hat{\mathbf{i}}_h$ has the same direction as the massless angular momentum vector $\mathbf{h}$ and $\hat{\mathbf{i}}_p$ completes the right-handed coordinate system, lying in the orbit plane. Using this coordinate frame, the position vector $\mathbf{r}$ and the velocity vector $\dot{\mathbf{r}}$ can be expressed as:

$$\mathbf{r} = \epsilon\hat{\mathbf{i}}_e + \psi\hat{\mathbf{i}}_p \tag{2.51}$$

$$\dot{\mathbf{r}} = \dot{\epsilon}\hat{\mathbf{i}}_e + \dot{\psi}\hat{\mathbf{i}}_p \tag{2.52}$$

Substitution of Equations 2.51 and 2.52 into Equation 2.20 gives:

$$\mathbf{h} = \left(\epsilon\dot{\psi} - \dot{\epsilon}\psi\right)\hat{\mathbf{i}}_h = h\hat{\mathbf{i}}_h \tag{2.53}$$

The study of Figure 2.1 allows to find the value of ϵ in terms of the eccentric anomaly E:

$$\epsilon = a\left(\cos E - e\right) \tag{2.54}$$

After simple geometrical transformations the ψ component can be found as:

$$\psi = a\sqrt{1-e^2}\sin E \tag{2.55}$$

Substitution of Equations 2.54 and 2.55 along with their derivatives into Equation 2.53 gives the following:

$$h = a^2\sqrt{1-e^2}\left(\overbrace{\cos^2 E + \sin^2 E}^{1} - e\cos E\right)\frac{dE}{dt} \tag{2.56}$$

Now let us equate the right-hand side of Equation 2.56 with the expression derived from Equation 2.36:

$$\sqrt{\mu p} = a^2\sqrt{1-e^2}\left(1 - e\cos E\right)\frac{dE}{dt} \tag{2.57}$$

Use of Equation 2.2 allows us to write:

$$\sqrt{\frac{\mu}{a^3}}dt = \left(1 - e\cos E\right)dE \tag{2.58}$$

By integrating of Equation 2.58 we obtain the following form of Kepler's Equation:

$$\sqrt{\frac{\mu}{a^3}}\left(t_1 - t_0\right) = \left(E - e\sin E\right)\Big|_{E_0}^{E_1} \tag{2.59}$$

Using Equation 2.59 and initial eccentric anomaly E_0 at initial time instant t_0 we can find eccentric anomaly E_1 at a current time t_1. However, Kepler's Equation needs to be solved using numerical method, for example Newton's method.

Now let us introduce the mean angular motion n defined as:

$$n = \sqrt{\frac{\mu}{a^3}} \tag{2.60}$$

and the notion of the mean anomaly M as:

$$M = M_0 + n\,(t - t_0) \tag{2.61}$$

wherein $0 \leqslant M \leqslant 2\pi$.

Using definitions given by Equations 2.60 and 2.61 we can rewrite Equation 2.59 to the classical form of the Kepler's Equation:

$$M = E - e \sin E \tag{2.62}$$

2.1.7 Perturbations

In this section we will consider the nature and magnitude of the uncontrolled disturbances, referred as perturbations.

One of the main sources of perturbations is the Earth oblateness. In the above sections we modeled the Earth as a point mass. Such model is not entirely consistent with reality. Due to the Earth's rotation, the equatorial radius is approximately twenty kilometers greater than the polar radius. Moreover, the Earth's mass is not centered at a point, but distributed unequally under the surface. Because of tidal effects, the mass distribution varies in time. An additional kind of perturbations are acting on satellites in low orbits, which are influenced by atmospheric effects such as drag.

The motion of a satellite is also disturbed by the presence and movement of the Moon, Venus and Jupiter as well as the Sun's gravity. An another kind of perturbations is induced by solar radiation pressure and solar wind.

Figure 2.4 reproduced from Ref. [2] presents the relative magnitude of the acceleration caused by the perturbation forces as a function of orbital radius.

2.2 Orbital Motion Relative to an Body Orbiting the Earth

In this dissertation we will consider formation consisting of two satellites: the chief satellite and the deputy spacecraft. The deputy spacecraft is controlled in order to perform rendezvous maneuver, while the chief satellite is uncontrolled. The chief

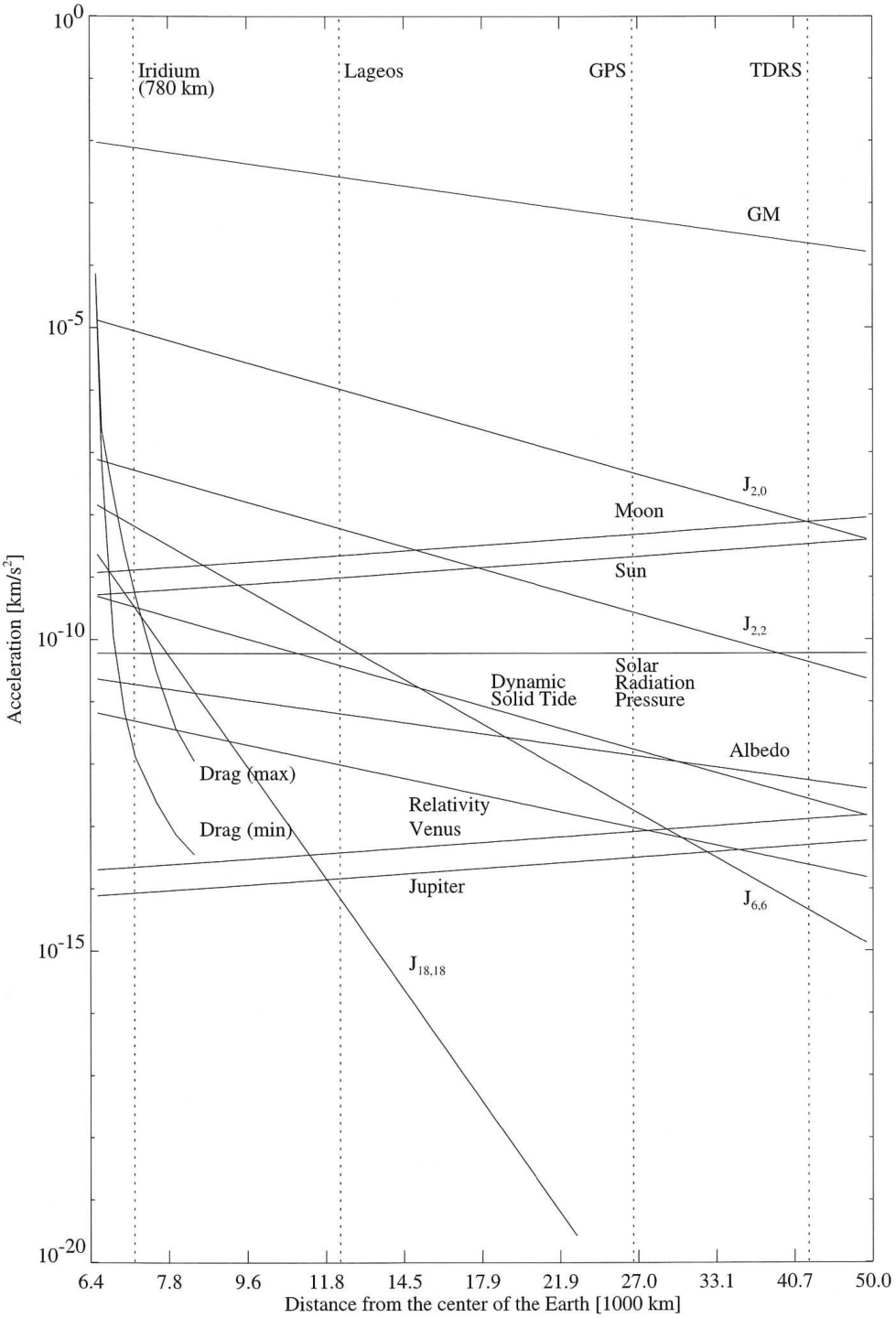

Figure 2.4: Magnitude of orbital perturbations vs satellite radius [2].

satellite determines reference point, furthermore chief satellite does not have to be a

physical object - it can be only a selected reference point.

2.2.1 Local-Vertical Local-Horizontal Coordinate Frame

In order to describe the motion of deputy spacecraft relative to the chief satellite, Cartesian local-vertical local-horizontal (LVLH) coordinate frame will be introduced. This reference frame sometimes is referred as Hill's frame. The frame is attached to the chief satellite and rotates with the chief's radius vector $\mathbf{r}_c$ as shown in Figure 2.5.

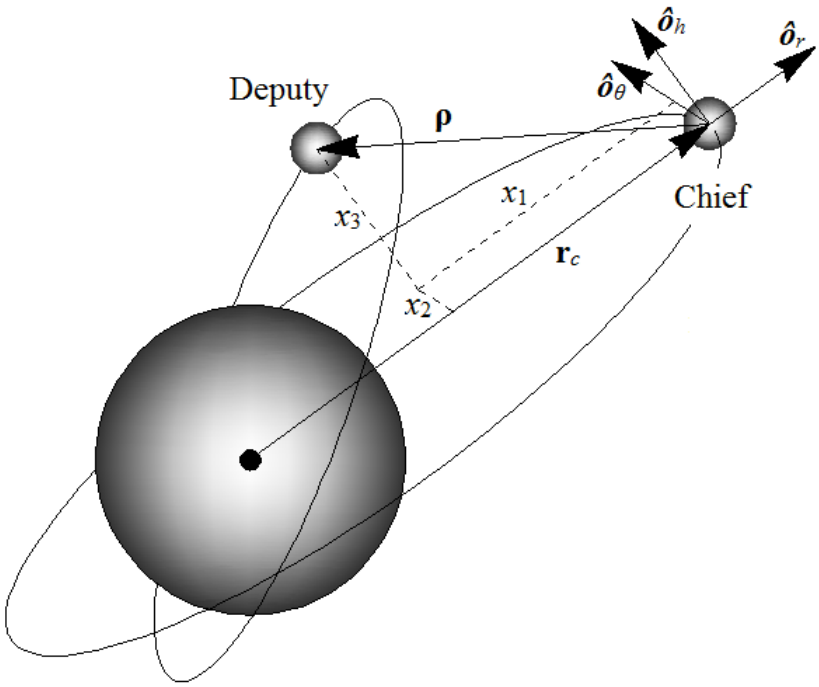

Figure 2.5: Local-vertical local-horizontal (LVLH) coordinate frame.

The orientation of LVLH frame is determined by the unit vector triad $\{\hat{\mathbf{o}}_r, \hat{\mathbf{o}}_\theta, \hat{\mathbf{o}}_h\}$ where vector $\hat{\mathbf{o}}_r$ lies in the chief's radial direction, $\hat{\mathbf{o}}_h$ is parallel to the orbit angular momentum vector, and $\hat{\mathbf{o}}_\theta$ completes the right-handed orthogonal triad. Position of the deputy satellite relative to the chief satellite can be expressed by Cartesian coordinate vector ρ:

$$\rho = x_1\hat{\mathbf{o}}_r + x_2\hat{\mathbf{o}}_\theta + x_3\hat{\mathbf{o}}_h \tag{2.63}$$

2.2.2 Nonlinear Equations of Relative Motion

This section presents the exact nonlinear equations of relative motion in LVLH frame, further called NERM. Derivation of these equations can be found inter alia in Ref. [66] and Ref. [68]. Here, they are derived in slightly different way and the impact of controlled and uncontrolled disturbances has been included.

According to Figure 2.5, the deputy satellite position vector can be written as:

$$\mathbf{r}_d = \mathbf{r}_c + \rho = (r_c + x_1)\,\hat{\mathbf{o}}_r + x_2\hat{\mathbf{o}}_\theta + x_3\hat{\mathbf{o}}_h \tag{2.64}$$

wherein r_c represents the current radius of the chief satellite orbit.

In the subsequent discussion we will assume that f denotes true anomaly of the chief satellite. According to Equation 2.25, massless angular momentum magnitude of the chief satellite is expressed by:

$$h = r_c^2\dot{f} \tag{2.65}$$

As shown in Section 2.1.3, in case of Keplerian motion the angular momentum h of the chief satellite is constant, therefore its first time derivative is equal to 0:

$$\dot{h} = 0 = 2r_c\dot{r}_c\dot{f} + r_c^2\ddot{f} \tag{2.66}$$

hence:

$$\ddot{f} = -2\frac{\dot{r}_c\dot{f}}{r_c} \tag{2.67}$$

Note that Equation 2.36 enables expression of the chief's true anomaly rate $\dot{f}$ in terms of the *semilatus rectum* value p:

$$\dot{f} = \sqrt{\frac{\mu p}{r_c^4}} \tag{2.68}$$

Considering Equation 2.65, the angular velocity vector of the rotating LVLH frame relative to the Earth-centered inertial frame is given through:

$$\omega = \dot{f}\hat{\mathbf{o}}_h = \frac{h}{r_c^2}\hat{\mathbf{o}}_h \tag{2.69}$$

Having regard Equation 2.67, the inertial angular acceleration vector of the LVLH

frame has the form:

$$\dot{\omega} = \ddot{f}\hat{\mathbf{o}}_h = -2\frac{\dot{r}_c\dot{f}}{r_c}\hat{\mathbf{o}}_h \tag{2.70}$$

In accordance with the relative acceleration formula (Ref. [67]) the second derivative of Equation 2.64 takes the form:

$$\ddot{\mathbf{r}}_d = \ddot{\mathbf{r}}_c + \dot{\omega} \times \rho + \omega \times (\omega \times \rho) + 2\omega \times \dot{\rho} + \ddot{\rho} \tag{2.71}$$

Note that the chief satellite position vector can be written as:

$$\mathbf{r}_c = r_c\hat{\mathbf{o}}_r \tag{2.72}$$

By substituting Equations 2.63, 2.69 and 2.70 into Equation 2.71 and using Equation 2.72 we obtain:

$$\begin{aligned} \ddot{\mathbf{r}}_d = \ddot{r}_c\hat{\mathbf{o}}_r + \ddot{f}\hat{\mathbf{o}}_h \times (x_1\hat{\mathbf{o}}_r + x_2\hat{\mathbf{o}}_\theta + x_3\hat{\mathbf{o}}_h) \\ +\dot{f}\hat{\mathbf{o}}_h \times \left(\dot{f}\hat{\mathbf{o}}_h \times (x_1\hat{\mathbf{o}}_r + x_2\hat{\mathbf{o}}_\theta + x_3\hat{\mathbf{o}}_h)\right) + 2\dot{f}\hat{\mathbf{o}}_h \times (\dot{x}_1\hat{\mathbf{o}}_r + \dot{x}_2\hat{\mathbf{o}}_\theta + \dot{x}_3\hat{\mathbf{o}}_h) \\ + (\ddot{x}_1\hat{\mathbf{o}}_r + \ddot{x}_2\hat{\mathbf{o}}_\theta + \ddot{x}_3\hat{\mathbf{o}}_h) \\ = \left(\ddot{r}_c - \ddot{f}x_2 - \dot{f}^2x_1 - 2\dot{x}_2\dot{f} + \ddot{x}_1\right)\hat{\mathbf{o}}_r \\ + \left(\ddot{f}x_1 - \dot{f}^2x_2 + 2\dot{x}_1\dot{f} + \ddot{x}_2\right)\hat{\mathbf{o}}_\theta \\ +\ddot{x}_3\hat{\mathbf{o}}_h \end{aligned} \tag{2.73}$$

Since it is assumed that the chief satellite is under influence of gravitational force only, its motion can be described by Equation 2.18. Substitution of Equation 2.72 into Equation 2.18 gives following form of the chief acceleration vector:

$$\ddot{\mathbf{r}}_c = -\frac{\mu}{r_c^3}\mathbf{r}_c = -\frac{\mu}{r_c^2}\hat{\mathbf{o}}_r \tag{2.74}$$

Through taking into account Equation 2.67 and the fact that Equation 2.74 leads to $\ddot{r}_c = -\frac{\mu}{r_c^2}$, we can rewrite Equation 2.73 into the following form:

$$\begin{aligned} \ddot{\mathbf{r}}_d = \left(-\frac{\mu}{r_c^2} + 2\frac{\dot{r}_c}{r_c}\dot{f}x_2 - \dot{f}^2x_1 - 2\dot{x}_2\dot{f} + \ddot{x}_1\right)\hat{\mathbf{o}}_r \\ + \left(-2\frac{\dot{r}_c}{r_c}\dot{f}x_1 - \dot{f}^2x_2 + 2\dot{x}_1\dot{f} + \ddot{x}_2\right)\hat{\mathbf{o}}_\theta + \ddot{x}_3\hat{\mathbf{o}}_h \end{aligned} \tag{2.75}$$

Let us assume that three kinds of forces are acting on the deputy satellite: gravitational, control force $\mathbf{u}$ calculated by a control system of the deputy satellite and some uncontrolled disturbance force $\mathbf{u}_{ud}$, including error between $\mathbf{u}$ and the actual force provided by the deputy satellite thrusters. Further, let us define the control vector:

$$\mathbf{u} = \begin{bmatrix} u_1 & u_2 & u_3 \end{bmatrix}^T \tag{2.76}$$

where the components u_1, u_2 and u_3 represent forces in the radial, in-track and cross-track directions respectively. Assuming that m_d denotes current mass of the deputy satellite, we can express the overall disturbance force $\mathbf{u}_d$ in terms of disturbance acceleration $\mathbf{a}_d$ from Equation 2.16:

$$\mathbf{u}_d = \begin{bmatrix} u_{d1} & u_{d2} & u_{d3} \end{bmatrix}^T = m_d \mathbf{a}_d = \mathbf{u} + \mathbf{u}_{ud} \tag{2.77}$$

In the presence of disturbances, Equation 2.17 can be applied in order to find the acceleration vector of the deputy satellite:

$$\ddot{\mathbf{r}}_d = -\frac{\mu}{r_d^3}\mathbf{r}_d + \mathbf{a}_d = -\frac{\mu}{r_d^3}\begin{bmatrix} r_c + x_1 \\ x_2 \\ x_3 \end{bmatrix} + \frac{1}{m_d}\begin{bmatrix} u_{d1} \\ u_{d2} \\ u_{d3} \end{bmatrix} \tag{2.78}$$

The current radius of the deputy satellite orbit can by found by:

$$r_d = \sqrt{(r_c + x_1)^2 + x_2^2 + x_3^2} \tag{2.79}$$

Equating coefficients in Equations 2.75 and 2.78 gives as the result the exact nonlinear equations of relative motion (NERM):

$$\ddot{x}_1 - 2\dot{f}\left(\dot{x}_2 - x_2\frac{\dot{r}_c}{r_c}\right) - x_1\dot{f}^2 - \frac{\mu}{r_c^2} = -\frac{\mu}{r_d^3}(r_c + x_1) + \frac{u_{d1}}{m_d} \tag{2.80}$$

$$\ddot{x}_2 + 2\dot{f}\left(\dot{x}_1 - x_1\frac{\dot{r}_c}{r_c}\right) - x_2\dot{f}^2 = -\frac{\mu}{r_d^3}x_2 + \frac{u_{d2}}{m_d} \tag{2.81}$$

$$\ddot{x}_3 = -\frac{\mu}{r_d^3}x_3 + \frac{u_{d3}}{m_d} \tag{2.82}$$

2.2.3 State-Space Representation

This section defines state-space representation of the relative motion model described in Section 2.2.2.

Let us assume the state vector:

$$\mathbf{x}_{rm} = \begin{bmatrix} x_1 & x_2 & x_3 & x_4 & x_5 & x_6 \end{bmatrix}^T \tag{2.83}$$

where x_1, x_2 and x_3 are components of the deputy satellite relative position vector in LVLH frame, according to Figure 2.5. Let x_4, x_5 and x_6 be components of the relative velocity vector. Then, using Equations 2.80, 2.81 and 2.82, we can write:

$$\dot{x}_1 = x_4 \tag{2.84}$$

$$\dot{x}_2 = x_5 \tag{2.85}$$

$$\dot{x}_3 = x_6 \tag{2.86}$$

$$\dot{x}_4 = 2\dot{f}x_5 - 2\dot{f}x_2\frac{\dot{r}_c}{r_c} + x_1\dot{f}^2 + \frac{\mu}{r_c^2} - \frac{\mu}{r_d^3}r_c - \frac{\mu}{r_d^3}x_1 + \frac{u_{d1}}{m_d} \tag{2.87}$$

$$\dot{x}_5 = -2\dot{f}x_4 + 2\dot{f}x_1\frac{\dot{r}_c}{r_c} + x_2\dot{f}^2 - \frac{\mu}{r_d^3}x_2 + \frac{u_{d2}}{m_d} \tag{2.88}$$

$$\dot{x}_6 = -\frac{\mu}{r_d^3}x_3 + \frac{u_{d3}}{m_d} \tag{2.89}$$

Assuming state vector $\mathbf{x}_{rm}$ given by Equation 2.83 and disturbance vectors defined by Equation 2.77, we can write Equations 2.84 ... 2.89 in the state-space form:

$$\dot{\mathbf{x}}_{rm} = \mathbf{A}_{rm}\mathbf{x}_{rm} + \mathbf{B}_{rm}\left(\mathbf{u} + \mathbf{u}_{ud}\right) + \mathbf{V}_{rm} \tag{2.90}$$

wherein the state matrix is defined as:

$$\mathbf{A}_{rm} = \begin{bmatrix} 0 & 0 & 0 & 1 & 0 & 0 \\ 0 & 0 & 0 & 0 & 1 & 0 \\ 0 & 0 & 0 & 0 & 0 & 1 \\ \dot{f}^2 - \frac{\mu}{r_d^3} & -2\dot{f}\frac{\dot{r}_c}{r_c} & 0 & 0 & 2\dot{f} & 0 \\ 2\dot{f}\frac{\dot{r}_c}{r_c} & \dot{f}^2 - \frac{\mu}{r_d^3} & 0 & -2\dot{f} & 0 & 0 \\ 0 & 0 & -\frac{\mu}{r_d^3} & 0 & 0 & 0 \end{bmatrix} \tag{2.91}$$

the input matrix:

$$\mathbf{B}_{rm} = \begin{bmatrix} 0 & 0 & 0 \\ 0 & 0 & 0 \\ 0 & 0 & 0 \\ \frac{1}{m_d} & 0 & 0 \\ 0 & \frac{1}{m_d} & 0 \\ 0 & 0 & \frac{1}{m_d} \end{bmatrix} \tag{2.92}$$

and the vector of the nonlinear term:

$$\mathbf{V}_{rm} = \begin{bmatrix} 0 & 0 & 0 & \mu\left(\frac{1}{r_c^2} - \frac{r_c}{r_d^3}\right) & 0 & 0 \end{bmatrix}^T \tag{2.93}$$

2.3 Mass Model of Deputy Satellite

For the purpose of this investigation author assumed a simple state-space model of the expelled propellant mass. The general concept of the model is based on the relationship between mass flow rate and the thrusters' parameter known as the specific impulse [69]. The relationship is given below:

$$\dot{m} = \frac{F_{thrust}}{I_{sp}g} \tag{2.94}$$

where $\dot{m}$ denotes the mass flow rate of the propellant being expelled, F_{thrust} is the force obtained from the thruster, g is the acceleration at the Earth's surface and I_{sp} denotes the specific impulse. The units of the I_{sp} are s.

Assume that $\mathbf{x}_{ep}$ having dimensions $\dim[\mathbf{x}_{ep}] = 1 \times 1$ denotes mass of the propellant expelled by the deputy satellite thrusters. Let us define state-space model of the expelled mass:

$$\dot{\mathbf{x}}_{ep} = \mathbf{A}_{ep}\mathbf{x}_{ep} + \mathbf{B}_{ep}\mathbf{u} \tag{2.95}$$

wherein the control vector $\mathbf{u}$ is defined by Equation 2.76. Let us assume that the expelled mass $\mathbf{x}_{ep}$ does not affect mass flow rate, therefore the state matrix $\mathbf{A}_{ep} = \mathbf{0}_{1,1}$.

The input matrix $\mathbf{B}_{ep}$ having dimensions $\dim[\mathbf{B}_{ep}] = 1 \times 3$ contains components which correspond to mass flow rate in the radial, in-track and cross-track directions respectively. The components are formulated based on Equation 2.94, however the sign of each component depends on the sign of corresponding component in the control vector $\mathbf{u}$. In the case where the expelled mass $x_{ep} = \|\mathbf{x}_{ep}\|$ is less than the initial propellant mass m_{p0} available to the deputy satellite, i-th component ($i = 1, 2, 3$) of the $\mathbf{B}_{ep}$ row matrix is defined as:

$$\forall x_{ep} < m_{p0} \left\{ u_i \geqslant 0 \Rightarrow B_{ep\,1,i} = \frac{1}{I_{sp}g} \right\} \tag{2.96}$$

$$\forall x_{ep} < m_{p0} \left\{ u_i < 0 \Rightarrow B_{ep\,1,i} = -\frac{1}{I_{sp}g} \right\} \tag{2.97}$$

In the case where the propellant mass available to the deputy satellite is fully expelled, the $\mathbf{B}_{ep}$ input matrix is a zero matrix:

$$\exists x_{ep} = m_{p0} \left\{ \mathbf{B}_{ep} = \begin{bmatrix} 0 & 0 & 0 \end{bmatrix} \right\} \tag{2.98}$$

Finally, the deputy spacecraft mass m_d, which is a parameter in the NERM model given in Section 2.2.2, can be found using the following formula:

$$m_d = m_{dry} + m_{p0} - x_{ep} \tag{2.99}$$

wherein m_{dry} denotes mass of the deputy satellite without available propellant.

Chapter 3

Theoretical Aspects of Model Predictive Control

Model predictive control (MPC), also referred to as moving horizon control or receding horizon control, is an advanced method of dynamic systems control. This dissertation considers discrete time predictive control only.

Model predictive controllers computes control action by periodical solving an optimal control problem over finite future horizon, possibly subject to constraints on the inputs and outputs. The optimal control problem is solved using the current state estimate of the controlled process as the initial state. The optimization yields an optimal control sequence, however only the first control action in this sequence is applied to the plant. The whole procedure is repeated at the next sampling instant.

The first presentation of MPC algorithm application took place at a conference in 1976. The algorithm was developed by J. Richalet and his collaborators from the Adersa company. The approach was described as Model Predictive Heuristic Control (MPHC), while the solution software is known as IDCOM, an acronym for Identification and Command. The distinguishing features of the IDCOM are linear impulse response model of the plant and quadratic cost function over a finite prediction horizon. The next milestone in the MPC development was algorithm named Dynamic Matrix Control (DMC) presented in 1980 by C. R. Cutler and B. L. Ramaker [70] from the Shell Oil company. The features of DMC algorithm include linear step response model of the plant and quadratic cost function over a finite prediction horizon. Still, IDCOM and DMC algorithms provided heuristic constraints handling. In order to overcome this weakness, in 1986 C. E. García and A. M. Morshedi proposed

algorithm known as QDMC (Quadratic Dynamic Matrix Control). The QDMC algorithm is characterized by full quadratic programming problem with state and control constraints and linear step response model of the plant.
The next relevant development of the MPC algorithms appeared in 1987. The algorithm presented by D. W. Clarke, C. Mothadi and P. S. Tuffs and described as Generalized Predictive Control (GPC) took into account large class of disturbances, current estimation of parameters and made use of linear discrete transfer function-based model of the plant.
Later development of MPC algorithms include making use of state-space model of the plant, estimation of unmeasured states and research on nonlinear models. Nowadays, the main directions of research are focused on robustness and stability of the algorithms.

An excellent overview of MPC algorithms and their history can be found in Ref. [71]. A meritorious handbook on the MPC is given in Ref. [72]. In case of Polish readers, Ref. [73] is strongly recommendable. An introduction to theoretical and practical aspects of the most commonly used MPC strategies is presented in Ref. [74]. A comprehensive survey on stability and optimality of the MPC is provided by [75]. An early comparison between the MPC and the other control strategies is performed in Ref. [76]. Ref. [77] delivers a survey on the contemporary MPC approaches.

A novel model predictive control scheme based on multi-objective optimization is developed in Ref. [78]. The problem of nonlinear model predictive control algorithms is presented by Cannon in Ref. [79]. Robust constrained model predictive control using linear matrix inequalities is proposed in Ref. [80]. Industrial applications of distributed model predictive control is given by Ref. [81]. A multi-objective optimization for the MPC can be also found in Ref. [82]. Ref. [83] presents nonlinear model predictive control using deterministic global optimization.

3.1 Principles of Model Predictive Control

This section describes the basic principles of model predictive control. Operation of model predictive control can be illustrated using Figure 3.1. The task of the controller is to calculate an optimal control sequence in order to move the predicted process response to the set-point. The measured process outputs $\mathbf{y}$ together with the current manipulated variable $\mathbf{u}$ are used to estimate the state vector. The state estimate $\hat{\mathbf{x}}$,

calculated by the state observer, serves as the feedback signal to the optimization algorithm. Using the model of the process and the current state estimate $\hat{\mathbf{x}}$ as initial condition, the controller obtains the future behaviour of the process output. This allows to find the optimal control vector $\mathbf{u}$ by minimization of the cost function, subject to the constraints, within optimization window called prediction horizon N_p (number of predictions). The cost function is typically expressed as a function of error between the desired set-point signal and the predicted output signal.

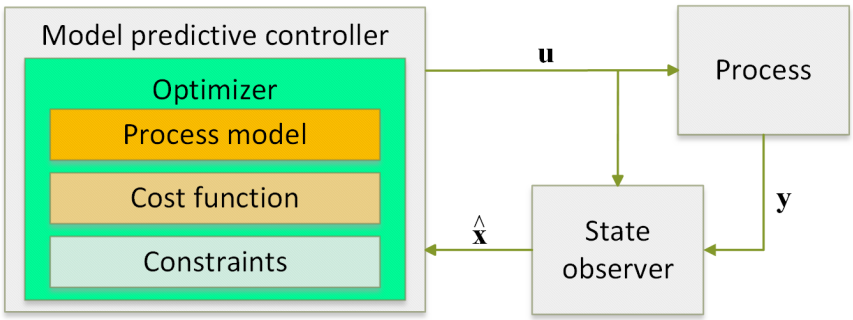

Figure 3.1: Basic operation diagram of model predictive control

Let us look more closely at the control calculations. Model predictive controllers are usually designed to find the change in the manipulated variable from one sampling instant to the next $\Delta\mathbf{u}(k)$ instead of solving for $\mathbf{u}(k)$ directly. The control increment $\Delta\mathbf{u}(k)$ can be expressed as:

$$\Delta\mathbf{u}(k) = \mathbf{u}(k) - \mathbf{u}(k-1) \tag{3.1}$$

wherein k is the current sampling instant. Furthermore, a distinguishing feature of MPC is its receding horizon approach. In fact, the result of the optimization procedure at a single sampling instant is a sequence of control moves (manipulated variables changes) $\Delta\mathbf{u}(k)$, $\Delta\mathbf{u}(k+1)$, $\cdots$, $\Delta\mathbf{u}(k+N_c-1)$, where N_c represents the control horizon (number of control moves). However, only the first control move $\Delta\mathbf{u}(k)$ from the sequence is applied to the process, ignoring the rest of the calculated control trajectory. At the next sampling instant, after new measurements become available, a new sequence is calculated in an optimal manner within the prediction horizon and again only the first control move is implemented. The whole procedure is repeated at each sampling instant.

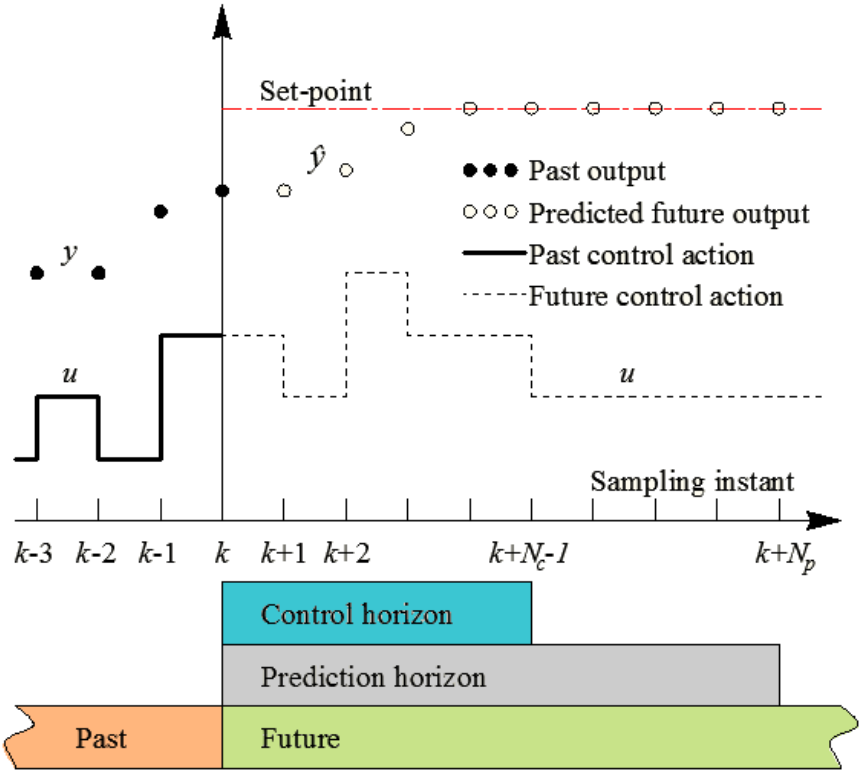

Figure 3.2: Illustration of MPC principle

The sequence of control moves calculated in a single sampling instant consists of N_c elements, the current control move $\Delta\mathbf{u}(k)$ and $N_c - 1$ future moves. Since the control horizon N_c is typically shorter than the prediction horizon N_p, the control value $\mathbf{u}$ is held after the N_c control moves ($\Delta\mathbf{u} = \mathbf{0}$), as shown in Figure 3.2. The chart refers to MPC of single-input single-output system for simplicity, and illustrates the sequence of future control moves u, calculated at the current sampling instant k, so that a set of N_p predicted outputs $\hat{y}$ reaches the set-point.

3.2 Mathematical Formulation of Model Predictive Control

Since linear models are most widely used in the MPC, this section presents general formulation of MPC assuming discrete-time, time-invariant linear state-space model

of the process. Let us express such model as:

$$\mathbf{x}(k+1) = \mathbf{A}\mathbf{x}(k) + \mathbf{B}\Delta\mathbf{u}(k) \tag{3.2}$$

$$\mathbf{y}(k) = \mathbf{C}\mathbf{x}(k) \tag{3.3}$$

Assuming that the process has n_u manipulated inputs, n_y outputs and n_x states, the $\mathbf{x}(k) \in \Re^{n_x}$ is the state vector at time k, $\mathbf{y}(k) \in \Re^{n_y}$ is the outputs vector and $\Delta\mathbf{u}(k) \in \Re^{n_u}$ is the vector of control moves to be determined by the controller. The control and state vectors must satisfy $\Delta\mathbf{u}(k) \in \Delta\mathscr{U}$ and $\mathbf{x}(k) \in \mathscr{X}$.

Usually, in case of MPC with quadratic optimization (and linear constraints), the set of admissible control moves $\Delta\mathscr{U}$ is a convex, compact subset of $\Re^{n_u}$ and the set of admissible states $\mathscr{X}$ is a convex, closed subset of $\Re^{n_x}$.

Typically, the control objective is to steer the state/output to the set-point value, with ability to tuning of control increment amplitude in order to enforce less or more aggressive behavior of the controller. This leads us to the essence of the model predictive control, that is minimization of the scalar cost function J at a given time k by solving for optimal control trajectory $\Delta\mathbf{u}(.) = \Delta\mathbf{u}(k), \Delta\mathbf{u}(k+1), \cdots, \Delta\mathbf{u}(k+N_c-1)$. In case of MPC based on quadratic optimization algorithms, one of the most commonly used cost functions has the following form:

$$\begin{aligned} J = \sum_{i=1}^{n_y}\sum_{j=1}^{N_p} \left[r_i - \hat{y}_i(k+j \mid k)\right]^T Q_i \left[r_i - \hat{y}_i(k+j \mid k)\right] \\ + \sum_{i=1}^{n_u}\sum_{j=0}^{N_p} \Delta u_i(k+j)^T R_i \Delta u_i(k+j) \end{aligned} \tag{3.4}$$

where:
r_i - reference (set-point) value for i-th process output,
$\hat{y}_i(k+j \mid k)$ - predicted value of i-th process output at j-th prediction horizon step, wherein the prediction is obtained using informations available at time k,
$\Delta u_i(k+j)$ - i-th control increment value at j-th prediction horizon step,
$Q_i > 0$ - tuning weight for i-th process output,
$R_i \geqslant 0$ - tuning weight for i-th control move.

The cost function is minimized subject to a set of linear inequality constraints:

$$\mathbf{M}_{const}\Delta\mathbf{U} \leqslant \mathbf{N}_{const} \tag{3.5}$$

where:

$$\Delta\mathbf{U} = \begin{bmatrix} \Delta\mathbf{u}(k) \\ \Delta\mathbf{u}(k+1) \\ \vdots \\ \Delta\mathbf{u}(k+N_c-1) \end{bmatrix} \tag{3.6}$$

It is sufficient that $\Delta\mathbf{U}$ contains only $N_c < N_p$ elements, since after the N_c control moves $\Delta\mathbf{u} = \mathbf{0}$. The constraints matrices $\mathbf{M}_{const}$ and $\mathbf{N}_{const}$ can reflect following constraints:

- on the control incremental variation: $\Delta\mathbf{u}^{min} \leqslant \Delta\mathbf{u}(k+j) \leqslant \Delta\mathbf{u}^{max}$,
- on the amplitude of the control: $\mathbf{u}^{min} \leqslant \mathbf{u}(k+j) \leqslant \mathbf{u}^{max}$,
- on output: $\mathbf{y}^{min} \leqslant \hat{\mathbf{y}}(k+j \mid k) \leqslant \mathbf{y}^{max}$.

Note that the predicted output values $\hat{\mathbf{y}}$ are calculated using the current state estimate $\hat{\mathbf{x}}(k)$. Particular detailed example of MPC formulation is presented in Chapter 4.

3.3 Reason and Properties of Model Predictive Control

The optimal control problems can be solved using necessary conditions of optimality in control space expressed by Pontryagin's maximum principle, or using Bellman's dynamic programming method. Solution based on Hamilton–Jacobi–Bellman equation need to be solved once, during controller design, what gives a relevant advantage over the Pontryagin's maximum principle approach. However, in case of nonlinear systems the solution based on Hamilton–Jacobi–Bellman equation is practically impossible to find. Much more convenient approach is to solve the optimal control problem periodically, within finite horizon using current state estimate as the initial condition. This makes MPC one of the few control method able to cope with nonlinear systems subject to constraints on control and state/output [84].

However, when a finite prediction horizon is used, the actual closed-loop control and state trajectories will differ from the predicted open-loop trajectories, even if no model-process mismatch and no disturbances are present. The cause is the fact that

standard control strategies obtains the feedback law a priori, while the MPC calculates the feedback law on-line, over finite horizon. The difference between repeated minimization over finite horizon and optimization over infinite horizon increases together with shortening of the prediction horizon. If too small horizon is chosen, there is no guarantee that the closed-loop system will be stable. Thus, the basic objective in prediction horizon tuning is to choose the length (number of sampling instants) which provides closed-loop stability [85].

The most important characteristics of the MPC are as follows:

- constraints on inputs and outputs are considered in a systematic, explicit manner,
- MPC allows the use of a nonlinear model for prediction,
- a specified cost function in MPC is optimized on-line,
- in general, the predicted behavior is different from the closed-loop behavior,
- the process model captures the dynamic and static interactions between input, output, and disturbance,
- MPC has the natural ability to control a multiple-input and multiple-output processes, including case of not equal number of inputs and outputs,
- to perform the prediction the process states must be measured or estimated.

Chapter 4

Control of Relative Motion

This chapter presents detailed design of the controller able to solve for quasi-optimal trajectory of spacecraft relative motion. The main goal was to design a relatively simple and reliable predictive controller which is able to cope with strong time variability and nonlinearity of the relative motion model.

Author introduced an output prediction system which takes into account the variability of model parameters over the prediction horizon. Let us refer this kind of MPC as MPC-EMP (**M**odel **P**redictive **C**ontrol with consideration of **E**volution of **M**odel **P**arameters).

For comparison, an approach based on assumption that model parameters are invariant within the prediction horizon is also presented. This approach will be further reffered as MPC-CMP (**M**odel **P**redictive **C**ontrol with **C**onstant **M**odel **P**arameters within the prediction horizon).

4.1 General Concept

The general scheme of the MPC-EMP algorithm is presented in Figure 4.1.

The controller is equipped with discrete time-variant nonlinear model of relative motion. This model is implemented as a set of functions capable to calculate the value of the next state $\mathbf{x}_m(k+1)$ and the output $\mathbf{y}_m(k)$ at a given sample instant k, depending on given state $\mathbf{x}_m(k)$ and control input $\mathbf{u}(k)$. Since the model is time-variant, part of these functions is responsible for calculation of the model parameters for given operation point.

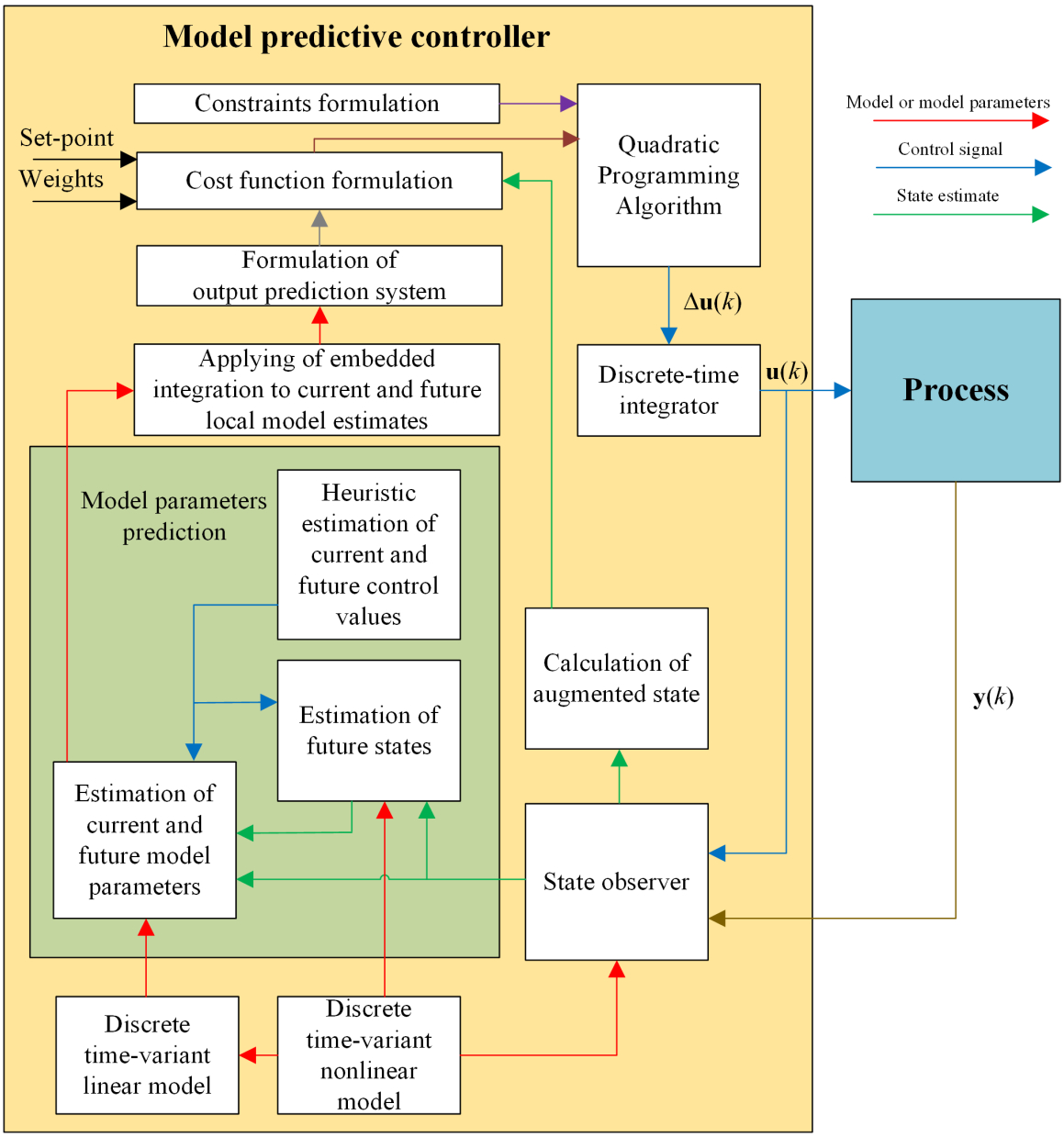

Figure 4.1: Operation diagram of MPC-EMP algorithm

Having this set of functions representing the nonlinear model, the controller inherits the subsequent set of functions representing time-variant linear model. Similarly, a part of functions enables for calculation of time-invariant parameters of a local linear model, depending on state, control input and time (for a local operation point). This allows to forecast a set of local linear models distributed over the prediction horizon (calculated for each sample time within the horizon) and hence enables for

consideration of the model parameters variance.

However, the model parameters over the prediction horizon are dependent on the current and future states $\mathbf{x}_m(k)$, $\mathbf{x}_m(k+1)$, ..., $\mathbf{x}_m(k+N_p)$ as well as the current and future control input values $\mathbf{u}(k)$, $\mathbf{u}(k+1)$, ..., $\mathbf{u}(k+N_p)$. In order to estimate parameters of the model at time k, the current state estimate $\hat{\mathbf{x}}_m(k)$ is provided by the state observer. Nevertheless, in order to estimate the future model parameters at sampling instants $k+1$, $k+2$, ..., $k+N_p$, the future states need to be estimated. Furthermore, the future states are dependent on the current and future control input values. Since the model parameters prediction takes place before calculation of the current control input $\mathbf{u}(k)$, the current and future control input estimates $\hat{\mathbf{u}}(k)$, $\hat{\mathbf{u}}(k+1)$, ..., $\hat{\mathbf{u}}(k+N_p)$ are found using a heuristic method.

The result of the model parameters prediction stage is a set of local linear models, one model for each sampling instant within the prediction horizon, wherein the models are represented by estimates of time-invariant local parameters.

In the next stage, each local model from the models set is augmented using an embedded integrator. This treatment allows the control system to reject constant disturbances without steady-state errors. The set of augmented models is then used to formulate an output prediction system, which allows to predict the output estimates $\hat{\mathbf{y}}(k)$, $\hat{\mathbf{y}}(k+1)$, ..., $\hat{\mathbf{y}}(k+N_p)$ used in the cost function.

Since the models with an embedded integrator are used to formulate the cost function, the current state estimate provided by the state observer need to be augmented according to the augmented model definition.

The cost function, equipped with the output prediction system, given augmented estimate of the current state, formulated with consideration of the set-point and weights, is fed to the optimization algorithm together with the constraints matrices.

The result of the optimization procedure is an open-loop control trajectory $\Delta\mathbf{u}(k)$, $\Delta\mathbf{u}(k+1)$, $\cdots$, $\Delta\mathbf{u}(k+N_c-1)$. Only the first control increment $\Delta\mathbf{u}(k)$ is accepted, and it need to be integrated before application to the process.

The result of the discrete integration, namely the control input $\mathbf{u}(k)$, together with the current measurements $\mathbf{y}(k)$ serve the state observer in order to estimate the state vector in the next sampling instant.

4.2 Internal Models Used by Controller

This section describes three classes of models utilized by the controller. Section 4.2.1 formulates the time-variant nonlinear model. Section 4.2.2 presents the linear time-variant model, which further is used to formulate linear model with an embedded integrator, described in Section 4.2.3.

Note that (in general) the state-space representation matrices should be treated as dependent on time, current state and control input. However, arguments k, $\mathbf{x}(k)$ and $\mathbf{u}(k)$ are often omitted here for the reason of clarity.

4.2.1 Nonlinear Model

The controller is equipped with time-variant nonlinear model of the controlled process, used by the state observer, for prediction of future states during model parameters prediction and to formulation of the linear model.

First, let us consider the model of the process in the continuous time domain. Since the deputy spacecraft mass $m_d(t)$ has relevant influence on dynamics of the system described by the NERM model, author decided to augment the relative motion model given by Equation 2.90 using the mass model described by Equation 2.95. This allows for estimation of the expelled propellant mass, and hence the mass of the deputy spacecraft.

Let us define an augmented state vector:

$$\mathbf{x}_m = \begin{bmatrix} \mathbf{x}_{rm} \\ \\ \mathbf{x}_{ep} \end{bmatrix} \tag{4.1}$$

where $\mathbf{x}_{rm}$ is the state vector in the model given by Equation 2.90, and $\mathbf{x}_{ep}$ is the state vector in the mass model expressed by Equation 2.95. Further, the subscript rm will refer to the matrices of the relative motion model described by Equation 2.90, and subscript ep denotes that matrix is taken from the mass model given by Equation 2.95.

It is assumed that the internal model of the controller does not consider the uncontrolled disturbance vector $\mathbf{u}_{ud}$. This assumption, together with the established nomenclature allows us to write an augmented, continuous, nonlinear state-space

model of relative motion:

$$\dot{\mathbf{x}}_m(t) = \overbrace{\begin{bmatrix} \mathbf{A}_{rm} & \mathbf{0}_{6,1} \\ \mathbf{0}_{1,6} & \mathbf{A}_{ep} \end{bmatrix}}^{\mathbf{A}_{cm}} \mathbf{x}_m(t) + \overbrace{\begin{bmatrix} \mathbf{B}_{rm} \\ \mathbf{B}_{ep} \end{bmatrix}}^{\mathbf{B}_{cm}} \mathbf{u}(t) + \overbrace{\begin{bmatrix} \mathbf{V}_{rm} \\ \mathbf{V}_{ep} \end{bmatrix}}^{\mathbf{V}_{cm}} \tag{4.2}$$

$$\mathbf{y}_m(t) = \overbrace{\mathbf{I}_7}^{\mathbf{C}_{cm}} \mathbf{x}_m(t) + \overbrace{\mathbf{0}_{7,3}}^{\mathbf{D}_{cm}} \mathbf{u}(t) \tag{4.3}$$

where $\mathbf{V}_{ep} = \mathbf{0}_{1,1}$ and $\mathbf{y}_m(t)$ denotes output variables of the augmented model.

Design of digital controller requires conversion of continuous state-space model into discrete equivalent. Derivation of this transformation was performed with temporary assumption that matrices $\mathbf{A}_{cm}$, $\mathbf{B}_{cm}$ and $\mathbf{V}_{cm}$ from Equation 4.2 are invariant within time range $[t_0, t]$.

In the case of Equation 4.2 the overall solution can be written as:

$$\mathbf{x}_m(t) = e^{\mathbf{A}_{cm} \cdot [t-t_0]} \mathbf{x}_m(t_0) + \int_{t_0}^{t} e^{\mathbf{A}_{cm} \cdot [t-\tau]} \mathbf{B}_{cm} \mathbf{u}(\tau)\, d\tau + \mathbf{V}_{cm} \cdot [t - t_0] \tag{4.4}$$

Note that the first term in the above equation is the homogenous solution and the second term is the particular solution (convolution of the input with the system's impulse response).

Solution for the system output given by Equation 4.3 can be written as:

$$\mathbf{y}_m(t) = \mathbf{C}_{cm} e^{\mathbf{A}_{cm} \cdot [t-t_0]} \mathbf{x}_m(t_0) + \mathbf{C}_{cm} \int_{t_0}^{t} e^{\mathbf{A}_{cm} \cdot [t-\tau]} \mathbf{B}_{cm} \mathbf{u}(\tau)\, d\tau + \mathbf{D}_{cm} \mathbf{u}(t) \tag{4.5}$$

Equation 4.4 allows us to calculate the state vector at time t given the state vector at the starting time t_0 and the control input signal between t_0 and t. Similarly, the output of the system can be calculated using Equation 4.5. Let us assume that $t_0 = kT$ where k denotes the current sampling instant and T is the sampling period. Furthermore, assume that the next sampling instance $t = kT + T = (k+1)T$. Now we can write:

$$\mathbf{x}_m((k+1)T) = e^{\mathbf{A}_{cm} T} \mathbf{x}_m(kT) + \int_{kT}^{kT+T} e^{\mathbf{A}_{cm} \cdot [(k+1)T - \tau]} \mathbf{B}_{cm} \mathbf{u}(\tau)\, d\tau + \mathbf{V}_{cm} T \tag{4.6}$$

Since a ZOH circuit holds the control constant over the entire sample period, we can

move the control input out of the integration (integration is only over one sample period) and assume $\mathbf{u}(\tau) = \mathbf{u}(kT)$. Then, after changing integration variable $\eta = (k+1)T - \tau$ and simplifying we can write:

$$\mathbf{x}_m(k+1) = e^{\mathbf{A}_{cm}T}\mathbf{x}_m(k) + \int_0^T e^{\mathbf{A}_{cm}\eta}\mathbf{B}_{cm}d\eta\mathbf{u}(k) + \mathbf{V}_{cm}T \tag{4.7}$$

Defining discrete state matrix:

$$\mathbf{A}_m = e^{\mathbf{A}_{cm}T} \tag{4.8}$$

discrete input matrix:

$$\mathbf{B}_m = \int_0^T e^{\mathbf{A}_{cm}\eta}\mathbf{B}_{cm}d\eta \tag{4.9}$$

and discrete nonlinear term matrix:

$$\mathbf{V}_m = \mathbf{V}_{cm}T \tag{4.10}$$

we obtain discrete state-space representation:

$$\mathbf{x}_m(k+1) = \mathbf{A}_m\mathbf{x}_m(k) + \mathbf{B}_m\mathbf{u}(k) + \mathbf{V}_m \tag{4.11}$$

$$\mathbf{y}_m(k) = \mathbf{C}_m\mathbf{x}_m(k) + \mathbf{D}_m\mathbf{u}(k) \tag{4.12}$$

where $\mathbf{C}_m = \mathbf{C}_{cm}$ and $\mathbf{D}_m = \mathbf{D}_{cm}$. Note that we can write:

$$\mathbf{A}_m = \mathbf{I} + \mathbf{A}_{cm}T\mathbf{\Psi} \tag{4.13}$$

and:

$$\mathbf{B}_m = \sum_{i=0}^{\infty}\frac{\mathbf{A}_{cm}^i T^i}{(i+1)!}T\mathbf{B}_{cm} = \mathbf{\Psi}T\mathbf{B}_{cm} \tag{4.14}$$

wherein:

$$\mathbf{\Psi} = \mathbf{I} + \frac{\mathbf{A}_{cm}T}{2!} + \frac{\mathbf{A}_{cm}^2T^2}{3!} + \dots \tag{4.15}$$

Due to the principle of model predictive control, where a current state of the process is required for prediction and control, and consequently the control input $\mathbf{u}(k)$ cannot affect the output $\mathbf{y}_m(k)$ at the same time, we give up writing the discrete feedthrough matrix $\mathbf{D}_m = \mathbf{0}_{7,3}$ from Equation 4.12:

$$\mathbf{y}_m(k) = \mathbf{C}_m\mathbf{x}_m(k) \tag{4.16}$$

4.2.2 Linear Model

In this dissertation the predictive controller uses a quadratic optimization algorithm. In order to ensure that the optimization problem will be quadratic and convex, the cost function is formulated based on local linear models. The linear model is obtained by linearization of the model given by Equations 4.11 and 4.16. More precisely, the nonlinear term matrix $\mathbf{V}_m$ from Equation 4.11 is omitted and further treated as disturbance for the process dynamics. Model parameters (elements of matrices $\mathbf{A}_m$ and $\mathbf{B}_m$) are calculated for the current or predicted operation points, depending on the need, forming local linear models. The linear model can be written using the following discrete state-space representation:

$$\mathbf{x}_m(k+1) = \mathbf{A}_m\mathbf{x}_m(k) + \mathbf{B}_m\mathbf{u}(k) \tag{4.17}$$

$$\mathbf{y}_m(k) = \mathbf{C}_m\mathbf{x}_m(k) \tag{4.18}$$

4.2.3 Linear Model with Embedded Integrator

Here we will discuss the linear model augmented using an embedded integrator. The use of such a model means that the optimized sequence will have the form $\Delta\mathbf{u}(k)$, $\Delta\mathbf{u}(k+1), \cdots, \Delta\mathbf{u}(k+N_c-1)$ instead of $\mathbf{u}(k)$, $\mathbf{u}(k+1), \cdots, \mathbf{u}(k+N_c-1)$. This kind of model is sometimes referred as Increment-Input-Output (IIO) model. The main reason for this approach is rejection of the steady-state error in presence of constant disturbances affecting the control loop.

Let us take a difference on both sides of the Equation 4.17:

$$\mathbf{x}_m(k+1) - \mathbf{x}_m(k) = \mathbf{A}_m(\mathbf{x}_m(k) - \mathbf{x}_m(k-1)) + \mathbf{B}_m(\mathbf{u}(k) - \mathbf{u}(k-1)) \tag{4.19}$$

The differences of the state variable can be denoted as:

$$\Delta\mathbf{x}_m(k+1) = \mathbf{x}_m(k+1) - \mathbf{x}_m(k) \tag{4.20}$$

and:

$$\Delta\mathbf{x}_m(k) = \mathbf{x}_m(k) - \mathbf{x}_m(k-1) \tag{4.21}$$

while the difference of the control variable can be expressed as:

$$\Delta \mathbf{u}(k) = \mathbf{u}(k) - \mathbf{u}(k-1) \tag{4.22}$$

Using the variable increments defined by the Equations 4.20, 4.21 and 4.22, we can write the difference of the state-space equation as:

$$\Delta \mathbf{x}_m(k+1) = \mathbf{A}_m \Delta \mathbf{x}_m(k) + \mathbf{B}_m \Delta \mathbf{u}(k) \tag{4.23}$$

The difference of the output equation can be written as:

$$\begin{aligned} \mathbf{y}_m(k+1) - \mathbf{y}_m(k) &= \mathbf{C}_m\left(\mathbf{x}_m(k+1) - \mathbf{x}_m(k)\right) \\ = \mathbf{C}_m \Delta \mathbf{x}_m(k+1) &= \mathbf{C}_m \mathbf{A}_m \Delta \mathbf{x}_m(k) + \mathbf{C}_m \mathbf{B}_m \Delta \mathbf{u}(k) \end{aligned} \tag{4.24}$$

Here, let us define the new state vector:

$$\mathbf{x}(k) = \begin{bmatrix} \Delta \mathbf{x}_m(k) \\ \mathbf{y}_m(k) \end{bmatrix} \tag{4.25}$$

Given Equations 4.23 and 4.24, we obtain the following state-space model with embedded integrator:

$$\overbrace{\begin{bmatrix} \Delta \mathbf{x}_m(k+1) \\ \mathbf{y}_m(k+1) \end{bmatrix}}^{\mathbf{x}(k+1)} = \overbrace{\begin{bmatrix} \mathbf{A}_m & \mathbf{0}_{7,7} \\ \mathbf{C}_m \mathbf{A}_m & \mathbf{I}_7 \end{bmatrix}}^{\mathbf{A}} \overbrace{\begin{bmatrix} \Delta \mathbf{x}_m(k) \\ \mathbf{y}_m(k) \end{bmatrix}}^{\mathbf{x}(k)} + \overbrace{\begin{bmatrix} \mathbf{B}_m \\ \mathbf{C}_m \mathbf{B}_m \end{bmatrix}}^{\mathbf{B}} \Delta \mathbf{u}(k) \tag{4.26}$$

$$\mathbf{y}(k) = \overbrace{\begin{bmatrix} \mathbf{0}_{7,7} & \mathbf{I}_7 \end{bmatrix}}^{\mathbf{C}} \overbrace{\begin{bmatrix} \Delta \mathbf{x}_m(k) \\ \mathbf{y}_m(k) \end{bmatrix}}^{\mathbf{x}(k)} \tag{4.27}$$

4.3 Model Parameters Estimation

The MPC-EMP algorithm requires the current and future model parameters, which need to be estimated. The parameters estimation is performed based on the procedures presented in Chapter 2. However, except the output matrix $\mathbf{C}_m$, the rest

of matrices in the state-space models described in Section 4.2 is dependent on time, state and control.

The current model parameters are calculated based on the current state estimate $\hat{\mathbf{x}}(k)$, provided by the state observer. Nevertheless, the current control input $\mathbf{u}(k)$ is still unavailable, since the model parameters estimation happens before the calculation of the $\mathbf{u}(k)$. Similarly, the future control inputs over the prediction horizon $\mathbf{u}(k+1)$, $\mathbf{u}(k+2)$, ..., $\mathbf{u}(k+N_p)$ are also unknown. This fact entails the need of preliminary forecast of the control estimates $\hat{\mathbf{u}}(k)$, $\hat{\mathbf{u}}(k+1)$, ..., $\hat{\mathbf{u}}(k+N_p)$. In this investigation, in order to find these estimates a simple heuristic method is used.

The control input is estimated using a variant of finite impulse response (FIR) filter, according to the below equation:

$$\forall i = 0, 1, \ldots, N_p \left\{ \hat{\mathbf{u}}(k+i) = \lambda_1 \mathbf{u}(k-1) + \lambda_2 \mathbf{u}(k-2) + \ldots + \lambda_{N_f} \mathbf{u}(k-N_f) \right\} \tag{4.28}$$

wherein $\lambda_1, \lambda_2, \ldots, \lambda_{N_f}$ are filter coefficients. Note that the zeroth coefficient λ_0 was chosen to be equal to 0, since the control value $\mathbf{u}(k)$ is unknown at this stage. For simplicity reasons, further we will assume that:

$$\forall j = 1, 2, \ldots, N_f \left\{ \lambda_j = \frac{1}{N_f} \right\} \tag{4.29}$$

where N_f is the filter order. This assumption makes the filter to be equivalent of a moving average filter. Note that the above formulation assumes the control estimate $\hat{\mathbf{u}}$ to be constant within the whole prediction horizon. The described method will be further referred as **H**euristic **C**ontrol trajectory **E**stimation (HCE).

Generally, the current control input estimate $\hat{\mathbf{u}}(k)$ enables for estimation of the current model parameters, while future control estimates $\hat{\mathbf{u}}(k+1)$, $\hat{\mathbf{u}}(k+2)$, ..., $\hat{\mathbf{u}}(k+N_p)$ enables to estimate sequentially the future states $\hat{\mathbf{x}}(k+1)$, $\hat{\mathbf{x}}(k+2)$, ..., $\hat{\mathbf{x}}(k+N_p)$ using nonlinear Equation 4.11. This allows to estimate the future model parameters.

4.4 Output Prediction System

This section describes the output prediction mechanism, whose task is to calculate the predicted process output trajectory over the prediction horizon with the future

control increments as the adjustable variables.

Let us organize the future control increments into the following block vector:

$$\Delta\mathbf{U} = \begin{bmatrix} \Delta\mathbf{u}(k) & \Delta\mathbf{u}(k+1) & \Delta\mathbf{u}(k+2) & \dots & \Delta\mathbf{u}(k+N_c-1) \end{bmatrix}^T \tag{4.30}$$

and define block vector of the predicted outputs:

$$\hat{\mathbf{Y}} = \begin{bmatrix} \hat{\mathbf{y}}(k+1 \mid k) & \hat{\mathbf{y}}(k+2 \mid k) & \hat{\mathbf{y}}(k+3 \mid k) & \dots & \hat{\mathbf{y}}(k+N_p \mid k) \end{bmatrix}^T \tag{4.31}$$

Then, the output prediction system can be expressed as:

$$\hat{\mathbf{Y}} = \mathbf{F}\hat{\mathbf{x}}(k) + \mathbf{\Phi}\Delta\mathbf{U} \tag{4.32}$$

Note that the predictions are based on the current state estimate $\hat{\mathbf{x}}(k)$.

The following Sections 4.4.1 and 4.4.2 will describe two approaches to formulate the matrices $\mathbf{F}$ and $\mathbf{\Phi}$.

4.4.1 Prediction without Consideration of Model Variability within Prediction Horizon

This section presents formulation of the output prediction system, with the assumption that the model given by Equations 4.26 and 4.27 is invariant within the prediction horizon. It means that only one local model is obtained (only for the current operation point $\hat{\mathbf{x}}(k)$) and is assumed to have constant parameters over the whole prediction horizon.

Based on this model, the future state estimates can be calculated sequentially using the set of the current and future control increments:

$$\hat{\mathbf{x}}(k+1 \mid k) = \mathbf{A}\hat{\mathbf{x}}(k) + \mathbf{B}\Delta\mathbf{u}(k) \tag{4.33}$$

$$\begin{aligned} \hat{\mathbf{x}}(k+2 \mid k) &= \mathbf{A}\hat{\mathbf{x}}(k+1 \mid k) + \mathbf{B}\Delta\mathbf{u}(k+1) \\ &= \mathbf{A}^2\hat{\mathbf{x}}(k) + \mathbf{AB}\Delta\mathbf{u}(k) + \mathbf{B}\Delta\mathbf{u}(k+1) \end{aligned} \tag{4.34}$$

$$\begin{aligned} \hat{\mathbf{x}}(k+3 \mid k) &= \mathbf{A}\hat{\mathbf{x}}(k+2 \mid k) + \mathbf{B}\Delta\mathbf{u}(k+2) \\ = \mathbf{A}^3\hat{\mathbf{x}}(k) &+ \mathbf{A}^2\mathbf{B}\Delta\mathbf{u}(k) + \mathbf{AB}\Delta\mathbf{u}(k+1) + \mathbf{B}\Delta\mathbf{u}(k+2) \end{aligned} \tag{4.35}$$

$$\vdots$$

$$\begin{aligned}\hat{\mathbf{x}}\left(k+N_p \mid k\right) = \mathbf{A}^{N_p}\hat{\mathbf{x}}\left(k\right) + \mathbf{A}^{N_p-1}\mathbf{B}\Delta\mathbf{u}\left(k\right) + \mathbf{A}^{N_p-2}\mathbf{B}\Delta\mathbf{u}\left(k+1\right) \\ + \ldots + \mathbf{A}^{N_p-N_c}\mathbf{B}\Delta\mathbf{u}\left(k+N_c-1\right)\end{aligned} \tag{4.36}$$

The expression $\hat{\mathbf{x}}\left(k+i \mid k\right)$ denotes predicted state value at i-th prediction horizon step, wherein the prediction is obtained using informations available at time k. Note that over the whole prediction horizon the same model $\mathbf{A}\left(k\right)$, $\mathbf{B}\left(k\right)$, $\mathbf{C}\left(k\right)$ is used. According to Equations 4.33 ... 4.36, the predicted outputs can be estimated using:

$$\hat{\mathbf{y}}\left(k+1 \mid k\right) = \mathbf{CA}\hat{\mathbf{x}}\left(k\right) + \mathbf{CB}\Delta\mathbf{u}\left(k\right) \tag{4.37}$$

$$\hat{\mathbf{y}}\left(k+2 \mid k\right) = \mathbf{CA}^2\hat{\mathbf{x}}\left(k\right) + \mathbf{CAB}\Delta\mathbf{u}\left(k\right) + \mathbf{CB}\Delta\mathbf{u}\left(k+1\right) \tag{4.38}$$

$$\begin{aligned}\hat{\mathbf{y}}\left(k+3 \mid k\right) = \mathbf{CA}^3\hat{\mathbf{x}}\left(k\right) + \mathbf{CA}^2\mathbf{B}\Delta\mathbf{u}\left(k\right) + \mathbf{CAB}\Delta\mathbf{u}\left(k+1\right) \\ + \mathbf{CB}\Delta\mathbf{u}\left(k+2\right)\end{aligned} \tag{4.39}$$

$$\vdots$$

$$\begin{aligned}\hat{\mathbf{y}}\left(k+N_p \mid k\right) = \mathbf{CA}^{N_p}\hat{\mathbf{x}}\left(k\right) + \mathbf{CA}^{N_p-1}\mathbf{B}\Delta\mathbf{u}\left(k\right) + \mathbf{CA}^{N_p-2}\mathbf{B}\Delta\mathbf{u}\left(k+1\right) \\ + \ldots + \mathbf{CA}^{N_p-N_c}\mathbf{B}\Delta\mathbf{u}\left(k+N_c-1\right)\end{aligned} \tag{4.40}$$

The above equations can be used to formulate the matrices $\mathbf{F}$ and $\mathbf{\Phi}$ according to Equation 4.32:

$$\mathbf{F} = \begin{bmatrix} \mathbf{CA} \\ \mathbf{CA}^2 \\ \mathbf{CA}^3 \\ \vdots \\ \mathbf{CA}^{N_p} \end{bmatrix} \tag{4.41}$$

$$\mathbf{\Phi} = \begin{bmatrix} \mathbf{CB} & 0 & 0 & \dots & 0 \\ \mathbf{CAB} & \mathbf{CB} & 0 & \dots & 0 \\ \mathbf{CA}^2\mathbf{B} & \mathbf{CAB} & \mathbf{CB} & \dots & 0 \\ \vdots & \vdots & \vdots & \ddots & \vdots \\ \mathbf{CA}^{N_p-1}\mathbf{B} & \mathbf{CA}^{N_p-2}\mathbf{B} & \mathbf{CA}^{N_p-3}\mathbf{B} & \dots & \mathbf{CA}^{N_p-N_c}\mathbf{B} \end{bmatrix} \tag{4.42}$$

4.4.2 Prediction with Consideration of Model Variability within Prediction Horizon

This section presents the prediction method proposed by author. In contrast to the method described in Section 4.4.1, the method described here takes into account the model time, state and control dependency over the prediction horizon. For every i-th prediction horizon step, $i = 1, 2, \dots, N_p$, the new future model parameters are calculated forming $\mathbf{A}(k+i)$, $\mathbf{B}(k+i)$ and $\mathbf{C}(k+i)$. However, in case of our relative motion model, the output matrix $\mathbf{C}$ is independent in the context of time, state and control. Although the matrices $\mathbf{A}$ and $\mathbf{B}$ are dependent on state and control, the arguments $\hat{\mathbf{x}}$ and $\Delta\mathbf{u}$ are omitted here for the reason of text clarity.

The future state estimates can be calculated sequentially:

$$\hat{\mathbf{x}}(k+1 \mid k) = \mathbf{A}(k)\,\hat{\mathbf{x}}(k) + \mathbf{B}(k)\,\Delta\mathbf{u}(k) \tag{4.43}$$

$$\begin{aligned} \hat{\mathbf{x}}(k+2 \mid k) &= \mathbf{A}(k+1)\,\hat{\mathbf{x}}(k+1 \mid k) + \mathbf{B}(k+1)\,\Delta\mathbf{u}(k+1) \\ &= \mathbf{A}(k+1)\,\mathbf{A}(k)\,\hat{\mathbf{x}}(k) + \mathbf{A}(k+1)\,\mathbf{B}(k)\,\Delta\mathbf{u}(k) + \mathbf{B}(k+1)\,\Delta\mathbf{u}(k+1) \end{aligned} \tag{4.44}$$

$$\begin{aligned} \hat{\mathbf{x}}(k+3 \mid k) &= \mathbf{A}(k+2)\,\hat{\mathbf{x}}(k+2 \mid k) + \mathbf{B}(k+2)\,\Delta\mathbf{u}(k+2) \\ &= \mathbf{A}(k+2)\,\mathbf{A}(k+1)\,\mathbf{A}(k)\,\hat{\mathbf{x}}(k) + \mathbf{A}(k+2)\,\mathbf{A}(k+1)\,\mathbf{B}(k)\,\Delta\mathbf{u}(k) \\ &\quad + \mathbf{A}(k+2)\,\mathbf{B}(k+1)\,\Delta\mathbf{u}(k+1) + \mathbf{B}(k+2)\,\Delta\mathbf{u}(k+2) \end{aligned} \tag{4.45}$$

$$\vdots$$

$$\begin{aligned}\hat{\mathbf{x}}\left(k+N_p \mid k\right) &= \mathbf{A}\left(k+Np-1\right)\mathbf{A}\left(k+Np-2\right)\ldots\mathbf{A}\left(k\right)\hat{\mathbf{x}}\left(k\right)\\ &+\mathbf{A}\left(k+Np-1\right)\mathbf{A}\left(k+Np-2\right)\ldots\mathbf{A}\left(k+1\right)\mathbf{B}\left(k\right)\Delta\mathbf{u}\left(k\right)\\ &+\mathbf{A}\left(k+Np-1\right)\mathbf{A}\left(k+Np-2\right)\ldots\mathbf{A}\left(k+2\right)\mathbf{B}\left(k+1\right)\Delta\mathbf{u}\left(k+1\right)\\ &+\ldots+\mathbf{A}\left(k+Np-1\right)\mathbf{A}\left(k+Np-2\right)\ldots\mathbf{A}\left(k+N_c\right)\\ &\cdot\mathbf{B}\left(k+Nc-1\right)\Delta\mathbf{u}\left(k+N_c-1\right)\end{aligned} \tag{4.46}$$

Consequently, the predicted output vectors can be calculated using:

$$\hat{\mathbf{y}}\left(k+1 \mid k\right) = \mathbf{C}\left(k\right)\mathbf{A}\left(k\right)\hat{\mathbf{x}}\left(k\right)+\mathbf{C}\left(k\right)\mathbf{B}\left(k\right)\Delta\mathbf{u}\left(k\right) \tag{4.47}$$

$$\begin{aligned}\hat{\mathbf{y}}\left(k+2 \mid k\right) &= \mathbf{C}\left(k+1\right)\mathbf{A}\left(k+1\right)\mathbf{A}\left(k\right)\hat{\mathbf{x}}\left(k\right)\\ &+\mathbf{C}\left(k+1\right)\mathbf{A}\left(k+1\right)\mathbf{B}\left(k\right)\Delta\mathbf{u}\left(k\right)+\mathbf{C}\left(k+1\right)\mathbf{B}\left(k+1\right)\Delta\mathbf{u}\left(k+1\right)\end{aligned} \tag{4.48}$$

$$\begin{aligned}\hat{\mathbf{y}}\left(k+3 \mid k\right) &= \mathbf{C}\left(k+2\right)\mathbf{A}\left(k+2\right)\mathbf{A}\left(k+1\right)\mathbf{A}\left(k\right)\hat{\mathbf{x}}\left(k\right)\\ &+\mathbf{C}\left(k+2\right)\mathbf{A}\left(k+2\right)\mathbf{A}\left(k+1\right)\mathbf{B}\left(k\right)\Delta\mathbf{u}\left(k\right)\\ &+\mathbf{C}\left(k+2\right)\mathbf{A}\left(k+2\right)\mathbf{B}\left(k+1\right)\Delta\mathbf{u}\left(k+1\right)+\mathbf{C}\left(k+2\right)\mathbf{B}\left(k+2\right)\Delta\mathbf{u}\left(k+2\right)\end{aligned} \tag{4.49}$$

$$\vdots$$

$$\begin{aligned}&\hat{\mathbf{y}}\left(k+N_p \mid k\right) =\\ &\mathbf{C}\left(k+Np-1\right)\mathbf{A}\left(k+Np-1\right)\mathbf{A}\left(k+Np-2\right)\ldots\mathbf{A}\left(k\right)\hat{\mathbf{x}}\left(k\right)\\ &+\mathbf{C}\left(k+Np-1\right)\mathbf{A}\left(k+Np-1\right)\mathbf{A}\left(k+Np-2\right)\ldots\mathbf{A}\left(k+1\right)\\ &\cdot\mathbf{B}\left(k\right)\Delta\mathbf{u}\left(k\right)\\ &+\mathbf{C}\left(k+Np-1\right)\mathbf{A}\left(k+Np-1\right)\mathbf{A}\left(k+Np-2\right)\ldots\mathbf{A}\left(k+2\right)\\ &\cdot\mathbf{B}\left(k+1\right)\Delta\mathbf{u}\left(k+1\right)\\ &+\ldots+\mathbf{C}\left(k+Np-1\right)\mathbf{A}\left(k+Np-1\right)\mathbf{A}\left(k+Np-2\right)\ldots\mathbf{A}\left(k+N_c\right)\\ &\cdot\mathbf{B}\left(k+Nc-1\right)\Delta\mathbf{u}\left(k+N_c-1\right)\end{aligned} \tag{4.50}$$

Then, Equations 4.47 ... 4.50 can serve to form the matrices $\mathbf{F}$ and $\mathbf{\Phi}$. Matrix $\mathbf{F}$ can

be written as:

$$\mathbf{F} = \begin{bmatrix} \mathbf{C}(k)\,\mathbf{A}(k) \\ \mathbf{C}(k+1)\,\mathbf{A}(k+1)\,\mathbf{A}(k) \\ \mathbf{C}(k+2)\,\mathbf{A}(k+2)\,\mathbf{A}(k+1)\,\mathbf{A}(k) \\ \vdots \\ \mathbf{C}(k+N_p-1)\,\mathbf{A}(k+N_p-1)\,\mathbf{A}(k+N_p-2)\ldots\mathbf{A}(k) \end{bmatrix} \tag{4.51}$$

Whilst the first column of the block matrix $\mathbf{\Phi}$ has the form:

$$\mathbf{\Phi}_{*,1} = \begin{bmatrix} \mathbf{C}(k)\,\mathbf{B}(k) \\ \mathbf{C}(k+1)\,\mathbf{A}(k+1)\,\mathbf{B}(k) \\ \mathbf{C}(k+2)\,\mathbf{A}(k+2)\,\mathbf{A}(k+1)\,\mathbf{B}(k) \\ \vdots \\ \mathbf{C}(k+N_p-1)\,\mathbf{A}(k+N_p-1)\,\mathbf{A}(k+N_p-2)\ldots\mathbf{A}(k+1)\,\mathbf{B}(k) \end{bmatrix} \tag{4.52}$$

The second column:

$$\mathbf{\Phi}_{*,2} = \begin{bmatrix} 0 \\ \mathbf{C}(k+1)\,\mathbf{B}(k+1) \\ \mathbf{C}(k+2)\,\mathbf{A}(k+2)\,\mathbf{B}(k+1) \\ \vdots \\ \mathbf{C}(k+N_p-1)\,\mathbf{A}(k+N_p-1)\ldots\mathbf{A}(k+2)\,\mathbf{B}(k+1) \end{bmatrix} \tag{4.53}$$

The third column:

$$\boldsymbol{\Phi}_{*,3} = \begin{bmatrix} 0 \\ 0 \\ \mathbf{C}\left(k+2\right)\mathbf{B}\left(k+2\right) \\ \vdots \\ \mathbf{C}\left(k+N_p-1\right)\mathbf{A}\left(k+N_p-1\right)\ldots\mathbf{A}\left(k+3\right)\mathbf{B}\left(k+2\right) \end{bmatrix} \tag{4.54}$$

$$\vdots$$

Finally, the N_c-th column of the $\boldsymbol{\Phi}$ matrix:

$$\boldsymbol{\Phi}_{*,N_c} = \begin{bmatrix} 0 \\ 0 \\ 0 \\ \vdots \\ \mathbf{C}\left(k+N_p-1\right)\mathbf{A}\left(k+N_p-1\right)\ldots\mathbf{A}\left(k+N_c\right)\mathbf{B}\left(k+N_c-1\right) \end{bmatrix} \tag{4.55}$$

4.5 Optimization

This section formulates the optimization problem being solved at each sampling instant of the controller. The class of optimization problem is associated with the model used for prediction of the output trajectory $\hat{\mathbf{y}}\left(k+1 \mid k\right)$, $\hat{\mathbf{y}}\left(k+2 \mid k\right)$, ..., $\hat{\mathbf{y}}\left(k+N_p \mid k\right)$. The process discussed in this dissertation is described by nonlinear and time-variant model given by Equations 4.11 and 4.16. MPC algorithms with nonlinear model used in optimization procedures, where the solution is found by nonlinear programming algorithms, are of limited use. However, they are objects of many theoretical investigations.

In the industry, the most widely used approach to predictive control of nonlinear objects is based on the linear models - the time-invariant linear approximation of the nonlinear model, or the models obtained by successive linearization of the nonlinear model, performed at some time intervals or operating points. The reason of such state

lies in the consequences of output trajectory prediction using nonlinear model. The nonlinear dependency between the predicted output $\hat{\mathbf{y}}(k+i \mid k)$ and the decision variables $\Delta\mathbf{u}$ causes that the optimization problem becomes non-quadratic and in general, non-convex.

There is lack of universal procedures being able to solve such control problem fast and reliable. What is more important from the practical point of view, the procedures with nonlinear optimization cannot guarantee required accuracy or predictable time for finding the solution. Moreover, part of the optimization techniques are able to find a local minimum only.

Above facts has formed the approach to the optimization problem considered in this dissertation. Since the model is nonlinear and strongly time-variant in the context of prediction horizon, author proposed generation of local time-invariant linear models for the current and predicted operation points within the prediction horizon, one model for each sampling instant within the horizon, obtained by linearization of Equations 4.11 and 4.16.

Agreeing to a certain inaccuracy, it is assumed that decision variables $\Delta\mathbf{u}(k)$, $\Delta\mathbf{u}(k+1)$, $\Delta\mathbf{u}(k+2)$, ..., $\Delta\mathbf{u}(k+N_c-1)$ do not affect the model parameters directly in the procedure of finding the optimal control increments sequence. The model parameters are calculated a priori, using estimate of the control increments trajectory $\Delta\hat{\mathbf{u}}(k)$, $\Delta\hat{\mathbf{u}}(k+1)$, $\Delta\hat{\mathbf{u}}(k+2)$, ..., $\Delta\hat{\mathbf{u}}(k+N_p)$ found in a heuristic manner.

This approach allows to attempting to use of quadratic programming solver. The detailed formulation of the optimization problem is described below.

4.5.1 Cost Function Formulation

The basic objective of the MPC algorithm is to bring the predicted output as close as possible to the set-point signal. Additionally, it is desired to tune the amplitude of the decision variable value within the control increment trajectory $\Delta\mathbf{U}$. This aims are reflected in the cost function, which is minimized in order to find control increments vector $\Delta\mathbf{U}$ at a given sample time k.

Let us assume that the set-point information is stored in the following vector:

$$\mathbf{R}_s = \begin{bmatrix} \mathbf{I}_7 & \mathbf{I}_7 & \cdots & \mathbf{I}_7 \end{bmatrix}^T \boldsymbol{\Xi}(k) = \bar{\mathbf{R}}_s \boldsymbol{\Xi}(k) \tag{4.56}$$

The cost function uses the augmented model described by Equations 4.26 and 4.27.

This model has 7 outputs, so the dimension of the $\bar{\mathbf{R}}_s$ matrix is $\dim\left[\bar{\mathbf{R}}_s\right] = 7 \cdot N_p \times 7$, while the set-point vector $\boldsymbol{\Xi}(k)$ has dimensions $\dim\left[\boldsymbol{\Xi}(k)\right] = 7 \times 1$.
Considering the requirements, let us formulate the cost function in the following form:

$$J = \left(\mathbf{R}_s - \hat{\mathbf{Y}}\right)^T \left(\mathbf{R}_s - \hat{\mathbf{Y}}\right) + \Delta\mathbf{U}^T \bar{\mathbf{R}} \Delta\mathbf{U} \tag{4.57}$$

wherein J is a scalar value of the cost function and $\hat{\mathbf{Y}}$ is the predicted output trajectory given by Equation 4.31. The first term is linked to the objective of minimizing the errors between the predicted output and the set-point signal while the second term reflects the consideration given to the amplitude of $\Delta\mathbf{U}$ when the objective function J is made to be as small as possible.

The positive-semidefinite matrix $\bar{\mathbf{R}}$ enables to tune the desired closed-loop performance (control increment amplitude within the control increment trajectory). If we assume that $\boldsymbol{\Theta}$ with dimensions $\dim\left[\boldsymbol{\Theta}\right] = 3 \times 1$ is the vector of tuning parameters, called control increment weights, the matrix $\bar{\mathbf{R}}$ has the following form:

$$\bar{\mathbf{R}} = \begin{bmatrix} \begin{bmatrix} \Theta_1 & 0 & 0 \\ 0 & \Theta_2 & 0 \\ 0 & 0 & \Theta_3 \end{bmatrix} & \mathbf{0}_{3,3} & \cdots & \mathbf{0}_{3,3} \\ \mathbf{0}_{3,3} & \begin{bmatrix} \Theta_1 & 0 & 0 \\ 0 & \Theta_2 & 0 \\ 0 & 0 & \Theta_3 \end{bmatrix} & \cdots & \mathbf{0}_{3,3} \\ \vdots & \vdots & \ddots & \vdots \\ \mathbf{0}_{3,3} & \mathbf{0}_{3,3} & \cdots & \begin{bmatrix} \Theta_1 & 0 & 0 \\ 0 & \Theta_2 & 0 \\ 0 & 0 & \Theta_3 \end{bmatrix} \end{bmatrix} \tag{4.58}$$

Note that the dimensionality of $\bar{\mathbf{R}}$ is $\dim\left[\bar{\mathbf{R}}\right] = 3 \cdot N_c \times 3 \cdot N_c$. For the case that $\boldsymbol{\Theta} = \mathbf{0}_{3,1}$ the cost function is interpreted as the situation where any attention is paid to how large amplitude of $\Delta\mathbf{U}$ might be and the only goal is to make the quadratic error $\left(\mathbf{R}_s - \hat{\mathbf{Y}}\right)^T \left(\mathbf{R}_s - \hat{\mathbf{Y}}\right)$ as small as possible. Large $\boldsymbol{\Theta}$ enforces careful

consideration how large the amplitude of $\Delta\mathbf{U}$ might be and attentive reduction of the error $\left(\mathbf{R}_s - \hat{\mathbf{Y}}\right)^T \left(\mathbf{R}_s - \hat{\mathbf{Y}}\right)$.

The cost function can be expressed in terms of the output prediction system given by Equation 4.32:

$$\begin{aligned} J = \left(\mathbf{R}_s - \mathbf{F}\hat{\mathbf{x}}\left(k\right)\right)^T \left(\mathbf{R}_s - \mathbf{F}\hat{\mathbf{x}}\left(k\right)\right) - 2\Delta\mathbf{U}^T\boldsymbol{\Phi}^T \left(\mathbf{R}_s - \mathbf{F}\hat{\mathbf{x}}\left(k\right)\right) \\ + \Delta\mathbf{U}^T \left(\boldsymbol{\Phi}^T\boldsymbol{\Phi} + \bar{\mathbf{R}}\right)\Delta\mathbf{U} \end{aligned} \tag{4.59}$$

In the optimization literature, the matrix $\left(\boldsymbol{\Phi}^T\boldsymbol{\Phi} + \bar{\mathbf{R}}\right)$ is commonly referred as the Hessian matrix.

4.5.2 Unconstrained Solution

Formulation of the cost function given in Section 4.5.1 enables simple, analytical unconstrained solution. To find the optimal $\Delta\mathbf{U}$, let us take the first derivative of the cost function J given by Equation 4.59:

$$\frac{\partial J}{\partial \Delta\mathbf{U}} = -2\boldsymbol{\Phi}^T \left(\mathbf{R}_s - \mathbf{F}\hat{\mathbf{x}}\left(k\right)\right) + 2\left(\boldsymbol{\Phi}^T\boldsymbol{\Phi} + \bar{\mathbf{R}}\right)\Delta\mathbf{U} \tag{4.60}$$

The necessary condition of the minimum $\frac{\partial J}{\partial \Delta\mathbf{U}} = 0$ enables an elegant, optimal unconstrained solution for the control increment trajectory:

$$\Delta\mathbf{U} = \left(\boldsymbol{\Phi}^T\boldsymbol{\Phi} + \bar{\mathbf{R}}\right)^{-1} \boldsymbol{\Phi}^T \left(\bar{\mathbf{R}}_s\boldsymbol{\Xi}\left(k\right) - \mathbf{F}\hat{\mathbf{x}}\left(k\right)\right) \tag{4.61}$$

Because of the receding horizon control principle, only the first subvector of $\Delta\mathbf{U}$ at time k is used for further application to the process:

$$\Delta\mathbf{u}\left(k\right) = \overbrace{\begin{bmatrix} \mathbf{I}_3 & \mathbf{0}_{3,3} & \dots & \mathbf{0}_{3,3} \end{bmatrix}}^{\iota} \left(\boldsymbol{\Phi}^T\boldsymbol{\Phi} + \bar{\mathbf{R}}\right)^{-1} \boldsymbol{\Phi}^T \left(\bar{\mathbf{R}}_s\boldsymbol{\Xi}\left(k\right) - \mathbf{F}\hat{\mathbf{x}}\left(k\right)\right) \tag{4.62}$$

wherein the dimensionality of the ι matrix is $\dim\left[\iota\right] = 3 \times 3 \cdot N_c$.

4.5.3 Constraints Formulation

Because of the nature of this investigation, only the basic operational constraints are considered. The constraints are applied on amplitude of the control variable, what

can be expressed as:

$$\mathbf{u}^{min} \leqslant \mathbf{u} \leqslant \mathbf{u}^{max} \tag{4.63}$$

The constraints are imposed for all the future sampling instants within the control horizon. Let us express the future control trajectory $\mathbf{U} = \begin{bmatrix} \mathbf{u}(k) & \mathbf{u}(k+1) & \dots & \mathbf{u}(k+N_c-1) \end{bmatrix}^T$ in terms of the control increment vector $\Delta\mathbf{U}$:

$$\begin{bmatrix} \mathbf{u}(k) \\ \mathbf{u}(k+1) \\ \mathbf{u}(k+2) \\ \vdots \\ \mathbf{u}(k+N_c-1) \end{bmatrix} = \overbrace{\begin{bmatrix} \mathbf{I}_3 \\ \mathbf{I}_3 \\ \mathbf{I}_3 \\ \vdots \\ \mathbf{I}_3 \end{bmatrix}}^{\mathbf{Z}_1} \mathbf{u}(k-1) + \overbrace{\begin{bmatrix} \mathbf{I}_3 & \mathbf{0}_{3,3} & \mathbf{0}_{3,3} & \dots & \mathbf{0}_{3,3} \\ \mathbf{I}_3 & \mathbf{I}_3 & \mathbf{0}_{3,3} & \dots & \mathbf{0}_{3,3} \\ \mathbf{I}_3 & \mathbf{I}_3 & \mathbf{I}_3 & \dots & \mathbf{0}_{3,3} \\ \vdots & \vdots & \vdots & \ddots & \vdots \\ \mathbf{I}_3 & \mathbf{I}_3 & \mathbf{I}_3 & \dots & \mathbf{I}_3 \end{bmatrix}}^{\mathbf{Z}_2} \overbrace{\begin{bmatrix} \Delta\mathbf{u}(k) \\ \Delta\mathbf{u}(k+1) \\ \Delta\mathbf{u}(k+2) \\ \vdots \\ \Delta\mathbf{u}(k+N_c-1) \end{bmatrix}}^{\Delta\mathbf{U}} \tag{4.64}$$

Assuming that $\mathbf{U}^{min}$ and $\mathbf{U}^{max}$ are column block vectors consisting of N_c vectors $\mathbf{u}^{min}$ and $\mathbf{u}^{max}$ respectively, Equation 4.64 enables formulation of the following inequality constraints on the control amplitude:

$$-\left(\mathbf{Z}_1\mathbf{u}(k-1) + \mathbf{Z}_2\Delta\mathbf{U}\right) \leqslant -\mathbf{U}^{min} \tag{4.65}$$

$$\left(\mathbf{Z}_1\mathbf{u}(k-1) + \mathbf{Z}_2\Delta\mathbf{U}\right) \leqslant \mathbf{U}^{max} \tag{4.66}$$

The constraints given by Equations 4.65 and 4.66 can be rewritten in compact form:

$$\overbrace{\begin{bmatrix} -\mathbf{Z}_2 \\ \mathbf{Z}_2 \end{bmatrix}}^{\mathbf{M}_{const}} \Delta\mathbf{U} \leqslant \overbrace{\begin{bmatrix} -\mathbf{U}^{min} + \mathbf{Z}_1\mathbf{u}\,(k-1) \\ \mathbf{U}^{max} - \mathbf{Z}_1\mathbf{u}\,(k-1) \end{bmatrix}}^{\mathbf{N}_{const}} \tag{4.67}$$

4.5.4 Constrained Solution

The constrained optimization problem is to find the decision variables vector $\Delta\mathbf{U}$ that minimizes the cost function described by Equation 4.59 subject to the inequality constraints given by Equation 4.67 at a given sample instant k. Because of the inequality constraints, the problem requires numerical solution. One of the objectives of this investigation was the ability to use of standard quadratic programming procedures. Therefore, the formulated problem is solved by simple and reliable Hildreth's quadratic programming procedure presented in Ref [72]. For research purposes, an alternative is a quadratic programming solver `quadprog` provided by MATLAB® software.

In this investigation is assumed that minimization of the cost function given by Equation 4.59 can be performed by solving the following optimal control problem:

$$\min_{\Delta\mathbf{U}} \frac{1}{2}\Delta\mathbf{U}^T\mathbf{H}\Delta\mathbf{U} + \varphi^T\Delta\mathbf{U} \tag{4.68}$$

subject to the inequality constraints formulated by Equation 4.67:

$$\mathbf{M}_{const}\Delta\mathbf{U} \leqslant \mathbf{N}_{const} \tag{4.69}$$

wherein the Hessian matrix $\mathbf{H}$ is represented by:

$$\mathbf{H} = \mathbf{\Phi}^T\mathbf{\Phi} + \bar{\mathbf{R}} \tag{4.70}$$

and the φ matrix takes the form:

$$\varphi = -\mathbf{\Phi}^T\left(\bar{\mathbf{R}}_s\mathbf{\Xi}\,(k) - \mathbf{F}\hat{\mathbf{x}}\,(k)\right) \tag{4.71}$$

In case of the MATLAB® `quadprog` solver, the result can be obtained using the following syntax:

```
DeltaU = quadprog(H, phi, Mconst, Nconst);
```

4.6 State Observer

Even if estimation of the current state is not necessary in research based on simulation, where all the states/outputs are available at each sample time, a state observer is introduced into this investigation in order to test the control loop behavior in presence of measurement noise and for the reason of approach generality. Moreover, the introduction of the state observer allows to reflect the situation where some of the output signals are unmeasured or need to be filtered.

The state observer is constructed using nonlinear model-based estimation and feedback principle where an error signal is deployed to improve the estimation:

$$\hat{\mathbf{x}}_m(k+1) = \overbrace{\mathbf{A}_m\hat{\mathbf{x}}_m(k) + \mathbf{B}_m\mathbf{u}(k) + \mathbf{V}_m}^{model} + \overbrace{\mathbf{K}_{ob}\left(\mathbf{y}_{meas}(k) - \mathbf{C}_m\hat{\mathbf{x}}_m(k)\right)}^{correction\,term} \tag{4.72}$$

wherein $\mathbf{K}_{ob}$ is the observer gain matrix, the model matrices $\mathbf{A}_m$, $\mathbf{B}_m$, $\mathbf{C}_m$ and $\mathbf{V}_m$ belongs to the nonlinear model given by Equations 4.11 and 4.16, and $\mathbf{y}_{meas}(k)$ is the vector of measurements at moment k.

Let us define the error state:

$$\tilde{\mathbf{x}}_m(k) = \mathbf{x}_m(k) - \hat{\mathbf{x}}_m(k) \tag{4.73}$$

The error satisfies the following difference Equation:

$$\tilde{\mathbf{x}}_m(k+1) = \mathbf{A}_m\left(\mathbf{x}_m(k) - \hat{\mathbf{x}}_m(k)\right) = \mathbf{A}_m\tilde{\mathbf{x}}_m(k) \tag{4.74}$$

Then, after substitution of $\mathbf{y}_{meas}(k) = \mathbf{C}_m\mathbf{x}_m(k)$ into the correction term from Equation 4.72 we can write:

$$\tilde{\mathbf{x}}_m(k+1) = \mathbf{A}_m\tilde{\mathbf{x}}_m(k) - \mathbf{K}_{ob}\mathbf{C}_m\tilde{\mathbf{x}}_m(k) = \left(\mathbf{A}_m - \mathbf{K}_{ob}\mathbf{C}_m\right)\tilde{\mathbf{x}}_m(k) \tag{4.75}$$

Now it is apparent that the observer gain matrix $\mathbf{K}_{ob}$ can be used to manipulate the convergence rate of the error. The stability of this closed-loop observer error system is guaranteed if and only if the eigenvalues of $\mathbf{A}_m - \mathbf{K}_{ob}\mathbf{C}_m$ are placed inside the unit circle.

Typically, for a multi-output system such as the considered, a Kalman filter is used in order to design the gain matrix $\mathbf{K}_{ob}$.

The current state estimate $\hat{\mathbf{x}}(k)$ used in the cost function is calculated according to the augmented state definition given by Equation 4.25:

$$\hat{\mathbf{x}}(k) = \begin{bmatrix} \Delta\mathbf{x}_m(k) \\ \mathbf{y}_m(k) \end{bmatrix} = \begin{bmatrix} \hat{\mathbf{x}}_m(k \mid k-1) - \hat{\mathbf{x}}_m(k-1 \mid k-2) \\ \mathbf{C}_m\hat{\mathbf{x}}_m(k \mid k-1) \end{bmatrix} \tag{4.76}$$

4.7 MPC-CMP Algorithm Architecture

For comparative purposes, an another algorithm is proposed. Let us call it as MPC-CMP (**M**odel **P**redictive **C**ontrol with **C**onstant **M**odel **P**arameters within the prediction horizon). The difference between the MPC-CMP and MPC-EMP algorithms is the approach to the model parameters within prediction horizon. The MPC-EMP algorithm considers evolution of the parameters, with utilization of the output prediction system described in Section 4.4.2, while the MPC-CMP algorithm generates only one local linear model of the process and uses it within the whole prediction horizon without any change of the parameters. This method of output prediction is described in Section 4.4.1.

The operation of the MPC-CMP algorithm can be illustrated using Figure 4.2 and is a simplification of activity performed by the MPC-EMP algorithm. The MPC-CMP algorithm can be considered as a classical algorithm with successive linearization.

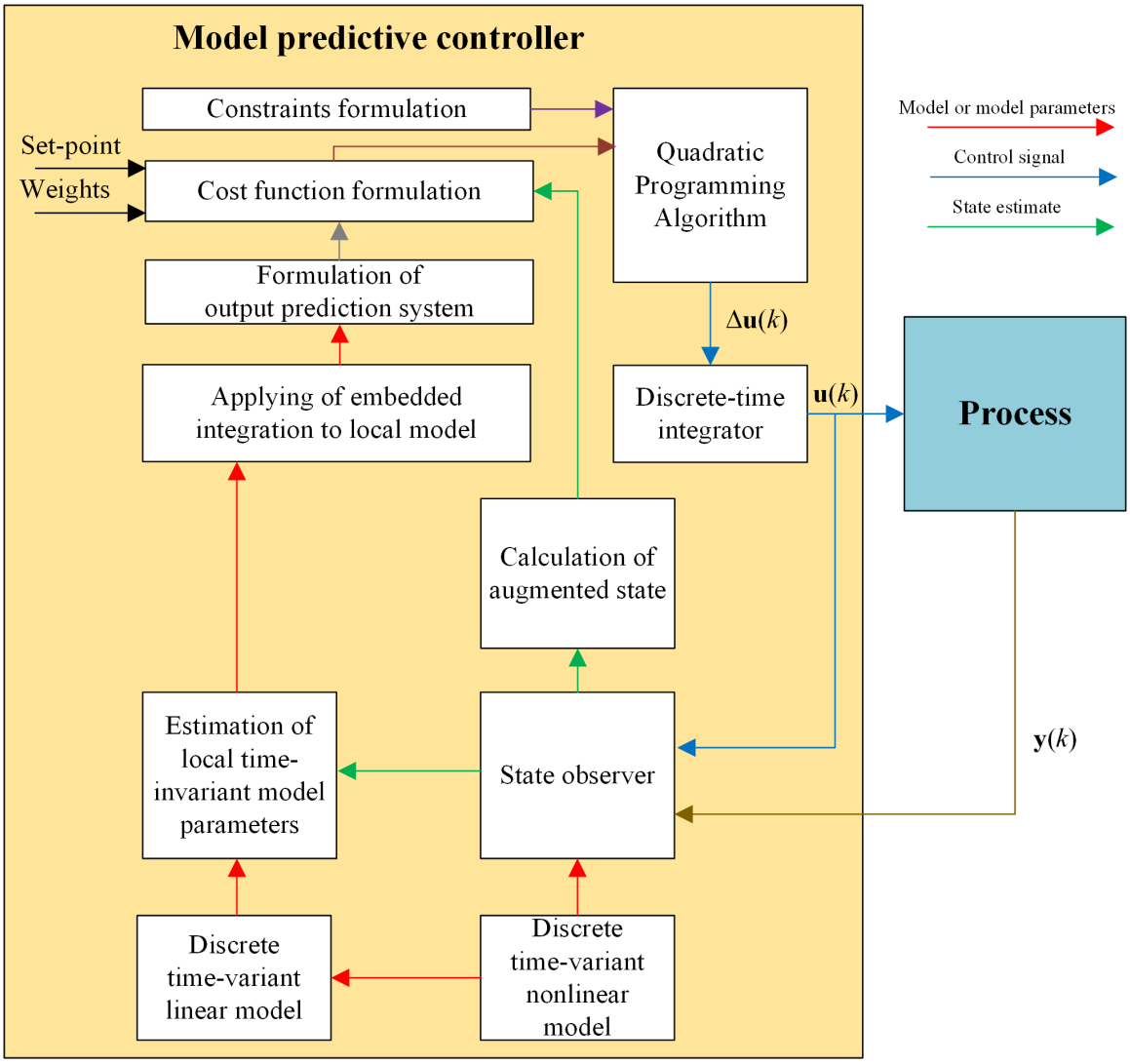

Figure 4.2: Operation diagram of MPC-CMP algorithm

Chapter 5

Implementation of Control System

In this chapter the implementation of the simulation environment for the control system will be presented. The basic aim of the implementation is to reflect the process of relative motion control by a simulation of the control loop. Implementation of the control loop includes the controller, input and output disturbances models, and a continuous nonlinear model of the process applied for simulation of relative motion between the both satellites (not to be confused with the internal models used the controller). The whole software package was developed using the MATLAB® numerical environment for purposes of this dissertation.

5.1 Control Loop Simulation

The control loop was implemented using Simulink® software, the part of the MATLAB® package. The block diagram of the control loop is presented in Figure 5.1. The main components of the control loop implementation are:

1. discrete predictive controller,
2. continuous model of the deputy spacecraft mass, whilst the controller observes only the expelled mass as the state x_7,
3. continuous nonlinear model of relative motion, described by Equation 2.90,
4. actuators model, which task is to add random uncontrolled disturbances to the control vector,
5. sensors model, which task is to add a random noise to the measurement channels.

The controller, the mass model as well as the relative motion model were implemented using Level-2 MATLAB® S-functions. The main purpose of the S-functions is to call appropriate methods of the controller and models implementation at current sampling instant.

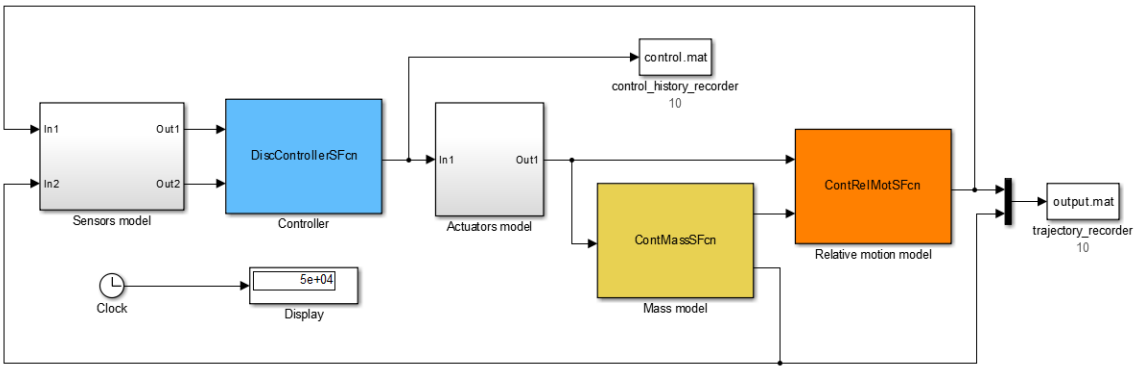

Figure 5.1: Control loop implementation

5.2 Process Implementation

The regulated process, namely the relative motion, is simulated using the continuous models given by Equation 4.2. However, the implementation of the process was decomposed into the principal relative motion model and the mass model, for reasons of handy diagnostics. Due to the complexity of the process models, they were implemented in MATLAB® environment using object-oriented programming strategy.

The operational principle of the process modeling software can be broadly described using the below step-by-step procedure:

1. Using the orbital elements of the chief satellite, given as a part of initial conditions, calculate the chief's mean angular motion n by application of Equation 2.60, and then for a given time moment t calculate the mean anomaly of the chief satellite M using Equation 2.61.

2. Adopting the chief's mean anomaly M, chief orbit eccentricity e and employing a numerical method, solve the Kepler's Equation 2.62 for an eccentric anomaly E.

3. Using the chief's eccentric anomaly E, find the true anomaly f by use of Equation 2.4.

4. Applying Equation 2.2, calculate *semilatus rectum* value p, and then find the radial distance r_c between the chief satellite and the Earth center by utilization of Equation 2.1.

5. Accepting the chief's radial distance value r_c, find true anomaly rate of the chief satellite $\dot{f}$ employing Equation 2.68.

6. Calculate the radial distance r_d between the deputy satellite and the Earth center by use of Equation 2.79, where the relative position x_1, x_2, x_3 is obtained using the state observer.

7. Obtain angular momentum h of the chief orbit according to Equation 2.36 and then calculate the chief's radial velocity $\dot{r}_c$ in the inertial frame using Equation 2.50.

8. For a given control vector $\mathbf{u}$, specific impulse I_{sp} and considering relation between the expelled mass x_{ep} and the initial propellant mass m_{p0} formulate the model of the expelled propellant mass according to Equation 2.95.

9. By an integration of Equation 2.95 and use of Equation 2.99 calculate mass m_d of the deputy spacecraft at the current time moment t.

10. Using the current model parameters $\dot{f}$, r_c, $\dot{r}_c$, r_d, μ and m_d formulate a form of nonlinear, continuous model of relative motion at the time moment t according to Equation 2.90.

11. Integrating Equation 2.90 calculate current value of the relative motion state $\mathbf{x}_{rm}$.

12. Applying Equation 4.3 calculate the current output vector $\mathbf{y}_m$ of the process, assuming the process state vector as compatible with Equation 4.1.

5.3 Controller Implementation

The basic requirement for the MPC-EMP controller implementation was to realize the algorithm presented in Figure 4.1. The controller implementation uses object-oriented

programming strategy in order to provide methods able to calculate the control value as the final result. The operation of the MPC-EMP controller (tailored for the model presented in this dissertation) can be described using step-form algorithm presented below. Note that every time the model parameters are calculated, exactly the same way is used as described in Section 5.2.

1. Using the heuristic estimation method given by Equation 4.28, find an approximation of control trajectory $\hat{\mathbf{u}}(k)$, $\hat{\mathbf{u}}(k+1)$, $\cdots$, $\hat{\mathbf{u}}(k+N_p)$.

2. Obtain the current state estimate $\hat{\mathbf{x}}_m(k)$ using the state observer given by Equation 4.72.

3. For the current and future discrete time moments $k+i$, where $i = 0, 1, \ldots, N_p$:

   - given the current state estimate $\hat{\mathbf{x}}_m(k)$ and control estimate $\hat{\mathbf{u}}$, calculate future state estimates $\hat{\mathbf{x}}_m(k+1)$, $\hat{\mathbf{x}}_m(k+2)$, $\ldots$, $\hat{\mathbf{x}}_m(k+N_p)$ iteratively using the discrete nonlinear model given by Equation 4.11.
   - using the estimated state values $\hat{\mathbf{x}}_m(k)$, $\hat{\mathbf{x}}_m(k+1)$, $\ldots$, $\hat{\mathbf{x}}_m(k+N_p)$ estimate the state matrices $\mathbf{A}_m(\hat{\mathbf{x}}_m(k+i), k+i)$ of the discrete model of relative motion according to Equation 4.17.

4. For the current and future discrete time moments $k+j$, where $j = 0, 1, \ldots, N_c-1$, using the estimated state values $\hat{\mathbf{x}}_m(k)$, $\hat{\mathbf{x}}_m(k+1)$, $\ldots$, $\hat{\mathbf{x}}_m(k+N_c-1)$, and having the current and future control estimate $\hat{\mathbf{u}}$, calculate estimated input matrices $\mathbf{B}_m(\hat{\mathbf{x}}_m(k+j), \hat{\mathbf{u}}, k+j)$ consistent with Equation 4.17.

5. Formulate an output matrix $\mathbf{C}_m$ according to Equation 4.18.

6. Given a set of triplets $\mathbf{A}_m(\hat{\mathbf{x}}_m(k+i), k+i)$, $\mathbf{B}_m(\hat{\mathbf{x}}_m(k+j), \hat{\mathbf{u}}, k+j)$ and $\mathbf{C}_m$ formulate a set of Increment-Input-Output (IIO) models (linear models with an embedded integrator) according to Equations 4.26 and 4.27 and expressed by a set of triplets $\mathbf{A}(\hat{\mathbf{x}}_m(k+i), k+i)$, $\mathbf{B}(\hat{\mathbf{x}}_m(k+j), \hat{\mathbf{u}}, k+j)$ and $\mathbf{C}$.

7. Calculate the $\mathbf{F}$ and $\mathbf{\Phi}$ matrices in Equation 4.32 using formulation of the output prediction system described in Section 4.4.2.

8. Formulate the $\bar{\mathbf{R}}_s$ matrix consistent with Equation 4.56.

9. Construct the $\bar{\mathbf{R}}$ matrix according to Equation 4.58.

10. Calculate the augmented state estimate $\hat{\mathbf{x}}(k)$ using Equation 4.76.

11. Given $\mathbf{F}$, $\mathbf{\Phi}$, $\bar{\mathbf{R}}$, $\bar{\mathbf{R}}_s$, $\hat{\mathbf{x}}(k)$ and set-point information $\mathbf{\Xi}(k)$ formulate the $\mathbf{H}$ and φ matrices after Equations 4.70 and 4.71.

12. Construct the matrices $\mathbf{M}_{const}$ and $\mathbf{N}_{const}$ reflecting the constraints given by Equation 4.67.

13. Using quadratic programming solver, for a given matrices $\mathbf{H}$, φ, $\mathbf{M}_{const}$ and $\mathbf{N}_{const}$ calculate the open-loop control trajectory $\Delta\mathbf{U}$.

14. According to the model predictive control principle, using the matrix ι from Equation 4.62 obtain the first element of $\Delta\mathbf{U}$ at time k, namely $\Delta\mathbf{u}(k)$.

15. Calculate the control variable $\mathbf{u}(k)$ using Equation 4.22.

The above procedure is repeated at each sampling instant.

Chapter 6

Numerical Experiments

This chapter presents the results of the simulations which attempt to confirm the theses of this dissertation. The simulations were performed using software described in Chapter 5, with chosen initial conditions and parameters. The initial conditions are given in the form of classical orbital elements in order to facilitate their interpretation. The classical orbital elements, the six quantities determining shape and orientation of the orbit in space are defined in many references, a recommendable one is Ref. [66]. The controller parameters were chosen in a way to provide possibly best closed-loop performance in each of the simulations.

6.1 Simulation I: Large Separation, MPC-CMP Algorithm

The simulation described in this section reflects the situation where the orbital rendezvous is performed with inconvenient initial conditions, with large separation and inopportune velocity vector. The purpose of this simulation is to test the capabilities of the MPC-CMP algorithm, being an equivalent of the classical MPC algorithms with successive linearization. The simulation represents the process behavior over 70 000 s (nearby 20 h).

6.1.1 Simulation Setup

The initial conditions for relative motion given in Table 6.1 corresponds to the following vector in LVLH frame:

$$\mathbf{x}_{rm} \approx \begin{bmatrix} 257\,\text{km} \\ -19\,827\,\text{km} \\ 2095\,\text{km} \\ -0{,}559\,\text{km/s} \\ -2{,}252\,\text{km/s} \\ 1{,}542\,\text{km/s} \end{bmatrix} \tag{6.1}$$

Table 6.1: Simulation I: Initial conditions for relative motion.

Orbit parameter	Symbol	Value for Chief	Value for Deputy	Unit
Semi-major axis	a	24000	28000	km
Eccentricity	e	0,5	0,7	-
Inclination	i	160	120	°
Longitude of the ascending node	Ω	60	10	°
Argument of periapsis	ω	120	50	°
Mean anomaly at epoch 0	M_0	120	90	°

Table 6.2 presents assumed parameters of the deputy satellite. Please note that the parameters have rather theoretical character, especially the specific impulse. Such choice was necessary because of initial conditions, however the result for expelled mass have relevant meaning in the context of comparison. Moreover, such maneuver could be realizable with the utilization of multi-stage thruster system of the deputy spacecraft.

The tuning parameters for the controller are given in Table 6.3. Because of relatively long duration of the control process, which enforces a long prediction horizon,

Table 6.2: Simulation I: Assumed parameters of the deputy satellite.

Parameter	Symbol	Value	Unit
Satellite mass without available propellant	m_{dry}	100	kg
Initial propellant mass	m_{p0}	900	kg
Specific impulse	I_{sp}	1200	s

the sampling time T_s is relatively large. Elongation of the prediction horizon by excessive increasing of the sampling instants number N_p is not preferred because of numerical difficulties and large computational effort. In the other hand, long sampling time of the controller entails inaccuracy due to assumption that parameters of the internal model used by the controller are invariant within the sampling period. Hence the choice of the sampling period is a kind of design compromise.

Table 6.3: Simulation I: Controller setup.

Parameter	Symbol	Value	Unit
Sampling time	T_s	300	s
Prediction horizon	N_p	120	-
Control horizon	N_c	5	-
Set-point	$\boldsymbol{\Xi}$	$\mathbf{0}_{7,1}$	m, m/s, kg
Control constraint (lower)	$\mathbf{u}^{min}$	$-100 \cdot \begin{bmatrix} 1 & 1 & 1 \end{bmatrix}^T$	N
Control constraint (upper)	$\mathbf{u}^{max}$	$100 \cdot \begin{bmatrix} 1 & 1 & 1 \end{bmatrix}^T$	N
Control increment weight	$\boldsymbol{\Theta}$	$5 \cdot 10^7 \cdot \begin{bmatrix} 1 & 1 & 1 \end{bmatrix}^T$	-

6.1.2 Simulation Results

Figure 6.1 presents trajectory of the relative position in LVLH frame, described by the components x_1, x_2 and x_3 of the state vector $\mathbf{x}_m(t)$ defined according to Equation 4.1.

Figure 6.2 shows trajectory of the relative velocity in LVLH frame, characterized

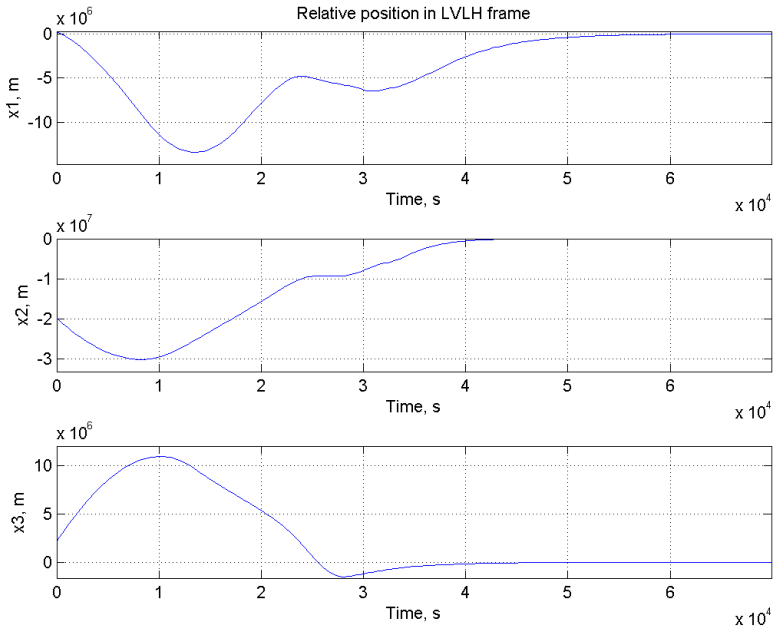

Figure 6.1: Simulation I: Relative position in LVLH frame.

by the states x_4, x_5 and x_6.

Figure 6.3 presents history of the expelled propellant mass, expressed by the state x_7.

Figure 6.4 shows history of the control signal in LVLH frame, expressed by the control vector $\mathbf{u}$.

The visualization of the deputy and chief satellites position is presented in Figure 6.5.

The study of Figures 6.1 and 6.2 denotes that the rendezvous maneuver was accomplished after 60 000 s. The visualization of the maneuver depicted in Figure 6.5 gives an impression that the maneuver objective was possible to meet much earlier. Additionally, Figure 6.4 indicates that even after the rendezvous at 60 000 s the controller need to perform significant corrections in order to maintain the set-point. The MPC-EMP controller used in the next simulation will attempt to cope with that imperfections.

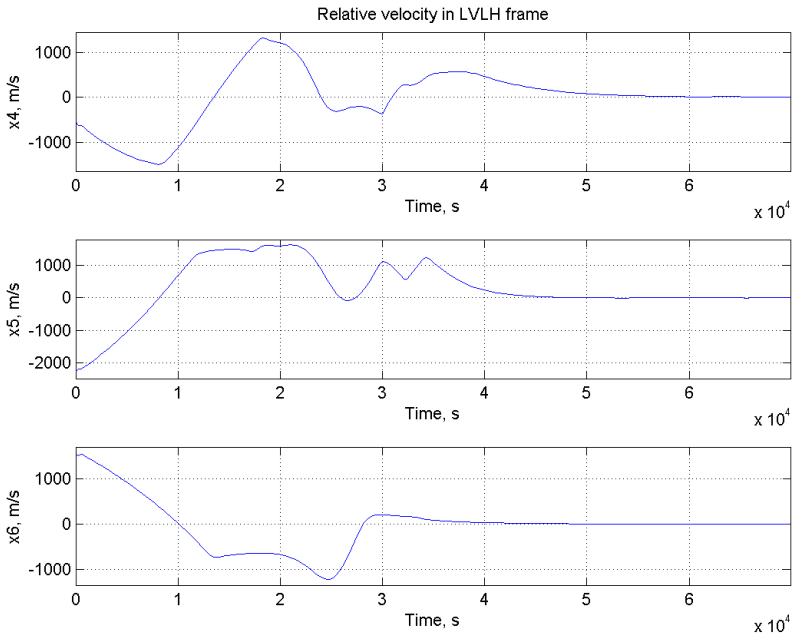

Figure 6.2: Simulation I: Relative velocity in LVLH frame.

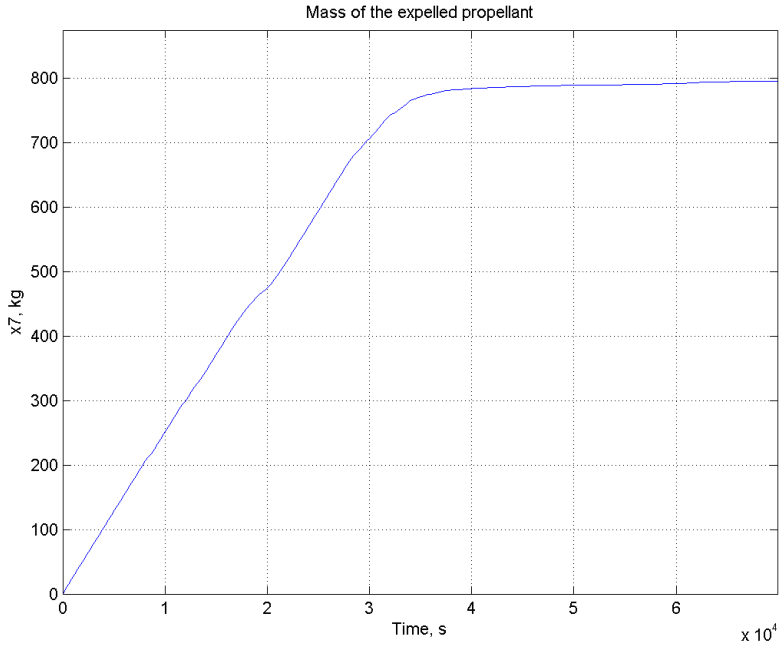

Figure 6.3: Simulation I: History of the expelled mass.

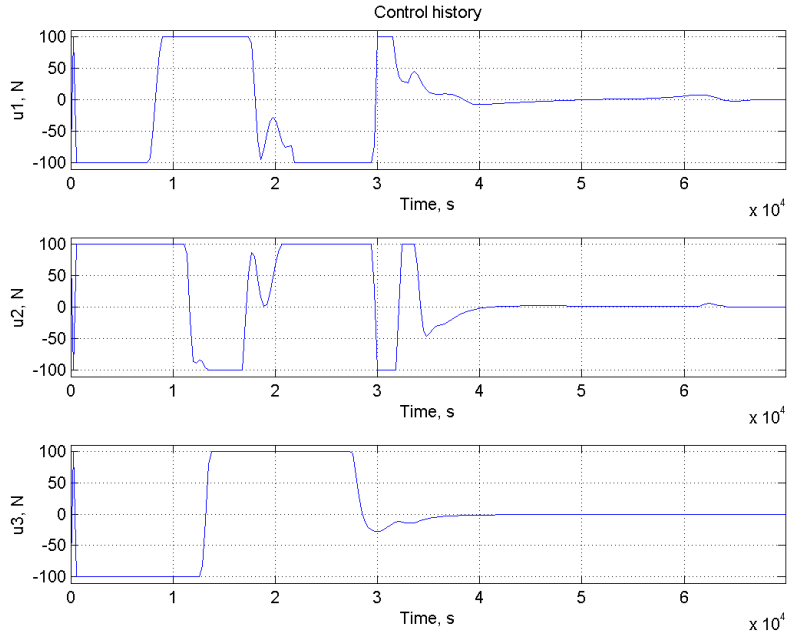

Figure 6.4: Simulation I: Control history.

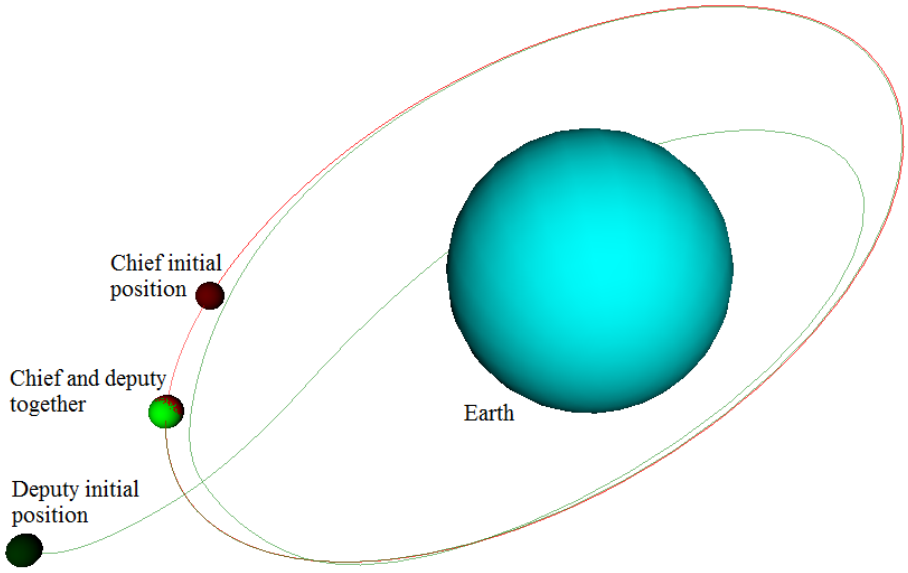

Figure 6.5: Simulation I: Visualization of the rendezvous maneuver.

6.2 Simulation II: Large Separation, MPC-EMP Algorithm

All the initial conditions and spacecraft parameters used in this simulation are the same as in Simulation I, the only change is the controller. This simulation is focused on finding differences between control loop behavior provided by the MPC-EMP algorithm and MPC-CMP algorithm used in Simulation I. Still, the simulation represents the process behavior over 70 000 s.

6.2.1 Simulation Setup

The initial conditions are the same as given in Table 6.1, while the deputy spacecraft parameters remains the same as these in Table 6.2. The tuning parameters for the MPC-EMP controller are given in Table 6.4.

Table 6.4: Simulation II: Controller setup.

Parameter	Symbol	Value	Unit
Sampling time	T_s	300	s
Prediction horizon	N_p	50	-
Control horizon	N_c	5	-
Set-point	$\boldsymbol{\Xi}$	$\mathbf{0}_{7,1}$	m, m/s, kg
Control constraint (lower)	$\mathbf{u}^{min}$	$-100 \cdot \begin{bmatrix} 1 & 1 & 1 \end{bmatrix}^T$	N
Control constraint (upper)	$\mathbf{u}^{max}$	$100 \cdot \begin{bmatrix} 1 & 1 & 1 \end{bmatrix}^T$	N
Control increment weight	$\boldsymbol{\Theta}$	$1 \cdot 10^9 \cdot \begin{bmatrix} 1 & 1 & 1 \end{bmatrix}^T$	-
Filter order in HCE algorithm	N_f	50	-

6.2.2 Simulation Results

The trajectory of relative position in LVLH frame, described by the states x_1, x_2 and x_3 of the state vector $\mathbf{x}_m(t)$ defined according to Equation 4.1 is depicted in Figure 6.6.

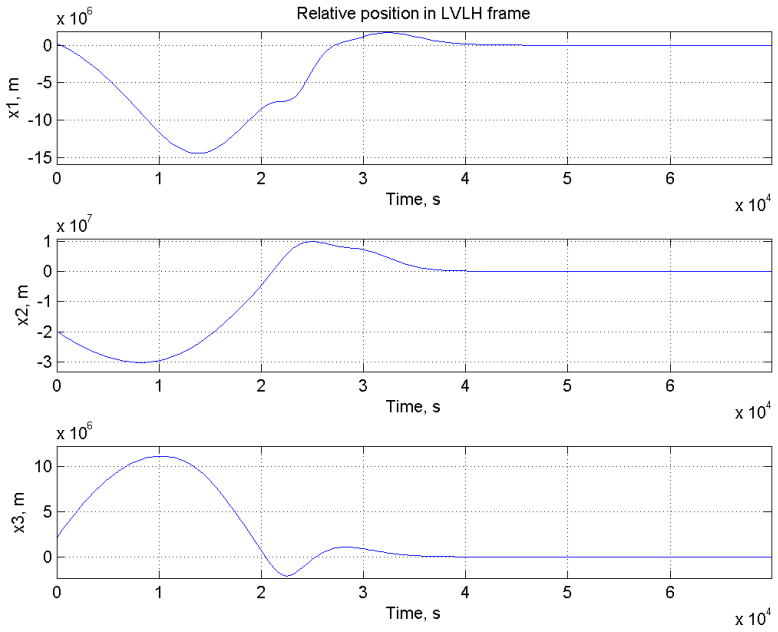

Figure 6.6: Simulation II: Relative position in LVLH frame.

The trajectory of relative velocity in LVLH frame, described by the states x_4, x_5 and x_6, is presented in Figure 6.7.

Figure 6.8 presents history of the expelled propellant mass, expressed by the state x_7.

Figure 6.9 shows history of the control signal in LVLH frame, represented by the control vector $\mathbf{u}$.

The visualization of the deputy and chief satellites position is depicted in Figure 6.10, where the deputy and chief satellites performed almost one revolution together.

The study of Figures 6.6 and 6.7 denotes that the rendezvous maneuver was successfully accomplished after approximately 50 000 s, what is a significantly better result than the performance obtained using MPC-CMP algorithm in Simulation I. Such accomplishment is not possible using MPC-CMP algorithm, even in the case of zero control increment weight, $\boldsymbol{\Theta} = \mathbf{0}_{3,1}$.

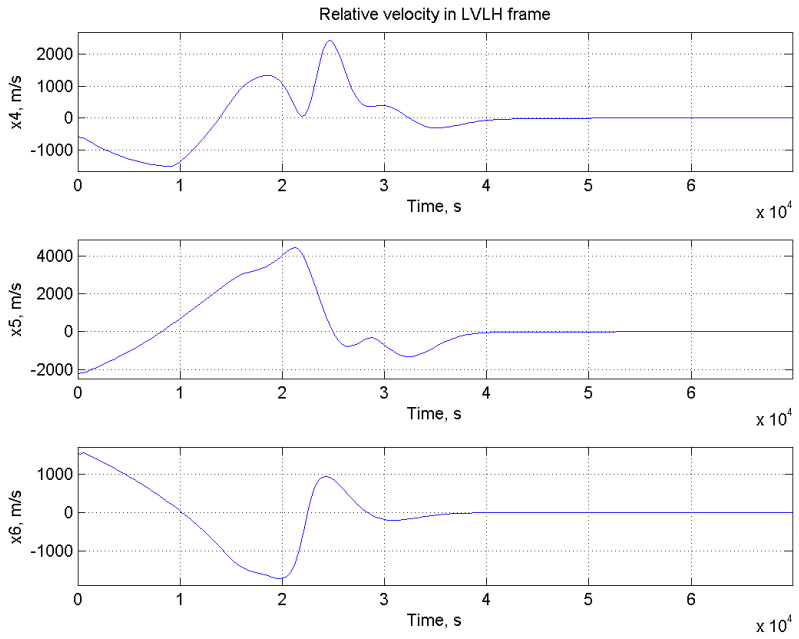

Figure 6.7: Simulation II: Relative velocity in LVLH frame.

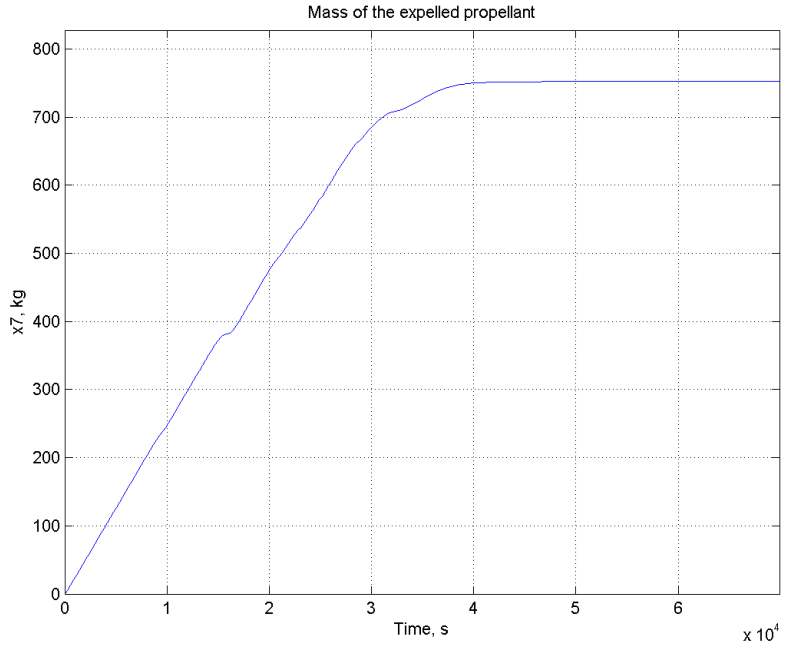

Figure 6.8: Simulation II: History of the expelled mass.

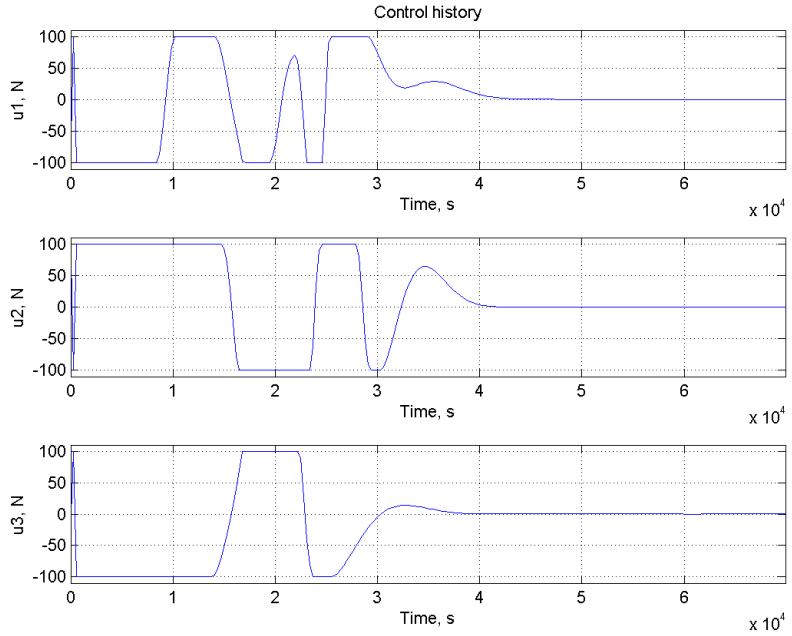

Figure 6.9: Simulation II: Control history.

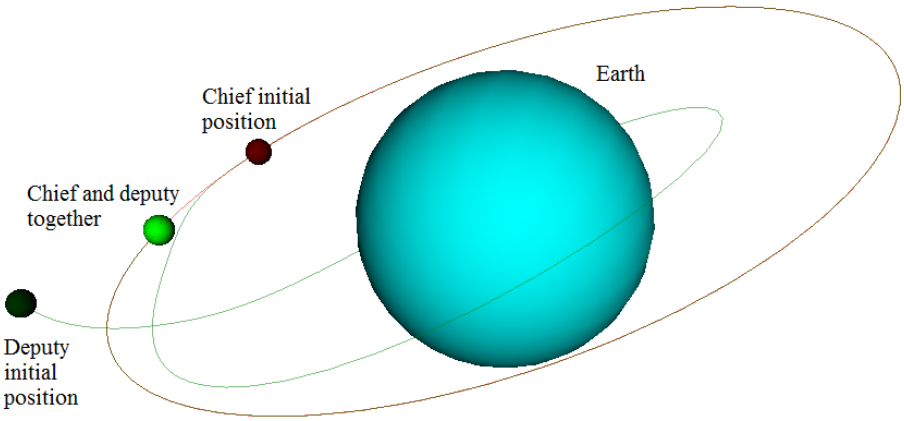

Figure 6.10: Simulation II: Visualization of the rendezvous maneuver.

6.3 Simulation III: Application of T–H Model of Relative Motion

This simulation presents the case where Tschauner–Hempel model is used for output trajectory prediction and state estimation, as replacement to the nonlinear model. The formulation of the Tschauner–Hempel model is given in Appendix A. The controller uses the MPC-EMP algorithm where the replacement of the nonlinear model through the Tschauner–Hempel model is the only modification. The aim of this simulation is to verify the ability of linearized model to serve as an internal model for predictive controller in formulated problem of relative motion. The simulation represents the process behavior over 70 000 s.

6.3.1 Simulation Setup

The initial conditions given in Table 6.5 corresponds to the following vector in LVLH frame:

$$\mathbf{x}_{rm} \approx \begin{bmatrix} -35\,287\,\text{km} \\ -8133\,\text{km} \\ 1697\,\text{km} \\ 3{,}963\,\text{km/s} \\ -3{,}649\,\text{km/s} \\ -0{,}539\,\text{km/s} \end{bmatrix} \tag{6.2}$$

Table 6.6 presents assumed parameters of the deputy satellite. In case of this simulation the parameters are physically achievable.

The tuning parameters for the MPC-EMP controller are given in Table 6.7.

Table 6.5: Simulation III: Initial conditions for relative motion.

Orbit parameter	Symbol	Value for Chief	Value for Deputy	Unit
Semi-major axis	a	40000	37000	km
Eccentricity	e	0,8	0,75	-
Inclination	i	260	270	$^\circ$
Longitude of the ascending node	Ω	60	55	$^\circ$
Argument of periapsis	ω	120	135	$^\circ$
Mean anomaly at epoch 0	M_0	30	0	$^\circ$

Table 6.6: Simulation III: Assumed parameters of the deputy satellite.

Parameter	Symbol	Value	Unit
Satellite mass without available propellant	m_{dry}	100	kg
Initial propellant mass	m_{p0}	900	kg
Specific impulse	I_{sp}	300	s

Table 6.7: Simulation III: Controller setup.

Parameter	Symbol	Value	Unit
Sampling time	T_s	300	s
Prediction horizon	N_p	70	-
Control horizon	N_c	5	-
Set-point	$\boldsymbol{\Xi}$	$\mathbf{0}_{7,1}$	m, m/s, kg
Control constraint (lower)	$\mathbf{u}^{min}$	$-100 \cdot \begin{bmatrix} 1 & 1 & 1 \end{bmatrix}^T$	N
Control constraint (upper)	$\mathbf{u}^{max}$	$100 \cdot \begin{bmatrix} 1 & 1 & 1 \end{bmatrix}^T$	N
Control increment weight	$\boldsymbol{\Theta}$	$15 \cdot 10^{10} \cdot \begin{bmatrix} 1 & 1 & 1 \end{bmatrix}^T$	-
Filter order in HCE algorithm	N_f	150	-

6.3.2 Simulation Results

Obtained trajectory of LVLH position determined by the states x_1, x_2 and x_3 is presented in Figure 6.11.

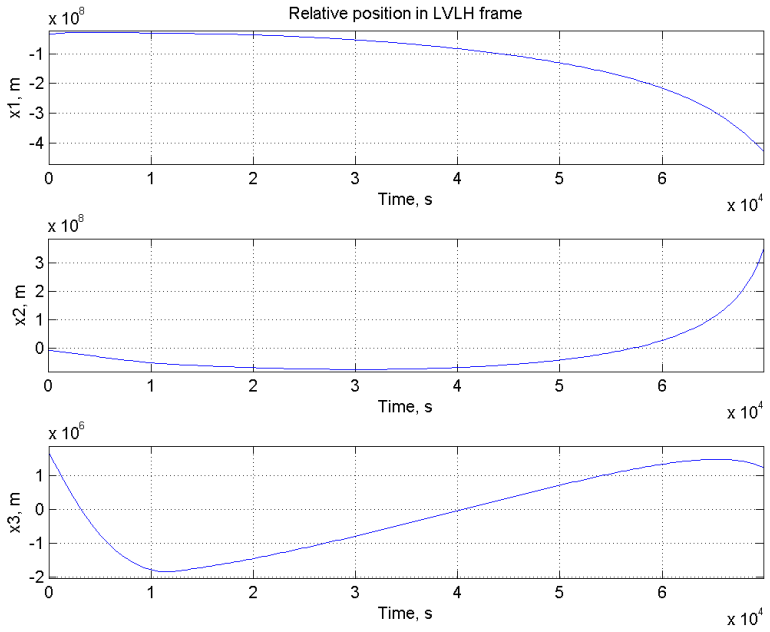

Figure 6.11: Simulation III: Relative position in LVLH frame.

The trajectory of relative velocity in LVLH frame, described by the states x_4, x_5 and x_6, is depicted in Figure 6.12.

Figure 6.13 describes history of the expelled propellant mass, represented by the state x_7.

The control history is plotted in Figure 6.14.

The calculated position of both the satellites is visualized using Figure 6.15.

Analysis of Figures 6.11, 6.12 and 6.15 denotes that controller behavior was completely erroneous. The reason of such performance is utilization of linearized model, which is suitable for small separations. Figure 6.13 implies fast loss of the whole available propellant, what prevents any kind of trajectory corrections even if the separation would become small due to the process dynamics. Although a large spectrum of tuning parameters was tested, any set of parameters was able to provide desired closed-loop performance.

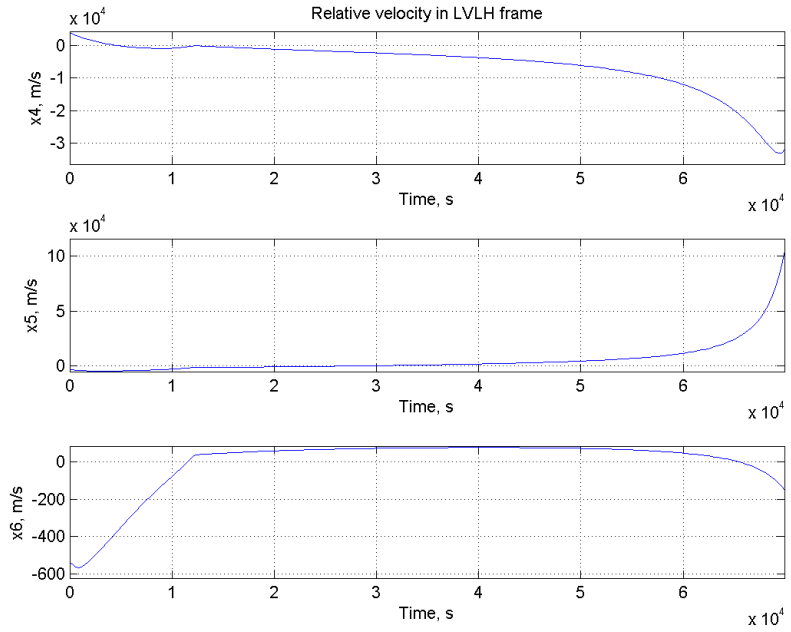

Figure 6.12: Simulation III: Relative velocity in LVLH frame.

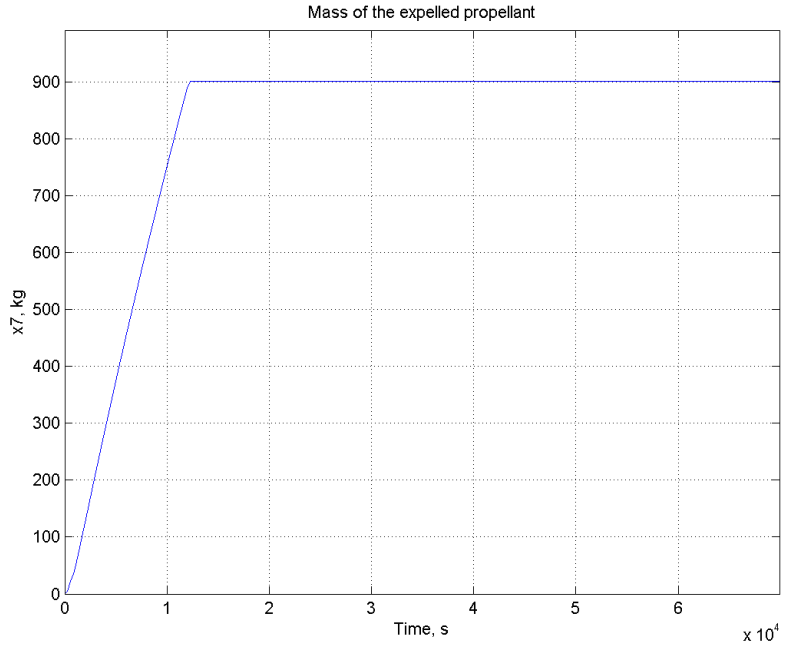

Figure 6.13: Simulation III: History of the expelled mass.

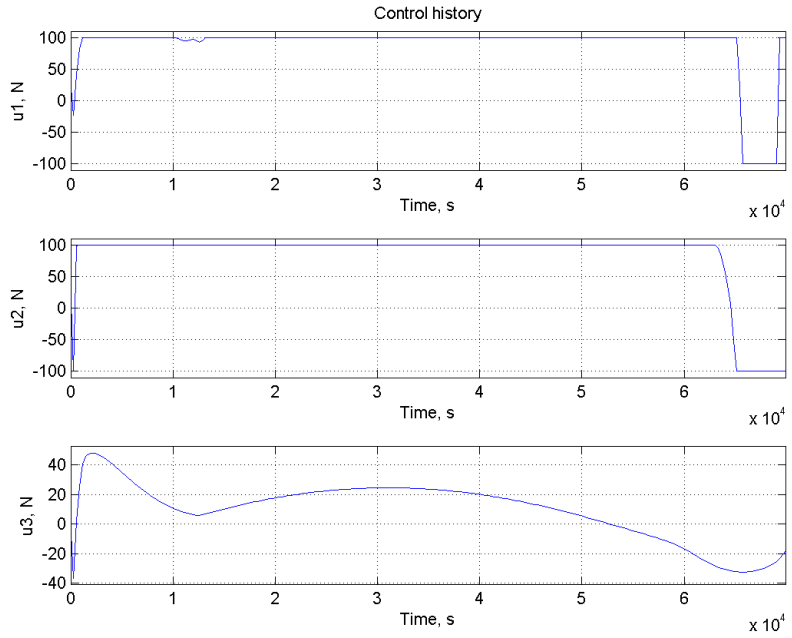

Figure 6.14: Simulation III: Control history.

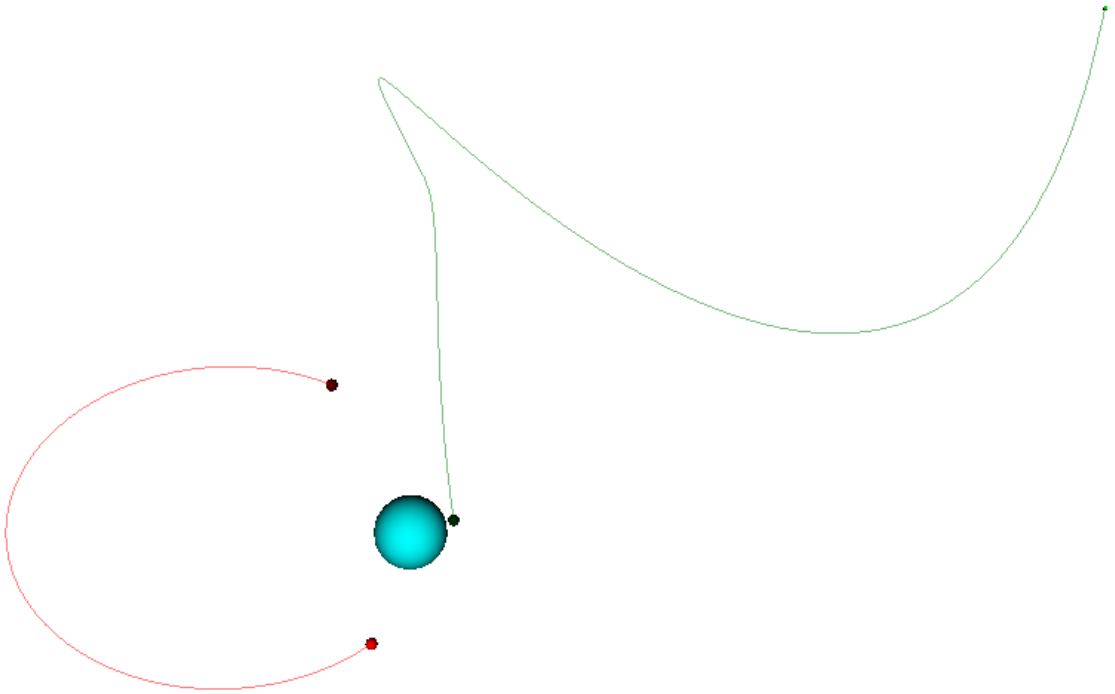

Figure 6.15: Simulation III: Visualization of the calculated position for both the satellites.

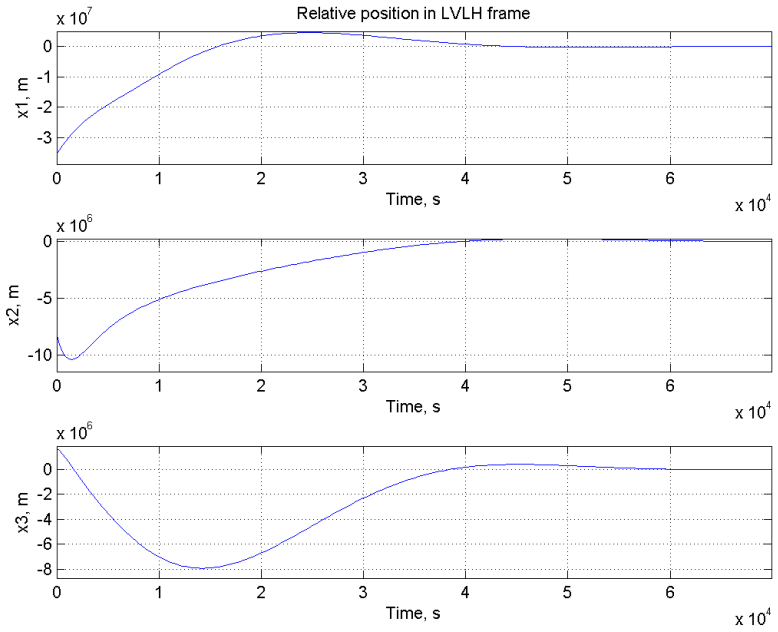

Figure 6.16: Simulation IV: Relative position in LVLH frame.

6.4 Simulation IV: Application of Nonlinear Model of Relative Motion

All the initial conditions and deputy spacecraft parameters used in this simulation are the same as in Simulation III. Tuning parameters of the controller are exactly the same as used in Simulation III and they are given in Table 6.7. Still, the MPC-EMP algorithm is used for the maneuver control. However, in contrast to Simulation III, the controller uses the nonlinear model of relative motion, given by Equation 4.11. The simulation represents the process behavior over 70 000 s.

6.4.1 Simulation Results

The relative motion trajectory is plotted in Figures 6.16 and 6.17.

Figure 6.18 represents history of the expelled propellant mass, expressed by the state x_7.

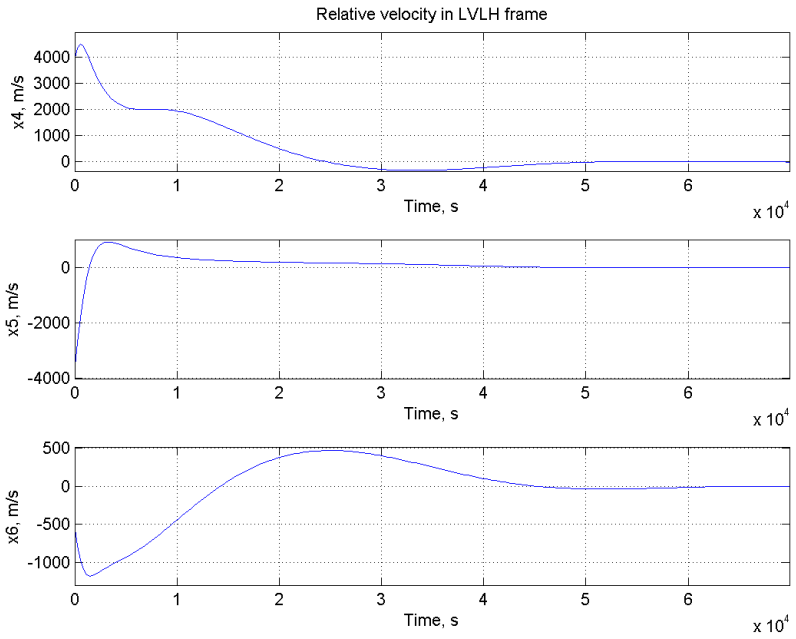

Figure 6.17: Simulation IV: Relative velocity in LVLH frame.

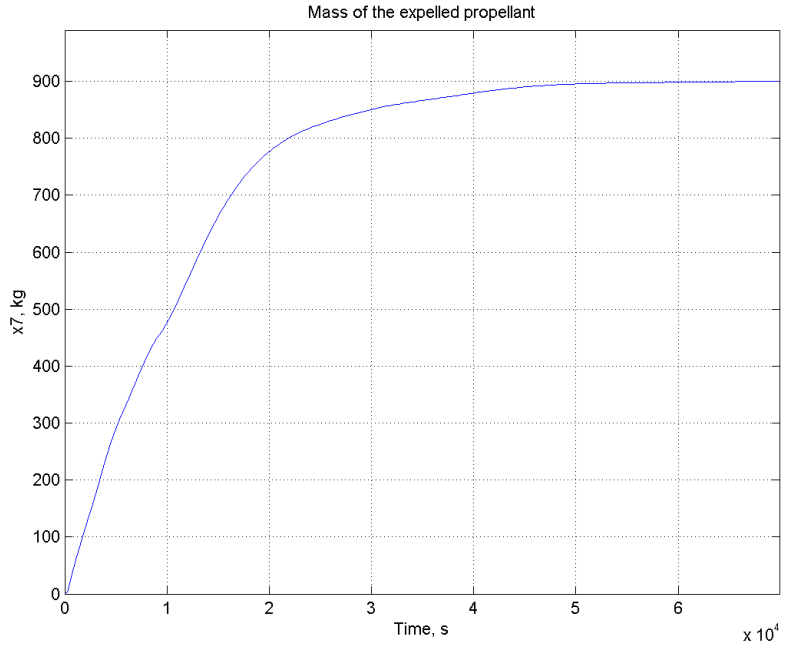

Figure 6.18: Simulation IV: History of the expelled mass.

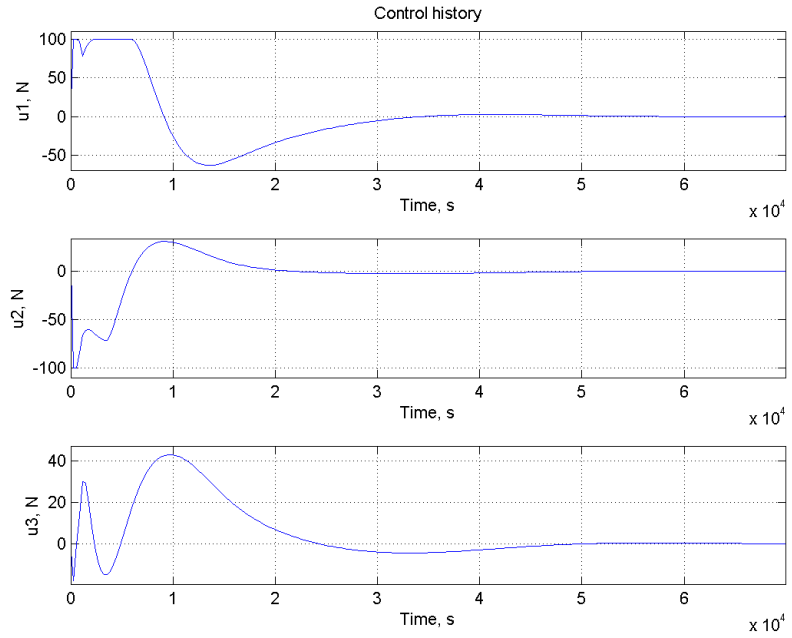

Figure 6.19: Simulation IV: Control history.

The control history **u** is plotted in Figure 6.19.

The position of both the satellites is visualized by Figure 6.20.

Study of Figures 6.16, 6.17 and 6.20 enables us to determine that the control objective was met. Figure 6.18 implies that almost the whole propellant was used, nevertheless it was sufficient amount. The comparison between Simulations III and IV gives clear conclusion that usage of the nonlinear model has strong advantages over linearized model, such as Tschauner–Hempel model. In this simulation, the MPC-EMP algorithm equipped with the nonlinear model enabled for rendezvous maneuver with the initial separation of 36 252 km.

6.5 Simulation V: MPC-EMP Algorithm, Disturbed Process

Simulation presented here reflects behavior of a control process perturbed by uncontrolled disturbances. The perturbations were simulated by an addition of uncontrolled disturbances in the form of random noise to the control signal. The noise was assumed

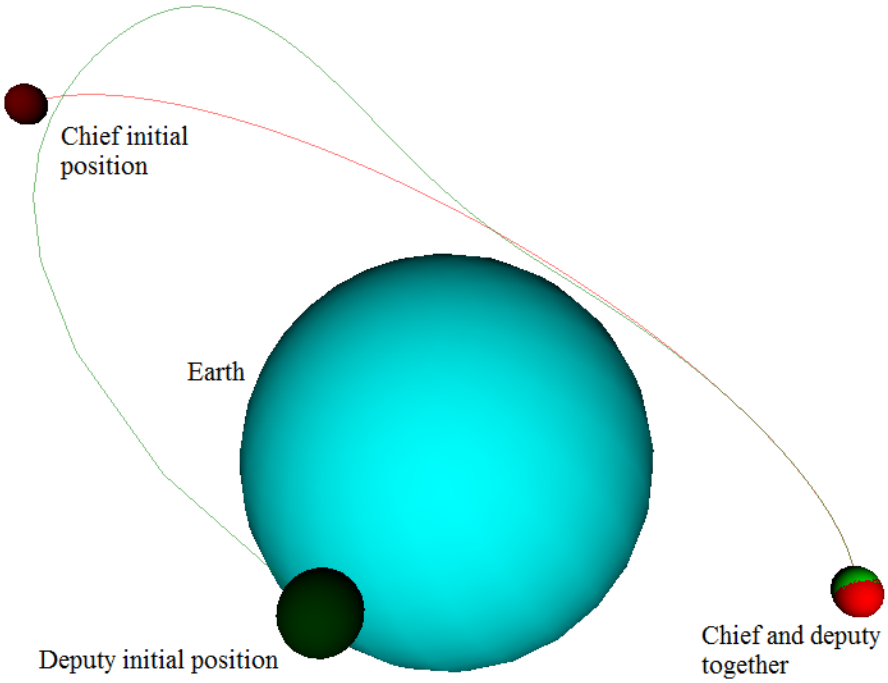

Figure 6.20: Simulation IV: Visualization of the rendezvous maneuver.

to have a uniform distribution and have consequences in acceleration disturbances in range $\left[-0{,}05\,\frac{\mathrm{m}}{\mathrm{s}^2}, 0{,}05\,\frac{\mathrm{m}}{\mathrm{s}^2}\right]$. Referring to Figure 2.4, this level of noise exceeds the magnitude of orbital perturbations encountered in the space flight practice.

Also a measurement noise was added to the output signal, with an assumption of its uniform distribution in range $[-1, 1]$. The simulation represents the process behavior over 40 000 s (approximately 11 h).

6.5.1 Simulation Setup

The initial conditions for relative motion are described by the following vector in LVLH frame:

$$\mathbf{x}_{rm} \approx \begin{bmatrix} -3000\,\text{km} \\ -5000\,\text{km} \\ -2000\,\text{km} \\ 0{,}1\,\text{km/s} \\ 0{,}1\,\text{km/s} \\ 0{,}05\,\text{km/s} \end{bmatrix} \tag{6.3}$$

The chief is moving in a Molniya orbit, with orbital elements given in Table 6.8.

Table 6.8: Simulation V: Classical orbital elements of the chief satellite.

Orbit parameter	Symbol	Value	Unit
Semi-major axis	a	26554	km
Eccentricity	e	0.72	-
Inclination	i	63.4	°
Longitude of the ascending node	Ω	0	°
Argument of periapsis	ω	270	°
Mean anomaly at epoch 0	M_0	40	°

Table 6.9 presents assumed parameters of the deputy satellite.

Table 6.9: Simulation V: Assumed parameters of the deputy satellite.

Parameter	Symbol	Value	Unit
Satellite mass without available propellant	m_{dry}	5000	kg
Initial propellant mass	m_{p0}	7000	kg
Specific impulse	I_{sp}	350	s

Table 6.10: Simulation V: Controller setup.

Parameter	Symbol	Value	Unit
Sampling time	T_s	300	s
Prediction horizon	N_p	80	-
Control horizon	N_c	12	-
Set-point	$\boldsymbol{\Xi}$	$\mathbf{0}_{7,1}$	m, m/s, kg
Control constraint (lower)	$\mathbf{u}^{min}$	$-1500 \cdot \begin{bmatrix} 1 & 1 & 1 \end{bmatrix}^T$	N
Control constraint (upper)	$\mathbf{u}^{max}$	$1500 \cdot \begin{bmatrix} 1 & 1 & 1 \end{bmatrix}^T$	N
Control increment weight	$\boldsymbol{\Theta}$	$2 \cdot 10^8 \cdot \begin{bmatrix} 1 & 1 & 1 \end{bmatrix}^T$	-
Filter order in HCE algorithm	N_f	65	-

The tuning parameters for the controller are given in Table 6.10.

6.5.2 Simulation Results

Figure 6.21 presents trajectory of the relative position in LVLH frame, described by the components x_1, x_2 and x_3 of the state vector $\mathbf{x}_m(t)$.

Figure 6.22 shows trajectory of the relative velocity in LVLH frame, characterized by the states x_4, x_5 and x_6.

Figure 6.23 presents history of the expelled propellant mass, expressed by the state x_7.

Figure 6.24 shows history of the control signal in LVLH frame, expressed by the control vector $\mathbf{u}$.

The visualization of the deputy and chief satellites position is presented in Figure 6.25.

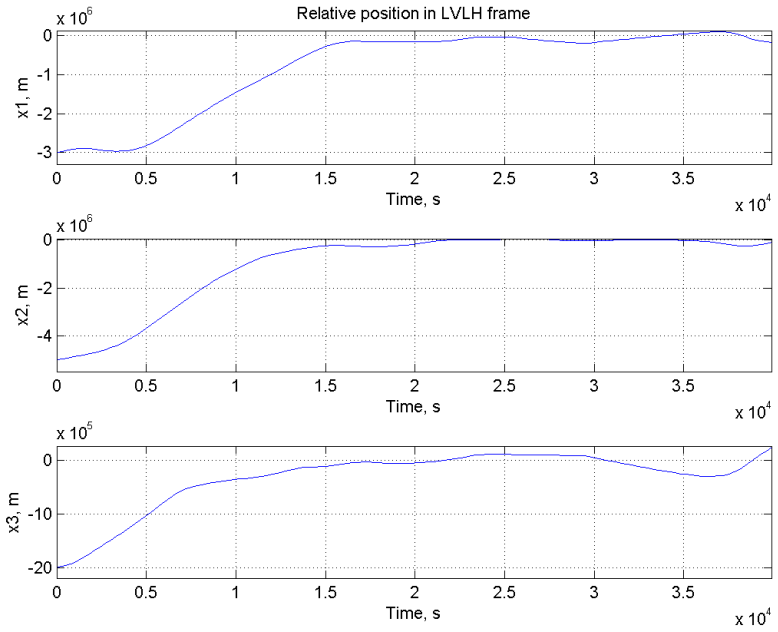

Figure 6.21: Simulation V: Relative position in LVLH frame.

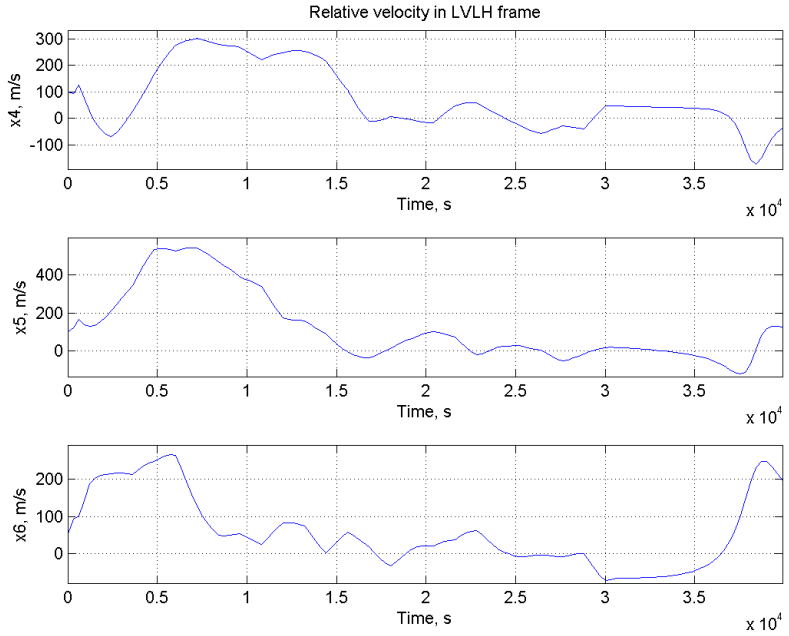

Figure 6.22: Simulation V: Relative velocity in LVLH frame.

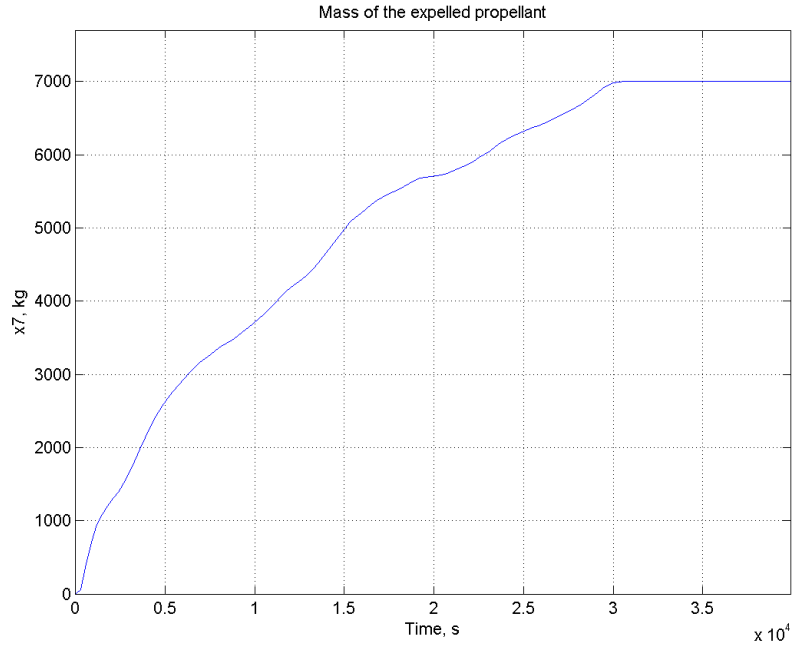

Figure 6.23: Simulation V: History of the expelled mass.

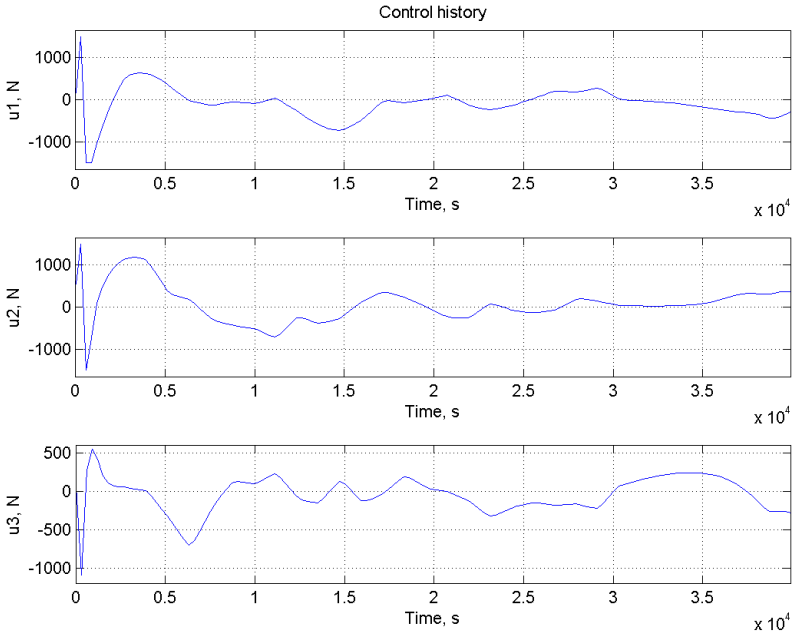

Figure 6.24: Simulation V: Control history.

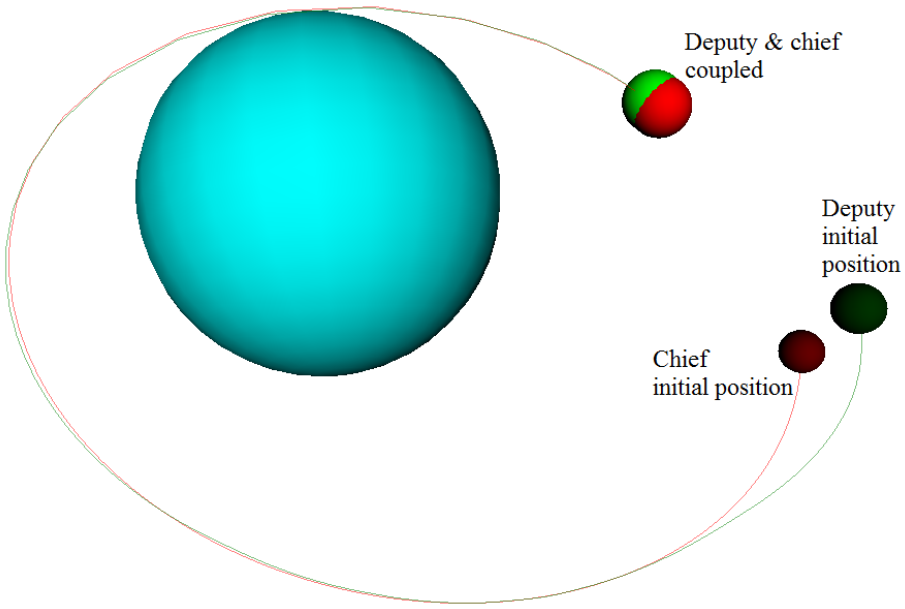

Figure 6.25: Simulation V: Visualization of the rendezvous maneuver.

6.6 Simulation VI: MPC-EMP Algorithm, Transient Response

This simulation was performed in order to find a transient response of the closed-loop system. The step disturbance was applied at the moment 1200 s as a vector $\begin{bmatrix} 100\,\mathrm{N} & 100\,\mathrm{N} & 100\,\mathrm{N} \end{bmatrix}^T$ added to the control signal $\mathbf{u}$. The simulation represents process behavior over 40 000 s (about 11 h).

6.6.1 Simulation Setup

The initial conditions for relative motion represents situation where the deputy and chief satellites are concatenated, what can be expressed as $\mathbf{x}_{rm} = \mathbf{0}_{6,1}$. The chief satellite is moving in an orbit with the same orbital elements as given in Table 6.8. The chosen parameters of the deputy spacecraft are given in Table 6.9. Similarly, the controller tuning parameters were the same as given in Table 6.10.

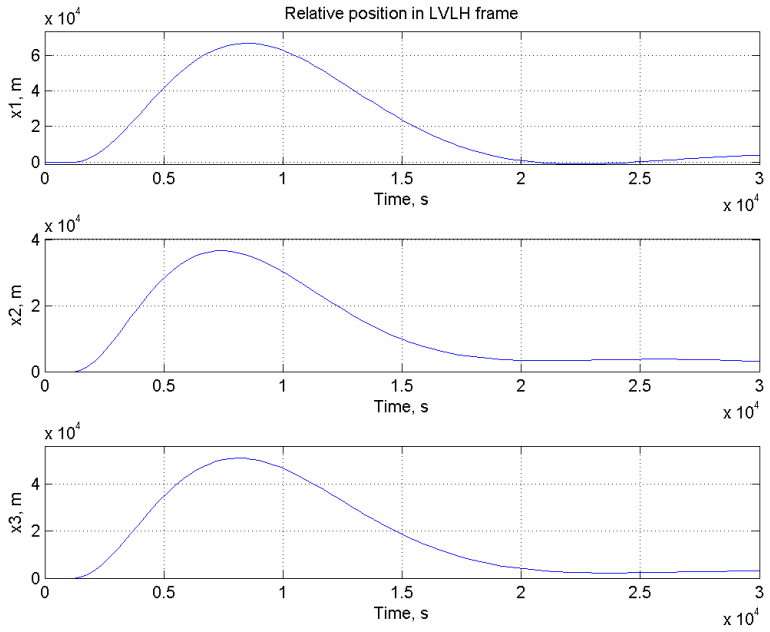

Figure 6.26: Simulation VI: Relative position in LVLH frame.

6.6.2 Simulation Results

Figure 6.26 presents trajectory of the relative position in LVLH frame, described by the components x_1, x_2 and x_3 of the state vector $\mathbf{x}_m(t)$.

Figure 6.27 shows trajectory of the relative velocity in LVLH frame, characterized by the states x_4, x_5 and x_6.

Figure 6.28 presents history of the expelled propellant mass, expressed by the state x_7.

Figure 6.29 shows history of the control signal in LVLH frame, expressed by the control vector $\mathbf{u}(k)$.

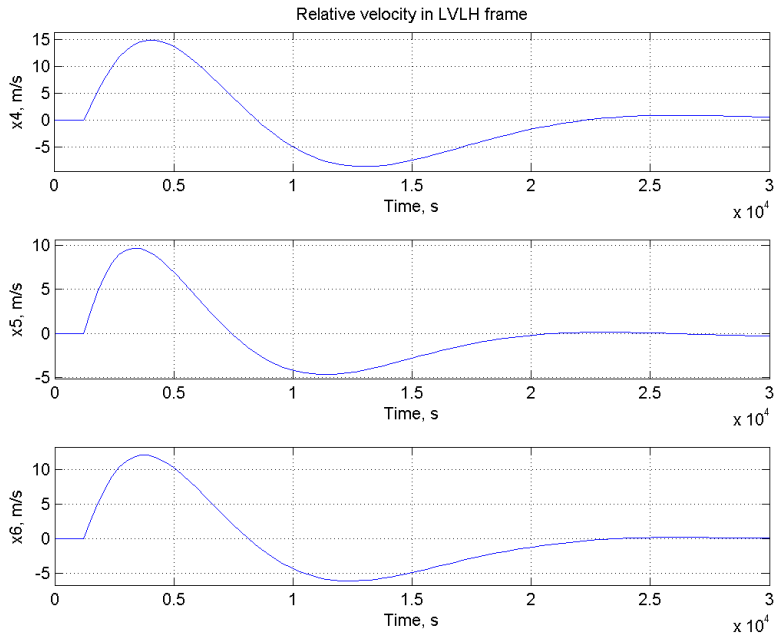

Figure 6.27: Simulation VI: Relative velocity in LVLH frame.

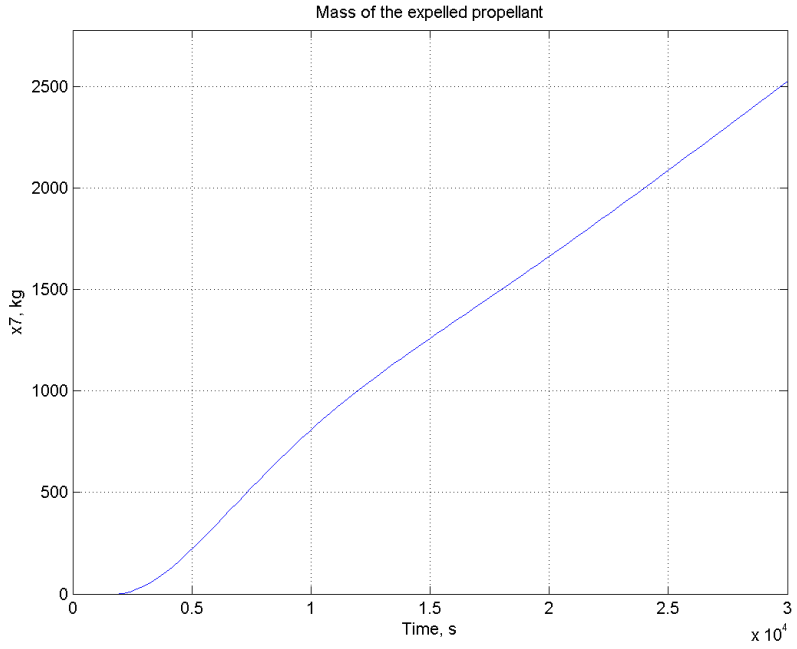

Figure 6.28: Simulation VI: History of the expelled mass.

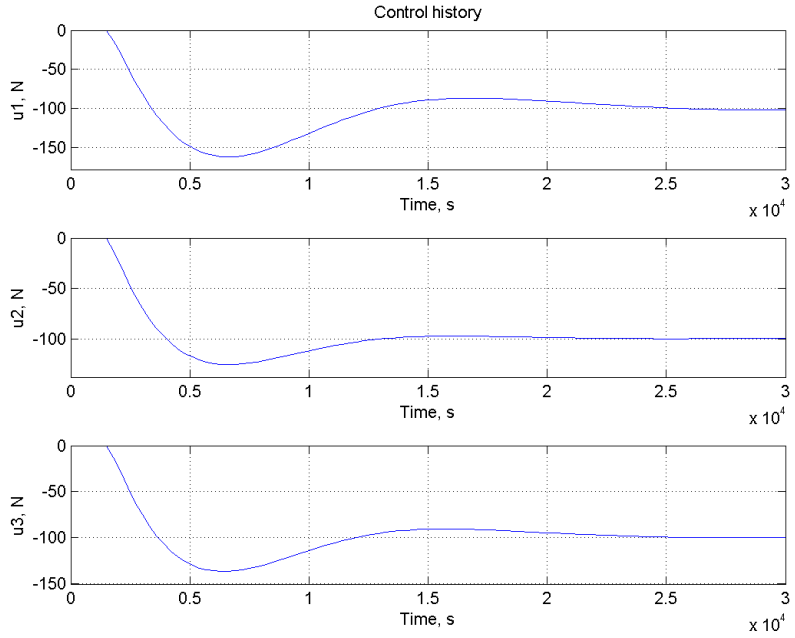

Figure 6.29: Simulation VI: Control history.

Chapter 7

Evaluation of Solution

Study of Chapter 6 enables a preliminary conclusion that main requirements for the proposed controller are met. In this chapter we will discuss the results more closely, as well as evaluate the solution in general context.

7.1 Results Interpretation

First, let us consider the comparison between Simulation I described in Section 6.1 and Simulation II presented in Section 6.2. The formulation of the problem, the same in both the simulations, includes large separation (approximately 20 000 km) and inconvenient initial conditions for relative velocity. Note that such set of initial conditions would prevent desired control performance in case where predictive controller uses linearized models, such as Tschauner-Hempel equations. The results of Simulation I, where the MPC-CMP algorithm was utilized, indicates that the rendezvous maneuver was accomplished, what can be counted as a success. However, the control process was burdened with a number of imperfections: wasting the possibility of earlier rendezvous, the need for corrections in order to prevent secondary separation and unnecessary propellant expenditure. The results of Simulation II, where MPC-EMP algorithm was used (algorithm with consideration of model parameters evolution over the prediction horizon) seems to be able to overcome these weaknesses. The maneuver was accomplished significantly earlier (around 2 hour and 45 minutes). Furthermore, the comparison between Figures 6.3 and 6.8 indicates that maneuver controlled by MPC-EMP algorithm costs visibly less, approximately 7% of the propellant mass, what has significant meaning in the context of mission economical aspects. In contrast to the MPC-CMP algorithm from Simulation I, the MPC-EMP controller

has negligible difficulties with maintaining of the set-point after achievement of the maneuver objectives, as indicates Figure 6.9.

Now, let us discuss the differences in control performance arising in case of application of different internal models for the controller. Such situation is reflected by Simulations III and IV. Both the simulations are characterized by the same initial conditions, spacecraft parameters and controller settings. In Simulation III the Tschauner–Hempel equations are used as the internal model for the controller, while in Simulation IV the controller utilizes the NERM-based model given by Equation 4.11. Analysis of Figures 6.11, 6.12 and 6.15 implies the conclusion that the behavior of the controller based on linearized (Tschauner–Hempel) model leads to radical malfunctions. The figures presented in Section 6.4, showing the results of Simulation IV, proves that utilization of the NERM-based model enables physically achievable rendezvous maneuver for such initial conditions. Moreover, the initial separation between the satellites was equal to 36 252 km, hence meeting of the control objective can be counted as a considerable success.

Simulation V reflects the situation where the control loop is exposed to strong input and output uncontrolled disturbances. The simulation has revealed a sensitivity of the MPC-EMP algorithm to strong perturbations. Figure 6.22 clearly shows that control system has difficulties with maintaining of the control objective. Frequent interventions performed by the controller leads to full expenditure of the propellant, what illustrates Figure 6.23. Nevertheless, such strong disturbances are not present during orbital flights. Moreover, even the presented behavior of the control system is sufficient for guidance purposes, wherein the close proximity operations are controlled by another, specialized algorithm. The magnitude of dynamic errors during stabilization process in the neighborhood of the control objective could be decreased through application of smaller control increment weights.

Simulation VI was conducted in order to analyze the transient response of the system controlled by the MPC-EMP controller. Study of Figures 6.26, 6.27 and 6.29 indicates that the controller, with some minor error, enforced return of the relative motion state to the control objective. The simulation proved that the MPC-EMP algorithm is able to compensate the constant disturbances in an acceptable manner.

7.2 Solution Limitations

Basic limitation of the MPC-EMP algorithm presented in this dissertation is associated with the effective length of the prediction horizon. The reasons of limitations on prediction horizon length are as follows:

1. the output prediction systems described in Section 4.4 using the state-space representation of the model implies matrix chain multiplication. The number of multiplications is proportional to the length of the prediction horizon, what causes numerical difficulties in case of long prediction horizons.

2. Another limitation on the prediction horizon length, even more restrictive than the previous is caused by imperfections of future model parameters estimation. The model parameters cannot be predicted accurately in too far future, mainly because of their implicit and explicit dependence on future control signal, which determines the future states of the process, shaping the future model parameters. Excessive elongation of the prediction horizon entails degradation of the closed-loop performance.

The consequences of the horizon length limitation are following:

1. for some subspace of initial conditions (a very large separations and relative velocities exceeding the values presented in Chapter 6) the stability of the control system is impossible to provide because of inability to sufficiently long prediction of complicated dynamics behavior.

2. Insufficiently long prediction horizon prevents purposefulness of further increasing of the control increment weight, what implies relative fast and aggressive control process. Too large control increment weights lead to control system instability.

7.3 Scope of Applicability

In the context of spacecraft relative motion, the presented MPC-EMP algorithm can be applied for wide range of initial conditions, far exceeding the capabilities of MPC algorithms based on linearized models. The presented method seems to be feasible in case of unoptimized, unfavorable set of initial conditions, where preliminary

arrangements of the maneuver are infeasible and immediate action need to be taken. Together with the relatively fast character of the control process, these attributes may prove to be relevant for military applications.
In general, the MPC-EMP algorithm may be utilized as a control strategy for wide range of problems, including control of objects with strong nonlinearity and time variance.

7.4 Anticipated Benefits of the Solution

The application of the MPC-EMP algorithm to the orbital rendezvous in an elliptical orbit lets hope the following benefits:

1. possibility of rendezvous maneuver for large separations (tens of thousands kilometers) and orbit eccentricities exceeding 0,8,
2. propellant savings (several percent) relative to approaches based on classical MPC algorithms with successive linearization,
3. relatively simple implementation,
4. possibility of an autonomous, impromptu maneuvers,
5. utilization of reliable and relatively simple optimization algorithm.

7.5 Comparison with Other Solutions

In this section, a chosen investigations applicable to elliptical orbit case will be compared with the approach presented in this dissertation. The objectives and features of the presented solution differs from the classical orbital rendezvous approaches. The solution is designed to be able to cope with exceptionally large separations, like tens of thousands kilometers. This approach is unusual in existing space rendezvous technology, where the large separations between deputy spacecraft and chief in a circular orbit are typically reduced by Hohmann maneuvers. However, proposed strategy gives a possibility of an impromptu rendezvous maneuvers in an elliptical orbit with radically shorter duration. In light of this feature, the MPC-EMP algorithm can be also used for guidance purposes.

In Ref. [29] general dynamics between spacecraft has been derived and 6 degree of freedom GNC system for relative motion between spacecraft on general elliptic orbits has been developed. The linearized dynamics allows application only for small separation distance. The control design is focused on H_∞ multi variable robust control.

Investigation presented in Ref. [26] utilizes model predictive control with linear cost function (including 1-norm of fuel use) and a novel, J_2-modified linearized relative orbital dynamics based on Gauss' Variational Equations. The work is focused on accuracy of a formation maintenance and safe docking paths, the separations less that 5000 m are considered.

In Ref. [86] the problem of relative motion was analyzed and analytical solutions has been provided. A LQR control for relative motion has been proposed and development of optimal feedback control that include nonlinear effects has been studied. The research assumes relative motion with initial separations approximately 10 km.

In Ref. [68] the relationship between the Hill-Clohessy-Wiltshire equations and relative motion in elliptic orbits has been explored. The Hill-Clohessy-Wiltshire equations have been generalized using Lyapunov-Floquet transformations to describe relative motion in elliptic orbits. Lyapunov-Floquet transformations were used by linear quadratic regulator to compute a time-varying gain matrix.

In Ref. [14] an analytic treatment of the problem of impulsive terminal rendezvous in near-circular orbit is presented. A typical large transfer where the two vehicles are initially separated by 2000 km is achieved with an interception error of 5 km.

In light of the last reference, which seems to consider the problem of large separations, the results obtained using the approach presented in this dissertation appear to be satisfactory.

Chapter 8

Conclusions and Future Work

In this dissertation, the problem of control of orbital relative motion was analyzed. Detailed derivation of nonlinear mathematical model of relative dynamics has been presented. A novel model predictive control algorithm has been proposed in order to solve the problem of rendezvous maneuver in a highly elliptical orbit. Below sections describes detailed summary of the proposed solution.

8.1 Relative Dynamics

Chapter 2 derived basic laws of orbital mechanics, assuming closed Keplerian orbit. The motion has been considered as the two-body problem, and orbital integrals of motion has been found. Using this basis a full, nonlinear, time-variant model of satellite relative motion has been derived in Cartesian coordinate frame. A model of deputy spacecraft mass has been proposed.

8.2 Control of Relative Motion

Chapter 3 presented principles and properties of the model predictive control.

Chapter 4 formulated a novel model predictive control algorithm MPC-EMP. Both the principal relative motion model and the spacecraft mass model have been concatenated into an augmented model of relative motion and discretized. The principal concept of the control process improvement has been consideration of model parameters evolution within the prediction horizon. Such possibility has been embedded into output prediction system. Furthermore, a detailed description of model predictive control formulation has been provided.

Chapter 5 depicted overall description of simulation methodology and control algorithm implementation.

Chapter 6 presented results of conducted simulations with necessary comments. The results has been depicted as control and state trajectories. Visualization of the relative position also has been presented.

Chapter 7 interpreted the results of simulations as well as presented a discussion on the approach with references to chosen alternative solutions.

8.3 Future Research and Extensions

Since the Earth oblateness effect plays a noticeable role in the relative motion dynamics, further work will incorporate the J_2 effect introduced into the mathematical model.

In order to capture the practical spacecraft rendezvous requirements, it is recommended to consider a complete set of constraints, including soft constraints on state vector and constraints related to sensors, for example constraints on line of sight cone.

More realistic projection of the process during simulation could be obtained using more advanced perturbation modeling, including the J_2 effect and the third bodies impact. This entails the connected problem - modeling of a relative state sensor system and design of state observer, using Kalman filtering principles.

One of the exigent problems is the formal stability analysis. In case of model predictive control using successive linearization, there is lack of common methods providing the stability proof. One of the challenges would be selection of an appropriate strategy for stability analysis of the MPC-EMP algorithm, which is a kind of broadening of algorithms with successive linearization.

Present structure of the MPC-EMP algorithm utilizes a simple method for preliminary estimation of future control trajectory, required for estimation of a future model parameters. The method is based on a FIR concept and provides results in a heuristic manner. A promising approach would be an application of auxiliary model predictive controller for preliminary estimation of future control and state trajectories.

Finally, an important investigation would be conducted with an assumption of linear cost function in the optimization procedure. The model predictive control algorithms utilizing linear programming generate trajectories that closely approximate “bang-off-bang” solutions rather than continuous thrusting plans, what entails

strategy more focused on optimization of propellant expenditure.

List of References

[1] Y. Luo, J. Zhang, and G. Tang, "Survey of orbital dynamics and control of space rendezvous," *Chinese Journal of Aeronautics*, vol. 27, no. 1, pp. 1 – 11, 2014.

[2] O. Montenbruck and E. Gill, *Satellite Orbits: Models, Methods, and Applications*. Springer, 2005.

[3] C. Brezinski, *Computational Aspects of Linear Control*. Numerical Methods and Algorithms, Springer US, 2002.

[4] G. W. Hill, "Researches in the lunar theory," *American Journal of Mathematics*, vol. 1, pp. 5–26,129–147,24–260, 1878.

[5] W. H. Clohessy and P. S. Wiltshire, "Terminal guidance system for satellite rendezvous," *Journal of Aerospace Sciences*, vol. 27, pp. 653–658, September 1960.

[6] D. F. Lawden, *Optimal Trajectories for Space Navigation*. London: Butterworths, 1963.

[7] J. Tschauner and P. Hempel, "Rendezvous zu einem in elliptischer bahn umlaufenden ziel," *Astronautica Acta*, vol. 11, no. 2, pp. 104–109, 1965.

[8] R. G. Melton, "Time-explicit representation of relative motion between elliptical orbits," *Journal of Guidance, Control, and Dynamics*, vol. 23, no. 4, pp. 604–610, 2000.

[9] T. E. Carter, "State transition matrices for terminal rendezvous studies: Brief survey and new example," *Journal of Guidance, Control, and Dynamics*, vol. 21, pp. 148–155, January 1998.

[10] K. Yamanaka and F. Ankersen, "New state transition matrix for relative motion on an arbitrary elliptical orbit," *Journal of Guidance, Control, and Dynamics*, vol. 25, pp. 60–66, January 2002.

[11] K. T. Alfriend and Y. Kashiwagi, "Minimum-time orbital rendezvous between neighboring elliptic orbits," *Journal of Optimization Theory and Applications*, vol. 4, no. 4, pp. 260–276, 1969.

[12] H. S. London, "Second approximation to the solution of the rendezvous equations," *AIAA Journal*, vol. 1, no. 7, pp. 1691–1693, 1963.

[13] C. D. Karlgaard and F. H. Lutze, "Second-order relative motion equations," *Journal of Guidance, Control, and Dynamics*, vol. 26, no. 1, pp. 41–49, 2003.

[14] J. A. Kechichian, "Techniques of accurate analytic terminal rendezvous in near-circular orbit," *Acta Astronautica*, vol. 26, no. 6, pp. 377–394, 1992.

[15] R. Z. Zhu and Y. L. Li, "Analytic solution of the nonlinear equation of relative motion with small constant thrust," *Chinese Space Science and Technology*, vol. 20, no. 2, pp. 20–29, 2000.

[16] I. M. Ross, "Linearized dynamic equations for spacecraft subject to j perturbations," *Journal of Guidance, Control, and Dynamics*, vol. 26, no. 4, pp. 657–659, 2003.

[17] D.-W. Gim and K. T. Alfriend, "State transition matrix of relative motion for the perturbed noncircular reference orbit," *Journal of Guidance, Control, and Dynamics*, vol. 26, no. 6, pp. 956–971, 2003.

[18] S. A. Schweighart and R. J. Sedwick, "High-fidelity linearized j model for satellite formation flight," *Journal of Guidance, Control, and Dynamics*, vol. 25, no. 6, pp. 1073–1080, 2002.

[19] G. E. Pollock, J. W. Gangestad, and J. M. Longuski, "Analytical solutions for the relative motion of spacecraft subject to lorentz-force perturbations," *Acta Astronautica*, vol. 68, no. 1-2, pp. 204–217, 2011.

[20] G. Zhang and D. Zhou, "A second-order solution to the two-point boundary value problem for rendezvous in eccentric orbits," *Celestial Mechanics and Dynamical Astronomy*, vol. 107, no. 3, pp. 319–336, 2010.

[21] K. Yamada, M. Kimura, T. Shima, and S. Yoshikawa, "New state transition matrix for formation flying in j_2-perturbed elliptic orbits," *Journal of Guidance, Control, and Dynamics*, vol. 35, no. 2, pp. 536–547, 2012.

[22] L. S. Breger and J. P. How, "J_2-modified GVE-based MPC for formation flying spacecraft," in *AIAA Guidance, Navigation, and Control Conference (GNC)*, (San Francisco, California, US), August 2005.

[23] K. T. Alfriend and H. Yan, "Evaluation and comparison of relative motion theories," *Journal of Guidance, Control, and Dynamics*, vol. 28, no. 2, pp. 254–261, 2005.

[24] P. Labourdette and A. A. Baranov, "Strategies for on-orbit rendezvous circling mars," *Advances in the Astronautical Sciences*, vol. 109, no. 2, pp. 1351–1368, 2002.

[25] J. Zhang, Y. Luo, and G. Tang, "Hybrid planning for leo long-duration multi-spacecraft rendezvous mission," *Science China - Technological Sciences*, vol. 55, no. 1, pp. 233–243, 2012.

[26] L. S. Breger, *Control of Spacecraft in Proximity Orbits*. PhD thesis, Massachusetts Institute of Technology, Cambridge, Massachusetts, US, June 2007.

[27] M. Okasha and B. Newman, "Relative motion guidance, navigation and control for autonomous orbital rendezvous," in *Proceedings of AIAA Guidance, Navigation and Control Conference 2011*.

[28] A. A. Baranov, "An algorithm for calculating parameters of multi-orbit maneuvers in remote guidance," *Cosmic Research*, vol. 28, no. 1, pp. 61–67, 1990.

[29] F. Ankersen, *Guidance, Navigation, Control and Relative Dynamics for Spacecraft Proximity Maneuvers*. PhD thesis, Aalborg University, Aalborg, Denmark, December 2010.

[30] E. J. Mora, F. Ankersen, and J. B. Serrano, "Mimo control for 6dof relative motion," in *Proceedings of 3'rd ESA International Conference on Spacecraft Guidance, Navigation and Control Systems*, November 1996.

[31] C. L. Karr and L. M. Freeman, "Genetic-algorithm-based fuzzy control of spacecraft autonomous rendezvous," *Engineering Applications of Artificial Intelligence*, vol. 10, no. 3, pp. 293–300, 1997.

[32] T. Chen and S.-J. Xu, "Fuzzy controller for terminal approach of autonomous rendezvous and docking with non-cooperative target," *Yuhang Xuebao*, vol. 27, no. 3, pp. 416–421, 2006.

[33] E. A. Youmans and F. H. Lutze, "Neural network control of space vehicle intercept and rendezvous maneuvers," *Journal of Guidance, Control, and Dynamics*, vol. 21, no. 1, pp. 116–121, 1998.

[34] N. K. Philip and N. K. Malik, "Guidance and control aspect of space rendezvous and docking," *Journal of Spacecraft Technology*, vol. 3, pp. 48–56, January 1993.

[35] M. Shibata and A. Ichikawa, "Orbital rendezvous and flyaround based on null controllability with vanishing energy," *Journal of Guidance, Control, and Dynamics*, vol. 30, no. 4, pp. 934–945, 2007.

[36] V. Kapila, A. G. Sparks, J. M. Buffington, and Q. Yan, "Spacecraft formation flying: Dynamics and control," *Journal of Guidance, Control, and Dynamics*, vol. 23, no. 3, pp. 561–564, 2000.

[37] R. Sharma, P. Sengupta, and S. R. Vadali, "Near-optimal feedback rendezvous in elliptic orbits accounting for nonlinear differential gravity," *Journal of Guidance, Control, and Dynamics*, vol. 30, no. 6, pp. 1803–1813, 2007.

[38] D. P. Scharf, F. Y. Hadaegh, and S. R. Ploen, "A survey of spacecraft formation flying guidance and control (part 2): Control," in *Proceedings of the American Control Conference*, pp. 2976–2985, 2004.

[39] S. D. Cairano, H. Park, and I. V. Kolmanovsky, "Model predictive control approach for guidance of spacecraft rendezvous and proximity maneuvering," *International Journal of Robust and Nonlinear Control*, vol. 22, no. 12, p. 1398–1427, 2012.

[40] J. R. Carpenter and R. H. Bishop, "Navigation filter estimate fusion for enhanced spacecraft rendezvous," *Journal of Guidance, Control, and Dynamics*, vol. 20, no. 2, pp. 338–345, 1997.

[41] H. Schaub and K. T. Alfriend, "Impulsive feedback control to establish specific mean orbit elements of spacecraft formations," *Journal of Guidance, Control, and Dynamics*, vol. 24, no. 4, pp. 739–745, 2001.

[42] X. Yang, J. Yu, and H. Gao, "An impulse control approach to spacecraft autonomous rendezvous based on genetic algorithms," *Neurocomputing*, vol. 77, no. 1, p. 189–196, 2012.

[43] C. D. Karlgaard, "Robust rendezvous navigation in elliptical orbit," *Journal of Guidance, Control, and Dynamics*, vol. 29, no. 2, pp. 495–499, 2006.

[44] H. Gao, X. Yang, and P. Shi, "Multi-objective robust h_∞ control of spacecraft rendezvous," *IEEE Transactions on Control Systems Technology*, vol. 17, no. 4, p. 794–802, 2009.

[45] M. Tillerson, G. Inalhan, and J. P. How, "Coordination and control of distributed spacecraft systems using convex optimization techniques," *International Journal of Robust and Nonlinear Control*, vol. 12, no. 2-3, pp. 207–242, 2002.

[46] B. Zhou, Z. Lin, and G.-R. Duan, "Lyapunov differential equation approach to elliptical orbital rendezvous with constrained controls," *Journal of Guidance, Control, and Dynamics*, vol. 34, no. 2, pp. 345–358, 2011.

[47] C. A. Kluever, "Feedback control for spacecraft rendezvous and docking," *Journal of Guidance, Control, and Dynamics*, vol. 22, no. 4, pp. 609–611, 1999.

[48] R. Bevilacqua, M. Romano, and O. Yakimenko, "Online generation of quasi-optimal spacecraft rendezvous trajectories," *Acta Astronautica*, vol. 64, no. 2–3, pp. 345–358, 2009.

[49] L. Breger, J. How, and A. Richards, "Model predictive control of spacecraft formations with sensing noise," in *Proceedings of the American Control Conference 2005*, pp. 2385–2390, IEEE, 2005.

[50] F. Gavilan, R. Vazquez, and E. F. Camacho, "Robust model predictive control for spacecraft rendezvous with online prediction of disturbance bounds," 2011.

[51] E. N. Hartley, P. A. Trodden, A. G. Richards, and J. M. Maciejowski, "Model predictive control system design and implementation for spacecraft rendezvous," *Control Engineering Practice*, vol. 20, no. 7, pp. 695–713, 2012.

[52] S.-G. Kim, J. L. Crassidis, Y. Cheng, A. M. Fosbury, and J. L. Junkins, "Kalman filtering for relative spacecraft attitude and position estimation," *Journal of Guidance, Control, and Dynamics*, vol. 30, no. 1, pp. 133–143, 2007.

[53] C. Petersen, A. Jaunzemis, M. Baldwin, M. J. Holzinger, and I. V. Kolmanovsky, "Model predictive control and extended command governor for improving robustness of relative motion guidance and control," *Proceedings of AAS/AIAA Space Flight Mechanics Meeting*, 2014.

[54] M. Saponara, V. Barrena, A. Bemporad, E. Hartley, J. Maciejowski, A. G. Richards, A. Tramutola, and P. A. Trodden, *Model Predictive Control Application to Spacecraft Rendezvous in Mars Sample Return Dcenario*. 2011. Conference Organiser: EUCASS.

[55] A. Weiss, I. Kolmanovsky, M. Baldwin, and R. S. Erwin, "Model predictive control of three dimensional spacecraft relative motion," in *Proceedings of the American Control Conference 2012*, pp. 173–178, IEEE, 2012.

[56] P. A. Capó-Lugo and P. M. Bainum, *Orbital Mechanics and Formation Flying: A Digital Control Perspective*. Woodhead Publishing in mechanical engineering, Woodhead Publishing Limited, 2011.

[57] W. Fehse, *Automated Rendezvous and Docking of Spacecraft*. Cambridge University Press, 2003.

[58] R. R. Bate, D. D. Mueller, and J. E. White, *Fundamentals of Astrodynamics*. New York City, New York, US: Dover Publications, Incorporated, 1971.

[59] V. A. Chobotov, *Orbital Mechanics, Third Edition*. AIAA Education Series, American Institute of Aeronautics and Astronautics, 2002.

[60] R. X. Meyer, *Elements of Space Technology*. Burlington: Academic Press, 1999.

[61] B. Wie, *Space Vehicle Dynamics and Control*. AIAA Education Series, American Institute of Aeronautics and Astronautics, 2008.

[62] W. Ley, K. Wittmann, and W. Hallmann, *Handbook of Space Technology*. American Institute of Aeronautics and Astronautics, 2009.

[63] J. D. Hadjidemetriou, "Analytic solutions of the two-body problem with variable mass," *Icarus*, vol. 5, no. 1–6, pp. 34–46, 1966.

[64] D. J. Jezewski and D. Mittleman, "Integrals of motion for the classical two-body problem with drag," *International Journal of Non-Linear Mechanics*, vol. 18, no. 2, pp. 119–124, 1983.

[65] F. Casella and M. Lovera, "High-accuracy simulation of orbital dynamics: An object-oriented approach," *Simulation Modelling Practice and Theory*, vol. 16, no. 8, pp. 1040–1054, 2008.

[66] H. Schaub and J. L. Junkins, *Analytical Mechanics of Space Systems*. Reston, Virginia, US: AIAA Education Series, October 2003.

[67] H. D. Curtis, *Orbital Mechanics for Engineering Students*. Elsevier Aerospace Engineering Series, Butterworth-Heinemann, 2005.

[68] R. E. Sherrill, *Dynamics and Control of Satellite Relative Motion in Elliptic Orbits using Lyapunov-Floquet Theory*. PhD thesis, Auburn University, Auburn, Alabama, US, May 2013.

[69] M. J. Sidi, *Spacecraft Dynamics and Control: A Practical Engineering Approach*. Cambridge Aerospace Series, Cambridge University Press, 1997.

[70] C. Cutler and B. Ramaker, "Dynamic matrix control-a computer control algorithm," 1979.

[71] S. J. Qin and T. A. Badgwell, "A survey of industrial model predictive control technology," *Control Engineering Practice*, vol. 11, pp. 733–764, July 2003.

[72] L. Wang, *Model Predictive Control System Design and Implementation Using MATLAB®*. Advances in Industrial Control, Springer, 2009.

[73] P. Tatjewski, *Sterowanie zaawansowane obiektów przemysłowych: Struktury i algorytmy*. Monografie - Komitet Automatyki i Robotyki Polskiej Akademii Nauk, Akademicka Oficyna Wydawnicza Exit, 2002.

[74] C. B. Eduardo F. Camacho, *Model Predictive Control*. Advanced Textbooks in Control and Signal Processing, Springer London, 2004.

[75] D. Q. Mayne, J. B. Rawlings, C. V. Rao, and P. O. M. Scokaert, "Constrained model predictive control: Stability and optimality," *Automatica*, vol. 36, no. 6, pp. 789–814, 2000.

[76] C. E. García, D. M. Prett, and M. Morari, "Model predictive control: Theory and practice - a survey," *Automatica*, vol. 25, no. 3, pp. 335–348, 1989.

[77] Y.-G. Xi, D.-W. Li, and S. Lin, "Model predictive control - status and challenges," *Acta Automatica Sinica*, vol. 39, no. 3, pp. 222–236, 2013.

[78] A. Bemporad and D. M. de la Pena, "Multiobjective model predictive control," *Automatica*, vol. 45, no. 12, pp. 2823–2830, 2009.

[79] M. Cannon, "Efficient nonlinear model predictive control algorithms," *Annual Reviews in Control*, vol. 28, no. 2, pp. 229–237, 2004.

[80] M. V. Kothare, V. Balakrishnan, and M. Morari, "Robust constrained model predictive control using linear matrix inequalities," *Automatica*, vol. 32, no. 10, pp. 1361–1379, 1996.

[81] P. D. Christofides, R. Scattolini, D. M. de la Pena, and J. Liu, "Distributed model predictive control: A tutorial review and future research directions," *Computers & Chemical Engineering*, vol. 51, no. 0, pp. 21 – 41, 2013.

[82] W. Wojsznis, A. Mehta, P. Wojsznis, D. Thiele, and T. Blevins, "Multi-objective optimization for model predictive control," *{ISA} Transactions*, vol. 46, no. 3, pp. 351–361, 2007.

[83] C. E. Long, P. K. Polisetty, and E. P. Gatzke, "Nonlinear model predictive control using deterministic global optimization," *Journal of Process Control*, vol. 16, no. 6, pp. 635–643, 2006.

[84] P. Bania, *Algorytmy sterowania optymalnego w nieliniowej regulacji predykcyjnej*. PhD thesis, Akademia Górniczo-Hutnicza im. Stanisława Staszica, Kraków, Poland, February 2008.

[85] R. Findeisen and F. Allgöwer, "An introduction to nonlinear model predictive control," in *Control, 21st Benelux Meeting on Systems and Control, Veidhoven*, pp. 1–23, 2002.

[86] P. Sengupta, *Dynamics and Control of Satellite Relative Motion in a Central Gravitational Field*. PhD thesis, Texas A&M University, College Station, Texas, US, December 2006.

Appendix A

Tschauner-Hempel Model of Relative Motion

This appendix describes the model of spacecraft relative motion based on system of linear differential equations proposed by Tschauner and Hempel. Derivation of these equations can be found in Ref. [7]. According to the assumed LVLH frame and nomenclature used in Chapter 2, the equations has the following form:

$$\ddot{x}_1 - 2\dot{f}\dot{x}_2 - \ddot{f}x_2 - \dot{f}^2 x_1 = 2\frac{\mu}{r_c^3}x_1 + \frac{u_{d1}}{m_d} \tag{A.1}$$

$$\ddot{x}_2 + 2\dot{f}\dot{x}_1 + \ddot{f}x_1 - \dot{f}^2 x_2 = -\frac{\mu}{r_c^3}x_2 + \frac{u_{d2}}{m_d} \tag{A.2}$$

$$\ddot{x}_3 = -\frac{\mu}{r_c^3}x_3 + \frac{u_{d3}}{m_d} \tag{A.3}$$

According to Equation 2.67, the above equations can be rewritten into the following form:

$$\ddot{x}_1 = 2\dot{f}\dot{x}_2 - 2\frac{\dot{r}_c}{r_c}\dot{f}x_2 + \dot{f}^2 x_1 + 2\frac{\mu}{r_c^3}x_1 + \frac{u_{d1}}{m_d} \tag{A.4}$$

$$\ddot{x}_2 = -2\dot{f}\dot{x}_1 + 2\frac{\dot{r}_c}{r_c}\dot{f}x_1 + \dot{f}^2 x_2 - \frac{\mu}{r_c^3}x_2 + \frac{u_{d2}}{m_d} \tag{A.5}$$

$$\ddot{x}_3 = -\frac{\mu}{r_c^3}x_3 + \frac{u_{d3}}{m_d} \tag{A.6}$$

Assuming the state vector given by Equation 2.83, the system of equations can be used to formulate a state-space representation of the model:

$$\dot{\mathbf{x}}_{rm} = \mathbf{A}_{th}\mathbf{x}_{rm} + \mathbf{B}_{th}\left(\mathbf{u} + \mathbf{u}_{ud}\right) \tag{A.7}$$

wherein the input matrix $\mathbf{B}_{th}$ has the same form as given by Equation 2.92 while the state matrix can be defined as:

$$\mathbf{A}_{th} = \begin{bmatrix} 0 & 0 & 0 & 1 & 0 & 0 \\ 0 & 0 & 0 & 0 & 1 & 0 \\ 0 & 0 & 0 & 0 & 0 & 1 \\ \dot{f}^2 + 2\frac{\mu}{r_c^3} & -2\frac{\dot{r}_c}{r_c}\dot{f} & 0 & 0 & 2\dot{f} & 0 \\ 2\frac{\dot{r}_c}{r_c}\dot{f} & \dot{f}^2 - \frac{\mu}{r_c^3} & 0 & -2\dot{f} & 0 & 0 \\ 0 & 0 & -\frac{\mu}{r_c^3} & 0 & 0 & 0 \end{bmatrix} \tag{A.8}$$